Collectively Enhanced Quantum Light-Matter Interactions

UNIVERSITY OF LEEDS

Oleg Kim

The University of Leeds

School of Physics and Astronomy

Submitted in accordance with the requirements for the degree of

Doctor of Philosophy

June, 2015

The candidate confirms that the work submitted is his own, except where work which has formed part of jointly authored publications has been included. The contribution of the candidate and the other authors to this work has been explicitly indicated below. The candidate confirms that appropriate credit has been given within the thesis where reference has been made to the work of others.

Chapter 4 is based on work from Kim, O. and Beige, A. (2013) Mollow triplet for cavity-mediated laser cooling. *Physical Review A* **88**, 053417. All of analytic and numerical calculations in the publication are attributable to the candidate. All of the above authors contributed to the remaining material.

This copy has been supplied on the understanding that it is copyright material and that no quotation from the thesis may be published without proper acknowledgement.

Acknowledgements

I would like to express my deepest thanks to my supervisor Dr. Almut Beige for support and guidance given to me through my PhD. Alongside, I wish to thank my OIST collaboration supervisor Dr. Thomas Busch for leading the collaboration and making it possible. I would also like to thank everyone (so as not to miss any names) who worked at or visited the Quantum Information group at the University of Leeds or the Quantum Systems Unit at the Okinawa Institute of Science and Technology between 2011 and 2015.

Abstract

In this thesis, we investigate dynamics of many-body atomic systems coupled to electromagnetic fields. We find that collective effects present in cavity-mediated laser cooling and high temperatures of bubble in sonoluminescence can be explained using a two-stage model which combines quantum-optical models and thermodynamical processes. We show how the collective processes are strongly dependent on mutual atomic coherences and how these coherences need to be recreated for the continous collective processes to take place.

The model mechanism behind both cavity-mediated laser cooling and sonoluminescence heating is alternating periods of thermalisation with cooling or heating cycles. The thermalisation stage is characterised by relatively weak interactions between the atomic system and its environment, while allowing the system to thermalise and to create phonon and electronic coherences necessary for the next stage. The second stage, when cooling or heating occurs, marks strong interactions of the atomic system with the surrounding radiation field, which renders interactions between the particles negligible. During this stage, the atomic coherences created earlier fuel the cooling or heating process, allowing the system to reach a more beneficial stationary state.

For cavity-mediated laser cooling of an atomic gas, we show that dispersing cooling pulses with periods of thermalisation in an asymmetric potential can result in very low temperatures of the atomic gas. By applying this to atomic interactions of sonoluminescence, we can describe different parts of the lifecycle of the cavitating bubble and how very high temperatures arise inside of it.

Abbreviations

k_B Boltzmann's constant

$\hbar$ Planck's constant

ε_0 Permittivity of free space

μ_0 Permeability of free space

tr   The *trace* operator

Contents

CONTENTS

List of Figures

LIST OF FIGURES

Chapter 1

Introduction

Laser cooling of atomic systems has been of interest for quite some time. It is a very prominent technique that allows to cool an atomic system to very low temperatures. A laser-cooled single atom provides an excellent way to obtain a quantum system which is close to theoretical models in quantum optics (cf. Neuhauser *et al.* (1978)). This makes a single trapped and laser-cooled atom the preferred subject for ultrahigh precision experiments, which test the foundations of quantum physics. The applications of laser cooling range from quantum metrology to quantum computing.

Powerful as it is, laser cooling is not very effective for simultaneous cooling of multiple particles (cf. Maunz *et al.* (2004)). Cooling of many body systems, such as atomic gases or condensates, is however essential for gaining insights in ultracold atomic physics, condensed matter physics and quantum optics. Experiments with ultracold atoms are important for studying and understanding quantum phenomena such as quantum phase transition, Bose-Einstein condensation, quantum magnetism or bosonic superfluidity (cf. Madison *et al.* (2013)). Such experiments require a proper technique that would yield very low temperatures and relatively fast cooling rates.

Coupling an atomic system to a quantised mode in an optical cavity was proposed as a solution for effective cooling of a many-body system. First indications of successful cavity-mediated laser cooling were first found in Vigneron (1995). Later on, it was repeatedly demonstrated that addition of an optical cavity can greatly enhance the cooling process for both single and multi-particle systems (cf. Maunz *et al.* (2004); McKeever *et al.* (2003); Nußmann *et al.* (2005)). One of the remarkable properties of cooling of many-body systems was the collective effect of the cooling process, where the cooling rate scales positively with the number of atoms in the system (cf. Domokos & Ritsch (2002)).

However, theoretical description of the cavity-mediated cooling process for many-body systems remains challenging. Many semiclassical approaches have been made to provide a qualitative description, but even full quantum mechanical models have trouble explaining the collective character that the cavity-mediated cooling possesses and the extremely low phonon numbers that it makes possible to obtain. In this thesis, we will present a radically different model which combines the quantum optics models together with framework of thermodynamics. By considering simultaneous coupling between atomic vibrational states, electronic states and the cavity field mode, we show that the cooling process reaches very low temperature when allowing the system to *thermalise* between cooling pulses. We demonstrate that the change in the temperature of the system originates in the fact that the phonon coherence ζ, which represents energy exchange between the atoms, attains a positive value. To maintain ζ above zero and continue the cooling process indefinitely, we introduce thermalisation periods between the cooling pulses, where we let the system evolve into a thermal state in an asymmetric potential without a cooling laser. We show how not only does such a thermal state revive the phonon coherence ζ, but also that thermalising the system is an exemplary method for doing this since it doesn't compromise the temperature of the system. Dispersing cooling pulses with periods of thermalisation therefore constitutes a continuous cooling cycle which results in very low temperatures.

Applying the same two-stage approach to model the phenomenon of sonoluminescence results in the theoretical description of heating processes and mechanisms behind them. As the lifecycle of the single bubble in sonoluminescence closely resembles the two-stage process of many-body cooling in an optical cavity, modelling it with thermalisation and atom-cavity-phonon interaction, as we did earlier, provides a relevant picture and identifies main properties of the process, with heating replacing cooling.

The design of this model for cooling and heating many particles collectively is the main result of this thesis. In addition, we also studied a single atom in the similar setup as a backdrop to many-body interactions. In the next section, we outline the full content of the thesis.

1.1   Our treatment of cooling of an atomic system

In this thesis, we model the cavity-mediated sideband cooling using the full quantum-mechanical description. We assume the dipole interaction between a system of har-

monically confined two-level atoms and a single-mode standing wave light field. Given such a scenario, we use the Jaynes-Cummings model as the starting point. The theory of quantum harmonic oscillators and of quantum electromagnetic field theory is given in chapters 2 and 3.

1.1.1 Cooling of a single particle

Using the master equation approach introduced in Cirac *et al.* (1993), we obtain a set of rate equations which describe the evolution of the mean vibrational energy. In chapter 4, we first treat cooling of a trapped single atom to show how our method applies to a simpler system and how it can be used to reproduce the already known results. For cooling a single atom, we find that the stationary state of the mean vibrational energy exhibits three sharp minima. The first minimum is located at the red sideband, which agrees with previous findings. The other two previously undiscovered minima are located to the either side of the sideband, separated from it by the amount equal to the Rabi frequency of the laser. The three resonances therefore resemble a Mollow triplet (cf. Mollow (1969)). The results of chapter 4 has been published in Kim & Beige (2013).

1.1.2 Cooling of an atomic gas

For cooling of a one-dimensional atomic gas in chapter 5, we apply the same master equation approach as for the single trapped atom. The rate equations demonstrate that the cooling process is collective and the mean vibrational energy of the system quickly reaches the stationary state with the cooling rate that scales positively with the number of atoms in the gas. As mentioned earlier, during the cooling process, the vibrational energy is decreased by the amount that is equal to the initial value of a phonon coherence ζ, which is destroyed later in the cooling process. By reviving this phonon coherence, the cooling process can be continued even after the atomic system reaches the stationary state. We demonstrate that an excellent method to achieve this is by alternating cooling and displacement stages. The purpose of the displacement stage is for the system to evolve into the thermal state where the phonon coherence ζ acquires a non-zero value. During the displacement stage, the atoms are aligned in an anharmonic, asymmetric trap with the purpose of drawing them away from the trap centre. As will be shown later, this results in a non-zero phonon coherence, needed for cooling, without compromising the temperature of the system.

1.2   Origin of cavity-mediated laser cooling

The predecessor of cavity-mediated laser cooling — free space laser cooling — was first proposed by Wineland & Dehmelt (1975), which marked the onset of theoretical and experimental investigations of laser cooling. Of the particular interest was the study of a trapped atom which allows to confine its wave function on small length scales and to greatly enhance its interactions with the electromagnetic field. Laser cooling of trapped atoms has been successfully demonstrated experimentally by Neuhauser *et al.* (1978) and Diedrich *et al.* (1989), and its theory was very well outlined in Stenholm (1986).

For laser cooling of a single atom, two major regimes have been identified. In the *weak-binding* limit, where the trap frequency v is smaller than the natural linewidth Γ of the optical transition of the atom, the final temperature is limited by $T = \frac{\hbar\Gamma}{2k_B}$. This is commonly known as the *Doppler cooling* limit. On the other hand, in the strong-binding limit, the frequency of the trap is larger than the natural linewidth of the optical transition, and the atom develops well-resolved absorption sidebands. In this case, the cooling laser can be tuned to one of the sidebands and the atom can be cooled to its lowest vibrational state. This is referred to as *sideband cooling*. Both the Doppler and the sideband cooling limits have been seen experimentally and well agree with the theoretical predictions (cf. Diedrich *et al.* (1989)).

Due to its ability to cool a single atom to very low temperatures, laser sideband cooling has been a prommient technique in many quantum optics experiments. Unfortunately, as mentioned earlier, it also has certain drawbacks, such as inability to efficiently cool large numbers of atoms simultaneously or to cool particles with a complex level structures, such as molecules (cf. Lev *et al.* (2008)). Alternative techniques have been proposed. One of suggestions involves working in the sideband regime while confining the atomic system in an optical cavity. This strongly enhances the interaction between the system and the surrounding radiation field. In addition, cavity-mediated cooling does not rely on spontaneous emission of the atoms and can be manipulated by cavity geometries.

1.3   Experimental and theoretical advances

First indications of cavity-mediated laser cooling of atomic systems were found in Vigneron (1995). Successfull cooling and trapping of single cesium atoms was reported by McKeever *et al.* (2003). In Maunz *et al.* (2004), it was shown that the

cooling mechanism results in extended storage times and improved localisation of the atoms. It was estimated that the observed cooling rate is at least five times larger than that in free space cooling, for comparable excitation of the atom. Nußmann *et al.* (2005) demonstrated that orthogonal configuration of cooling laser, trapping laser and cavity-axis result in high cooling efficiency, low temperatures and relatively long trapping times. Wolke *et al.* (2012) reported an atom-cavity system with a cavity bandwidth below the recoil limit and cooling at densities and temperatures incompatible with conventional laser cooling. Cooling at two-photon resonance was observed in Kampschulte *et al.* (2010) for a single atom in an optical cavity with electromagnetically induced transparency. In Chuah *et al.* (2013), dynamics of cavity cooling of a single ion beyond the Lamb-Dicke regime was investigated, where a cooling limit below the Doppler temperature was demonstrated.

The theory for cavity-mediated laser cooling of single atoms was first discussed in Mossberg *et al.* (1991) and Zaugg *et al.* (1993), which confirmed that atomic cooling can be significantly enhanced using an optical resonator. Later on, using the semi-classical approach, Domokos & Ritsch (2003) identified weak and strong coupling regimes, and highlighted the importance of correlations between particles. Hemmerling & Robb (2011) demonstrated cooling using a blue-detuned driving light. Moreover, the number of atoms enhanced the cooling rate in the atom-pump configuration while having no effect in the cavity-pump configuration. Murr (2006) showed that addition of a cavity leads to modification of the Doppler force in the Doppler limit. A laser cooling method for atoms at low saturation and large detuning was proposed by Vuletić & Chu (2000).

While the semiclassical approach can be used to describe many phenomena of cavity-mediated laser cooling, the master equation approach introduced in Cirac *et al.* (1993) allows for a fully quantum mechanical description of the cooling process. This is particularly practical for cavity cooling, which allows to cool particles to very low temperatures where quantum effects dominate the time evolution of the system and semiclassical models no longer apply (cf. Domokos & Ritsch (2003)). In addition, the precision of master equation calculations is easier to control than the precision of semiclassical calculations.

Subsequently, the master equation approach has been employed by many authors. Bad-cavity and low saturation limits were treated by Cirac *et al.* (1995) to show that an atom can be cooled to the ground state of the trap even in the strong confinement regime. A mechanism for the collective cooling of a large number of trapped particles was proposed by Beige *et al.* (2005), where the particles were coupled to the

quantised field of an optical cavity and driven by a red-detuned laser field. Zippilli & Morigi (2005) presented cooling and heating rates of motion of a single driven atom in an optical resonator. The motion was critically affected by quantum correlations induced by the mechanical coupling with the resonator. The cavity-mediated laser cooling was compared with ordinary sideband laser cooling in Blake *et al.* (2011a) and Blake *et al.* (2012). Within the validity range of the Lamb-Dicke approximation, it was shown that both techniques display striking similarities. For example, the mean phonon number stationary states obtain the same expression in the weak and strong confinement regimes. An efficient ground state cooling was demonstrated in Bienert & Morigi (2012) by using electromagnetically induced transparency. A good review on cavity-mediated laser cooling of a single atom is given by Ritsch *et al.* (2013).

Compared to single particles, cooling of many-body systems in an optical cavity exhibits a much richer and more complicated dynamics. Subsequently, much less of it is identified or understood. Multiple systematic experimental studies have been reported. Schleier-Smith *et al.* (2011) demonstrated cooling of a single collective vibrational mode of an atomic ensemble down to two phonons which was in a good agreement with an optomechanical model. The cooling rate was proportional to the total photon scattering rate by the ensemble, which demonstrated the collective character of the light-induced cooling process. Pulsed cooling was used in Gibbons *et al.* (2008) to obtain very long lifetimes of a one-dimensional optical lattice. Black *et al.* (2003) demonstrated that emission-induced self-organisation of two-level atoms can lead to strong cooling of vibrational motion of the atoms.

Lately, multiple different models for theoretical description for cooling of many-body systems have been suggested. Morigi & Eschner (2001) investigated Doppler cooling of a Coulomb crystal in a linear ion trap, where they were able to derive the semiclassical limit and the Lamb-Dicke limit of the cooling dynamics. In addition, they found a Fokker-Planck equation for the total mechanical energy of the system. Mishina (2014) showed that cooling of a one-dimensional atomic array in harmonic traps can be affected by trap inhomogeneities. The rate equations approach was used by Beige *et al.* (2005) to obtain low temperatures using red-detuned fields.

1.4   Sonoluminescence

When it comes to heating of a many-body atomic system, sonoluminescence is an intriguing phenomenon of strong light flashes from tiny bubbles in a liquid (cf. Bren-

ner *et al.* (2002); Lohse (2002)). The bubbles are driven by an ultrasonic wave and need to be filled with atomic species. Moss (1997) showed that the time dependence of the bubble radius is in good agreement with the laws of classical physics, since the bubble radius increases isothermally for most of the cycle. However, each expansion phase is followed by a rapid collapse phase. The accelerating bubble wall becomes so fast that the bubble becomes thermally isolated from the liquid. Close to its minimum radius of about $0.5\,\mu$m, a rapid increase of the energy density of the particles inside the bubble occurs which is accompanied by the sudden emission of light. Afterwards a re-expansion phase begins in which the bubble oscillates around its equilibrium radius until it regains its stability.

Measuring the spectra of the picosecond light flash at the end of the collapse and associating the continuum underlying these sonoluminescence spectra with blackbody or Bremsstrahlung radiation indicates temperatures of at least 10^3–10^4 K inside the bubble (cf. Barber & Putterman (1991); Didenko *et al.* (2000); Suslick & Flannigan (2008)). It is even possible to observe light emission in the ultraviolet regime which hints at temperatures of about 10^6 K, as was shown by Camara *et al.* (2004). Noteworthy is the discovery of sharp emission lines in the optical regime (cf. Brenner *et al.* (2002); Flannigan & Suslick (2007); Suslick & Flannigan (2008)), which indicate the population of highly excited energy eigenstates of noble gas and metal atoms that cannot be populated thermally but indicate the presence of a dense plasma.

Although sonoluminescence has been studied extensively, the origin of the sudden energy concentration during the final stage of the bubble collapse phase remains a mystery (cf. Putterman *et al.* (2001); Suslick & Flannigan (2008)). A valid theoretical model needs to include a mechanism for the formation of a plasma as well as a mechanism which can increase the temperature of the plasma even further by at least one order of magnitude. This mechanism needs to be able to operate in a solid state-like environment and on the very small length scale given by the radius of the bubble. The goal of chapter 6 is to identify cavity-mediated collective quantum effects on which such a heating mechanism might be based.

1. INTRODUCTION

Chapter 2

Theory of quantum harmonic oscillators

In this chapter we revisit the theory of harmonic oscillators. In Section 2.1, we begin by quantising a harmonic oscillator and present the description of its eigenstates, so-called number states, and energy levels in the second quantisation. Number states will be used to describe the states of vibrational states of the trapped particles and cavity radiation modes in the later chapters.

In Section 2.2, we present the theory for harmonic oscillators in the thermal state. Since the thermal state of a harmonic oscillator is a mixed state, it can be described by a canonical density operator. As we will see later, analytical treatment of the phonon coherence ζ of an atomic gas requires calculating thermal averages in the number state basis. Using the density operator, we calculate thermal averages of the number operator and the squared number operator, and relate them to the vibrational energy of the system.

2.1   Quantisation of a harmonic oscillator

Recall that a single one-dimensional oscillator of mass M in a harmonic trap of frequency ν can be described by the following Hamiltonian (cf. Loudon (1992)),

$$H = \frac{p^2}{2M} + \frac{1}{2}M\nu^2 x^2 \,, \tag{2.1}$$

where its momentum operator p and position operator x obey the usual commutator relation,

$$[x, p] = i\hbar \,. \tag{2.2}$$

If the exact form of the wave function of harmonic oscillator is not important, we can employ the second quantisation and introduce ladder operators,

$$
\begin{aligned}
b &= \sqrt{\frac{Mv}{2\hbar}} \left(x + \frac{i}{Mv} p \right) , \\
b^\dagger &= \sqrt{\frac{Mv}{2\hbar}} \left(x - \frac{i}{Mv} p \right) .
\end{aligned}
\tag{2.3}
$$

This means that operators b and $b^\dagger$ follow the bosonic relation,

$$
[b, b^\dagger] = 1 .
\tag{2.4}
$$

Using Eqs. (2.3), the Hamiltonian (2.1) is transformed to

$$
H = \hbar v \left(b^\dagger b + \frac{1}{2} \right) .
\tag{2.5}
$$

To solve the Schroedinger equation, consider an arbitrary eigenstate $|m\rangle$ with a corresponding eigenvalue E_m. The Schroedinger equation then reads,

$$
H|m\rangle = \hbar v \left(b^\dagger b + \frac{1}{2} \right) |m\rangle = E_m |m\rangle .
\tag{2.6}
$$

Multiplying both sides from the left by $b^\dagger$ yields

$$
\hbar v \left(b^\dagger b^\dagger b + \frac{1}{2} b^\dagger \right) |m\rangle = E_m b^\dagger |m\rangle
\tag{2.7}
$$

$$
\hbar v \left(b^\dagger b b^\dagger - \frac{1}{2} b^\dagger \right) |m\rangle = E_m b^\dagger |m\rangle
\tag{2.8}
$$

$$
\hbar v \left(b^\dagger b + \frac{1}{2} \right) b^\dagger |m\rangle = (E_m + \hbar v) \, b^\dagger |m\rangle .
\tag{2.9}
$$

The last equation is also a form of an energy eigenvalue equation with the eigenstate

$$
|m + 1\rangle = b^\dagger |m\rangle
\tag{2.10}
$$

and the eigenvalue $E_{m+1} = E_m + \hbar v$. This shows that for a given energy level E_m, there exists another level higher than the first by the amount $\hbar v$. The energy levels form an equally-spaced ladder without an upper limit, as illustrated in Fig. 2.1. Applying the so-called *creation* operator $b^\dagger$ shifts the energy level upwards.

Similarly, applying the *destruction* operator b shifts the energy level downwards,

$$
H \, b|m\rangle = (E_m - \hbar v) \, b|m\rangle ,
\tag{2.11}
$$
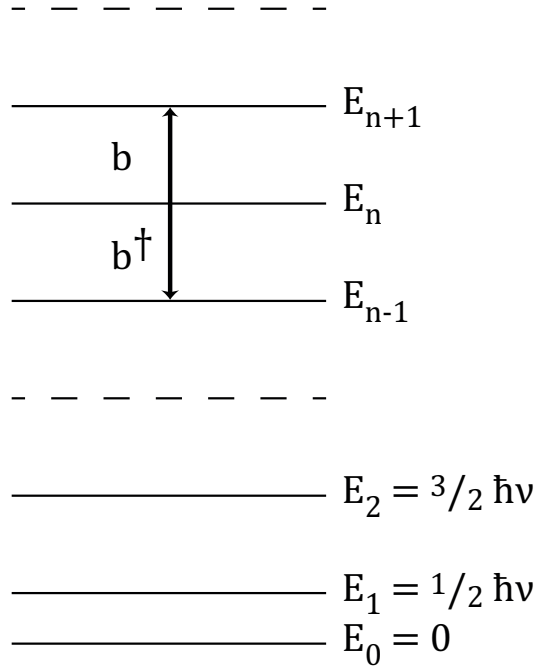
Figure 2.1: Energy-level diagram for the quantum-mechanical harmonic oscillator. Applying the creation operators $b^\dagger$ and the destruction operators b results in adding and subtracting an amount $\hbar v$, respectively.

to the state

$$|m - 1\rangle = b|m\rangle \tag{2.12}$$

with the eigenvalue $E_{m-1} = E_m - \hbar v$. There is, however, a lower bound, because kinetic and potential energies are positive quantities and the eigenvalues are not allowed to become negative. We can denote the lowest state, or the *ground* state, as $|0\rangle$ and assume that the only consistent solution to $H b|0\rangle = (E_m - \hbar v)b|0\rangle$ is

$$b|0\rangle = 0 \,, \tag{2.13}$$

since there are no lower eigenstates then the ground state. In this case, the Schroedinger equation reads,

$$\hbar v \left(b^\dagger b + \frac{1}{2} \right) |0\rangle = \frac{1}{2}\hbar v|0\rangle = E_0|0\rangle \,, \tag{2.14}$$

which shows that the energy of the ground state $|0\rangle$ is $E_0 = \frac{1}{2}\hbar v$. Therefore the full spectrum of energies follows,

$$E_m = \hbar v \left(m + \frac{1}{2} \right) \,, \tag{2.15}$$

where m is zero or a positive integer. The quantum number m therefore denotes the energy level of the harmonic oscillator or, in other words, the number of energy quanta that it possesses. Throughout the remainder of the thesis, we will refer to the energy quanta as *phonons*, if the harmonic oscillator is used to describe the vibrational energy of a particle, or as *photons*, if the harmonic oscillator is used to describe the energy of an electromagnetic field mode.

Fig. 2.1 shows the role of the ladder operators b and $b^\dagger$ in shifting the energy of the system by the amount of $\hbar v$. The eigenstates of the Hamiltonian (2.5) are simultaneous eigenstates to the *number operator* $b^\dagger b$ and it is evident from the Eqs. (2.5) and (2.15) that they satisfy

$$b^\dagger b |m\rangle = m|m\rangle\,. \tag{2.16}$$

The states $|m\rangle$ are called *number* states or *Fock* states. It is preferrable to normalise the eigenstates so that

$$\langle m|m\rangle = 1\,. \tag{2.17}$$

When the states are normalised, the relations between them need to be modified. We can generalise Eq. (2.12) to

$$b|m\rangle = C|m-1\rangle\,, \tag{2.18}$$

where C is an arbitrary constant. If we take the Hermitian conjugate of both sides, this implies that

$$\langle m|b^\dagger = \langle m-1|C\,. \tag{2.19}$$

Multipling Eqs. (2.18) and (2.19) shows that

$$\langle m|b^\dagger b|m\rangle = C^2\langle m-1|m-1\rangle\,,$$
$$m = C^2\,. \tag{2.20}$$

The phase of the normalisation constant is conventionally taken to be zero and Eq. (2.18) becomes

$$b|m\rangle = \sqrt{m}|m-1\rangle\,. \tag{2.21}$$

Similarly, we can show that

$$b^\dagger|m\rangle = \sqrt{m+1}|m+1\rangle\,. \tag{2.22}$$

Note that the ground state condition (2.13) is included as a special case in Eq. (2.21). Eqs. (2.21) and (2.22) are always more preferrable to use than Eqs. (2.10) and (2.12) because of the normalisation. The different energy eigenstates are orthogonal, so that the only non-vanishing matrix elements of operators b and $b^\dagger$ are those of the form

$$\langle m-1|b|m\rangle = \sqrt{m}\,,$$
$$\langle m+1|b^\dagger|m\rangle = \sqrt{m+1}\,. \tag{2.23}$$

Together with Eq. (2.17), this shows that the eigenstates obey the orthonormality condition

$$\langle m|n\rangle = \delta_{mn}\,, \tag{2.24}$$

where δ_{mn} is the Kronecker delta. From Eqs. (2.23), we can see immediately that operators b and $b^\dagger$ are not Hermitian, since every Hermitian operator A satisfies

$$\langle i|A|j\rangle = \langle j|A|i\rangle^*\,, \tag{2.25}$$

for arbitrary states $|i\rangle$ and $|j\rangle$. Therefore, the operators b and $b^\dagger$ cannot represent physically observable quantities. However, the convenience of the algebra of ladder operators and their representation of transfer between quantum energy levels is greatly appreciated in many areas of quantum mechanics.

2.2   Thermal properties of harmonic oscillators

When a harmonic oscillator is placed in a heat bath of constant temperature, its quantum state is no longer pure and therefore cannot be described by a single number state. Instead, the quantum harmonic oscillator will be in a *mixed* state, which is a statistical ensemble of pure states. Its exact energy will be unknown but would be a probabilistic mixture of energies of different states governed by the temperature of the surroundings. In this section, we derive expressions for thermal averages of different operators that will be used later in this thesis.

2.2.1   Average energy of the Hamiltonian

Consider a harmonic oscillator in a heat bath, where it cannot exchange energy with the neighbourhood so that it remains constant. Since the thermal mixed state of the harmonic oscillator cannot be represented by a single state, it is instead described by

its associated canonical density operator ρ, defined as (cf. Blaise & Henri-Rousseau (2011))

$$\rho = \frac{1}{Z} e^{-\beta H} , \qquad (2.26)$$

where Z is the partition function,

$$Z = \text{tr} \left(e^{-\beta H} \right) , \qquad (2.27)$$

β is the thermal Lagrange parameter related to temperature T as

$$\beta = \frac{1}{k_B T} , \qquad (2.28)$$

and H is the Hamiltonian of the harmonic oscillator.

The mean thermal average energy of a quantum harmonic oscillator is the average of the Hamiltonian over the canonical density operator,

$$\langle H \rangle = \text{tr} \left(\rho H \right) = \frac{1}{Z} \text{tr} \left(e^{-\beta H} H \right) = -\frac{1}{Z} \text{tr} \left(\frac{\partial e^{-\beta H}}{\partial \beta} \right) . \qquad (2.29)$$

The operations of trace and of partial differentiation commute and therefore,

$$\langle H \rangle = -\frac{1}{Z} \frac{\partial}{\partial \beta} \text{tr} \left(e^{-\beta H} \right) = -\frac{1}{Z} \frac{\partial Z}{\partial \beta} = -\frac{\partial \ln Z}{\partial \beta} . \qquad (2.30)$$

2.2.2 Canonical density operator

For a harmonic oscillator, the Hamiltonian is given by the Eq. (2.5),

$$H = \hbar \nu \left(b^\dagger b + \frac{1}{2} \right) , \qquad (2.31)$$

and Eqs. (2.26) and (2.27) become

$$\rho = \frac{1}{Z} \left(e^{-\beta \hbar \nu \left(b^\dagger b + \frac{1}{2} \right)} \right) , \qquad (2.32)$$

and

$$Z = e^{-\frac{1}{2}\beta \hbar \nu} \ \text{tr} \left(e^{-\beta \hbar \nu b^\dagger b} \right) , \qquad (2.33)$$

respectively. To perform the trace, it is convenient to use the basis of eigenstates of the number operator $b^\dagger b$, $|m\rangle$, described in the previous section, which have the orthonormality property (2.24),

$$\langle m | n \rangle = \delta_{mn} , \qquad (2.34)$$

This results in

$$Z = e^{-\frac{1}{2}\beta\hbar\nu} \sum_m \langle m | e^{-\beta\hbar\nu b^\dagger b} | m \rangle . \tag{2.35}$$

Expanding the exponential in the Taylor series and noting that

$$\left(b^\dagger b\right)^k |m\rangle = m^k |m\rangle \tag{2.36}$$

yields

$$Z = e^{-\frac{1}{2}\beta\hbar\nu} \sum_m \sum_{k=0}^{\infty} \langle m | \frac{(-\beta\hbar\nu b^\dagger b)^k}{k!} | m \rangle \tag{2.37}$$

$$= e^{-\frac{1}{2}\beta\hbar\nu} \sum_m \sum_{k=0}^{\infty} \langle m | \frac{(-\beta\hbar\nu m)^k}{k!} | m \rangle . \tag{2.38}$$

Now we can combine the Taylor series back into the exponential to obtain

$$Z = e^{-\frac{1}{2}\beta\hbar\nu} \sum_m \langle m | e^{-\beta\hbar\nu m} | m \rangle = e^{-\frac{1}{2}\beta\hbar\nu} \sum_m e^{-\beta\hbar\nu m} , \tag{2.39}$$

where we have used the orthonormality property of the eigenstates.

In case of strong trapping and relatively low temperatures, the inequality

$$\hbar\nu > k_B T \tag{2.40}$$

is satisfied, so that

$$e^{-\beta\hbar\nu} < 1 . \tag{2.41}$$

In this case, the geometric series in Eq. (2.39) converges, and the full expression becomes

$$Z = \frac{e^{-\frac{1}{2}\beta\hbar\nu}}{1 - e^{-\beta\hbar\nu}} = \frac{1}{2\sinh\left(\frac{1}{2}\beta\hbar\nu\right)} . \tag{2.42}$$

Moreover, the canonical density operator (2.26) can be written as

$$\rho = \left(1 - e^{-\beta\hbar\nu}\right) e^{-\beta\hbar\nu b^\dagger b} . \tag{2.43}$$

2.2.3 Thermal averages

Combining Eqs. (2.30) and (2.42) results in the expression for the thermal average energy of a harmonic oscillator,

$$\langle H \rangle = -\frac{\partial \ln Z}{\partial \beta} = \hbar\nu \left(\frac{1}{e^{\beta\hbar\nu-1}} + \frac{1}{2} \right) . \tag{2.44}$$

We can use this together with the Eq. (2.29) to find out the average of the number operator $b^\dagger b$. Recall that

$$
\begin{aligned}
\langle H \rangle = \mathrm{tr}\,(\rho H) &= \mathrm{tr}\left(\rho \hbar v \left(b^\dagger b + \frac{1}{2}\right)\right) \\
&= \hbar v \left(\mathrm{tr}\left(\rho b^\dagger b\right) + \frac{1}{2}\right) = \hbar v \left(\langle b^\dagger b \rangle + \frac{1}{2}\right).
\end{aligned}
\tag{2.45}
$$

Combining Eqs. (2.44) and (2.45) now yields an expression for the average of the number operator,

$$
\langle b^\dagger b \rangle = \frac{1}{e^{\beta \hbar v} - 1}.
\tag{2.46}
$$

Similarly to the Eq. (2.29), we can find out the thermal average of $\langle H^2 \rangle$,

$$
\langle H^2 \rangle = \frac{1}{Z}\,\mathrm{tr}\left(e^{-\beta H} H^2\right) = \frac{1}{Z}\,\mathrm{tr}\left(\frac{\partial^2 e^{-\beta H}}{\partial \beta^2}\right).
\tag{2.47}
$$

Again, we use the fact that the trace operation commutes with the differentiation operation and rewrite this as

$$
\langle H^2 \rangle = \frac{1}{Z}\frac{\partial^2}{\partial \beta^2}\,\mathrm{tr}\left(e^{-\beta H}\right) = \frac{1}{Z}\frac{\partial^2 Z}{\partial \beta^2}.
\tag{2.48}
$$

Now, observe that, using the product rule, we can show that

$$
\frac{\partial}{\partial \beta}\left(\frac{1}{Z}\frac{\partial Z}{\partial \beta}\right) = \left(\frac{\partial}{\partial \beta}\frac{1}{Z}\right)\frac{\partial Z}{\partial \beta} + \frac{1}{Z}\frac{\partial^2 Z}{\partial \beta^2} = -\frac{1}{Z^2}\left(\frac{\partial Z}{\partial \beta}\right)^2 + \frac{1}{Z}\frac{\partial^2 Z}{\partial \beta^2},
\tag{2.49}
$$

which leads to

$$
\frac{1}{Z}\frac{\partial^2 Z}{\partial \beta^2} = \frac{\partial}{\partial \beta}\left(\frac{1}{Z}\frac{\partial Z}{\partial \beta}\right) + \frac{1}{Z^2}\left(\frac{\partial Z}{\partial \beta}\right)^2.
\tag{2.50}
$$

Combining this with Eq. (2.48), and using Eq. (2.30), yields

$$
\langle H^2 \rangle = \frac{\partial}{\partial \beta}\left(\frac{1}{Z}\frac{\partial Z}{\partial \beta}\right) + \frac{1}{Z^2}\left(\frac{\partial Z}{\partial \beta}\right)^2 = -\frac{\partial \langle H \rangle}{\partial \beta} + \langle H \rangle^2.
\tag{2.51}
$$

For a harmonic oscillator, this can be rewritten as

$$
\left\langle \left(b^\dagger b + \frac{1}{2}\right)^2 \right\rangle = -\frac{1}{\hbar v}\left(\frac{\partial}{\partial \beta}\langle b^\dagger b + \frac{1}{2}\rangle\right) + \langle b^\dagger b + \frac{1}{2}\rangle^2
\tag{2.52}
$$

or

$$
\left\langle \left(b^\dagger b\right)^2 \right\rangle = -\frac{1}{\hbar v}\frac{\partial \langle b^\dagger b \rangle}{\partial \beta} + \langle b^\dagger b \rangle^2.
\tag{2.53}
$$

Using the last expression together with Eq. (2.46) results in full expression for the thermal average of the operator $\left(b^\dagger b\right)^2$,

$$\left\langle \left(b^\dagger b\right)^2 \right\rangle = -\frac{1}{\hbar \nu} \frac{\partial}{\partial \beta} \left(\frac{1}{e^{\beta \hbar \nu} - 1} \right) + \left(\frac{1}{e^{\beta \hbar \nu} - 1} \right)^2 = \frac{e^{\beta \hbar \nu} + 1}{\left(e^{\beta \hbar \nu} - 1 \right)^2}. \qquad (2.54)$$

The derivation of the thermal averages $\langle b^\dagger b \rangle$ and $\left\langle \left(b^\dagger b\right)^2 \right\rangle$ is the main result of this section. As we will see later, analytical treatment of the thermalisation process of an atomic gas requires calculating thermal averages in the number state basis. Using Eqs. (2.46) and (2.54), we can relate the thermal averages to the temperature of the system and therefore to its vibrational energy.

2.3   Conclusions

In this chapter, we outlined the theory of a harmonic oscillator in the second quatisation. The eigenstates of the system are represented by number states $|m\rangle$ and the energy transfer between the states is represented by ladder operators b and $b^\dagger$. Using this formalism, the treatment of a harmonic oscillator becomes relatively simple and straight-forward. The harmonic oscillator is used to describe the vibrational energy levels of trapped particles, in which case they are referred to as phonons, and the energy levels of a radiation mode, in which case they are referred to as photons. We will use these descriptions heavily when treating trapped atomic systems in both cavity-mediated cooling and sonoluminescence.

In addition to the theory of harmonic oscillator eigenstates, we looked at the mixed states which arise when a harmonic oscillator is placed in a thermal equilibrium. By considering the canonical density operator, we derived the expressions for thermal averages of the number operator $b^\dagger b$ and the squared number operator $\left(b^\dagger b\right)^2$. These will later be used to treat the atomic gas under thermalisation and to derive its phonon coherence ζ.

18

Chapter 3

Quantum theory of light-matter interactions

The theory of cavity-mediated laser cooling is based on the Jaynes-Cummings model, which describes the system of a two-level atom interacting with a standing wave radiation mode. In a nutshell, it consists of quantised radiation mode, quantised energy of a two-level atom and the interaction between the two. In this chapter, we show how each of these terms is obtained and put together under the Jaynes-Cummings model. We develop the quantised models for a free radiation field, starting from the Maxwell equations, and for a two-level atom. We obtain expressions for operators that can be used to completely describe our system and examine some of their properties. The atom-light interaction is modelled as the dipole interaction and represents the coupling between the atomic excited states and the ladder states of the quantised radiation field mode. The Hamiltonian of the atomic-radiation system is expressed completely in terms of quantum mechanical operators.

This chapter consists of three sections. In the first section, we show that free radiation can be expressed as a collection of harmonic oscillators, each representing a mode. The second section describes quantisation of a two-level atom in terms of projection operators. Lastly, in the third section we select a single radiation mode and model its interaction with the atom in the dipole approximation.

3.1 Electromagnetic field theory

3.1.1 Maxwell equations

Quantisation of the radiation field is based on the canonical transition from classical theory, where we replace field modes by corresponding quantum mechanical operators. In order to do that, we first rewrite the classical equations in a form appropriate for the conversion. We start with the treatment of the microscopic Maxwell equations for electric field $\mathbf{E}$ and magnetic field $\mathbf{B}$,

$$\nabla \times \mathbf{E} = -\frac{\partial \mathbf{B}}{\partial t}\,,$$

$$\frac{1}{\mu_0}\nabla \times \mathbf{B} = \varepsilon_0 \frac{\partial \mathbf{E}}{\partial t} + \mathbf{J}\,,$$

$$\varepsilon_0 \nabla \cdot \mathbf{E} = \sigma\,,$$

$$\nabla \cdot \mathbf{B} = 0\,, \tag{3.1}$$

with σ and $\mathbf{J}$ are the charge and current densities, respectively. These equations can be reformulated in terms of a vector potential $\mathbf{A}$ and a scalar potential φ, which are defined as

$$\mathbf{E} = -\nabla \varphi - \frac{\partial \mathbf{A}}{\partial t}\,, \tag{3.2}$$

$$\mathbf{B} = \nabla \times \mathbf{A}\,. \tag{3.3}$$

Eqs. (3.1) become

$$\nabla\left(\nabla \cdot \mathbf{A}\right) - \nabla^2 \mathbf{A} + \frac{1}{c^2}\frac{\partial}{\partial t}\nabla \varphi + \frac{1}{c^2}\frac{\partial^2 \mathbf{A}}{\partial t^2} = \mu_0 \mathbf{J}\,, \tag{3.4}$$

$$-\varepsilon_0 \left(\nabla^2 \varphi + \nabla \cdot \frac{\partial \mathbf{A}}{\partial t}\right) = \sigma\,. \tag{3.5}$$

Equations (3.4) and (3.5) are called the field equations.

The field equations are quite complicated due to the mixtures of terms involving $\mathbf{A}$ and φ. However, physical fields obtained from Eqs. (3.2) and (3.3) are the same for pairs $\{\mathbf{A}, \varphi\}$ and $\{\mathbf{A}', \varphi'\}$ that are related by the gauge transformation

$$\mathbf{A} = \mathbf{A}' - \nabla \Xi\,, \tag{3.6}$$

$$\varphi = \varphi' + \frac{\partial \Xi}{\partial t}\,, \tag{3.7}$$

where the gauge function Ξ is an arbitrary function of position $\mathbf{r}$ and time t. We can therefore impose conditions on $\mathbf{A}$ and φ that can be realised by a gauge transformation from an arbitrary pair of $\mathbf{A}$ and φ, therefore specifying a gauge for the electromagnetic field.

Gauge that is commonly used in electrodynamics is the so-called *Coulomb gauge*,

$$\nabla \cdot \mathbf{A} = 0 \,. \tag{3.8}$$

This simplifies the field equations (3.9) and (3.10) to

$$-\nabla^2 \mathbf{A} + \frac{1}{c^2} \frac{\partial}{\partial t} \nabla \varphi + \frac{1}{c^2} \frac{\partial^2 \mathbf{A}}{\partial t^2} = \mu_0 \mathbf{J} \,, \tag{3.9}$$

$$-\nabla^2 \varphi = \frac{\sigma}{\varepsilon_0} \,. \tag{3.10}$$

These are further simplified by employing Helmholtz' theorem (cf. Arfken *et al.* (2012)), according to which any vector field can be rewritten as a sum of its transverse component with zero divergence and longitudinal component with zero curl. This yields

$$\mathbf{E} = \mathbf{E}_{\mathrm{T}} + \mathbf{E}_{\mathrm{L}} \,, \tag{3.11}$$

$$\mathbf{J} = \mathbf{J}_{\mathrm{T}} + \mathbf{J}_{\mathrm{L}} \,. \tag{3.12}$$

Using these and the condition of the Coulomb gauge (3.8), we arrive at (cf. Loudon (1992))

$$-\nabla^2 \mathbf{A} + \frac{1}{c^2} \frac{\partial^2 \mathbf{A}}{\partial t^2} = \mu_0 \mathbf{J}_{\mathrm{T}} \,, \tag{3.13}$$

$$\frac{1}{c^2} \frac{\partial}{\partial t} \nabla \varphi = \mu_0 \mathbf{J}_{\mathrm{L}} \,, \tag{3.14}$$

as well as

$$\mathbf{E}_{\mathrm{T}} = -\frac{\partial \mathbf{A}}{\partial t} \,, \tag{3.15}$$

$$\mathbf{E}_{\mathrm{L}} = -\nabla \varphi \,. \tag{3.16}$$

We see that, in general, transverse variables are associated with the vector potential $\mathbf{A}$ while longitudinal variables are associated with the scalar potential φ. The Maxwell equations can be written as

$$\nabla \times \mathbf{E}_{\mathrm{T}} = -\frac{\partial \mathbf{B}}{\partial t} \,, \tag{3.17}$$

$$\frac{1}{\mu_0} \nabla \times \mathbf{B} = \varepsilon_0 \frac{\partial \mathbf{E}}{\partial t} + \mathbf{J}_{\mathrm{T}} \,, \tag{3.18}$$

$$\nabla \cdot \mathbf{E}_{\mathrm{T}} = 0 \,, \tag{3.19}$$

$$\nabla \cdot \mathbf{B} = 0 \,. \tag{3.20}$$

These transverse equations describe electromagnetic waves. In addition to this, we have

$$\nabla \cdot \mathbf{E}_{\mathrm{L}} = \frac{\sigma}{\varepsilon_0}\,, \tag{3.21}$$

$$\mathbf{J}_{\mathrm{L}} = -\varepsilon_0 \frac{\partial \mathbf{E}_{\mathrm{L}}}{\partial t}\,. \tag{3.22}$$

These longitudinal equations describe electric fields that arise from charge densities.

3.1.2   Field modes

Consider now radiation field in a region of free space,

$$\mathbf{J}_{\mathrm{T}} = 0\,. \tag{3.23}$$

We regard this region as a cube of side L and consider running wave solutions, also known as modes, with periodic boundary conditions. The vector potential is expanded as a sum of contributions from different modes,

$$\mathbf{A}(\mathbf{r}, t) = \sum_{\mathbf{k}\lambda} \mathbf{e}_{\mathbf{k}\lambda} A_{\mathbf{k}\lambda}(t)(\mathbf{r}, t)\,, \tag{3.24}$$

where the modal components are taken as

$$A_{\mathbf{k}\lambda}(t)(\mathbf{r}, t) = A_{\mathbf{k}\lambda}(t)e^{i\mathbf{k}\cdot\mathbf{r}} + A_{\mathbf{k}\lambda}^{*}(t)e^{-i\mathbf{k}\cdot\mathbf{r}}\,. \tag{3.25}$$

The wavevector $\mathbf{k}$ carries two modes, $\lambda = 1$ and $\lambda = 2$, and its components take values

$$k_{\mu} = \frac{2\pi n_{\mu}}{L}\,, \tag{3.26}$$

where μ denotes dimension, $\mu \in \{x, y, z\}$, and n_{μ} are zeros or integers. The $\mathbf{e}_{\mathbf{k}\lambda}$ are unit polarisation vectors and under the Coulomb gauge they satisfy

$$\mathbf{e}_{\mathbf{k}\lambda} \cdot \mathbf{k} = 0\,, \tag{3.27}$$

$$\mathbf{e}_{\mathbf{k}1} \cdot \mathbf{e}_{\mathbf{k}2} = \delta_{\lambda,\lambda'}\,, \tag{3.28}$$

where $\delta_{\lambda,\lambda'}$ is the Kronecker delta.

The modal components $A_{\mathbf{k}\lambda}(\mathbf{r}, t)$ of the vector potential are independent and for each of them, Eq. (3.13) leads to a harmonic equation of motion

$$\ddot{A}_{\mathbf{k}\lambda}(t) + \omega_k^2 A_{\mathbf{k}\lambda}(t) = 0\,, \tag{3.29}$$

where we defined the mode angular frequency $\omega_k = ck$. To calculate the field energy, we notice that the solution to Eq. (3.29) takes the form of (cf. Loudon (1992))

$$A_{k\lambda}(t) = A_{k\lambda} e^{-i\omega_k t} \tag{3.30}$$

and the full modal component to the vector potential in Eq. (3.25) becomes

$$A_{k\lambda}(t)(\mathbf{r}, t) = A_{k\lambda} e^{-i\omega_k t + i\mathbf{k}\cdot\mathbf{r}} + A_{k\lambda}^* e^{i\omega_k t - i\mathbf{k}\cdot\mathbf{r}}. \tag{3.31}$$

If we insert this into Eq. (3.24), we obtain the full expression for the vector potential $\mathbf{A}(\mathbf{r}, t)$. This allows us to calculated the tranverse electric field in Eq. (3.15),

$$\mathbf{E}_{\mathrm{T}}(\mathbf{r}, t) = \sum_{k\lambda} \mathbf{e}_{k\lambda} E_{k\lambda}(t)(\mathbf{r}, t) \tag{3.32}$$

with

$$E_{k\lambda}(t)(\mathbf{r}, t) = i\omega_k \left(A_{k\lambda}(t) e^{-i\omega_k t + i\mathbf{k}\cdot\mathbf{r}} - A_{k\lambda}^*(t) e^{i\omega_k t - i\mathbf{k}\cdot\mathbf{r}} \right), \tag{3.33}$$

and the magnetic field in Eq. (3.3),

$$\mathbf{B}(\mathbf{r}, t) = \sum_{k\lambda} \frac{1}{k} \mathbf{k} \times \mathbf{e}_{k\lambda} B_{k\lambda}(t)(\mathbf{r}, t) \tag{3.34}$$

with

$$B_{k\lambda}(t)(\mathbf{r}, t) = ik \left(A_{k\lambda}(t) e^{-i\omega_k t + i\mathbf{k}\cdot\mathbf{r}} - A_{k\lambda}^*(t) e^{i\omega_k t - i\mathbf{k}\cdot\mathbf{r}} \right). \tag{3.35}$$

The total energy of the radiation field is given by

$$\mathcal{E}_{\mathrm{R}} = \frac{1}{2} \int_{\mathrm{cavity}} dV \left(\varepsilon_0 E_{\mathrm{T}}(\mathbf{r}, t) \cdot E_{\mathrm{T}}(\mathbf{r}, t) + \frac{1}{\mu_0} B(\mathbf{r}, t) \cdot B(\mathbf{r}, t) \right), \tag{3.36}$$

which is calculated to be (cf. Loudon (1992))

$$\mathcal{E}_{\mathrm{R}} = \sum_{k\lambda} \mathcal{E}_{k\lambda} \tag{3.37}$$

with

$$\mathcal{E}_{k\lambda} = \varepsilon_0 V \omega_k^2 \left(A_{k\lambda} A_{k\lambda}^* + A_{k\lambda}^* A_{k\lambda} \right). \tag{3.38}$$

3.2 Canonical quantisation

We see that the Eq. (3.38) for the energy of radiation field mode is very similar to the expression for the energy of a quantum harmonic oscillator,

$$H_{k\lambda} = \frac{1}{2}\hbar\omega_k \left(c_{k\lambda}c_{k\lambda}^\dagger + c_{k\lambda}^\dagger c_{k\lambda} \right) , \tag{3.39}$$

where $c_{k\lambda}$ and $c_{k\lambda}^\dagger$ are annihilation and creation operators for the mode $k\lambda$, respectively. We now carry out canonical transition, where we replace classical vector potential amplitudes with quantum mechanical operators,

$$A_{k\lambda} \rightarrow \sqrt{\frac{\hbar}{2\varepsilon_0 V\omega_k}}\, c_{k\lambda} , \tag{3.40}$$

$$A_{k\lambda}^* \rightarrow \sqrt{\frac{\hbar}{2\varepsilon_0 V\omega_k}}\, c_{k\lambda}^\dagger . \tag{3.41}$$

With these subtitutions, the classical vector potential now becomes an *operator*,

$$\mathbf{A}(\mathbf{r}, t) = \sum_{k\lambda} \mathbf{e}_{k\lambda} A_{k\lambda}(t)(\mathbf{r}, t) \tag{3.42}$$

with

$$A_{k\lambda}(t)(\mathbf{r}, t) = \sqrt{\frac{\hbar}{2\varepsilon_0 V\omega_k}} \left(c_{k\lambda}e^{-i\omega_k t + i\mathbf{k}\cdot\mathbf{r}} + c_{k\lambda}^\dagger e^{i\omega_k t - i\mathbf{k}\cdot\mathbf{r}} \right) , \tag{3.43}$$

which leads to the full expressions for the electric and the magnetic field operators,

$$\mathbf{E}_T(\mathbf{r}, t) = i\sum_{k\lambda} \mathbf{e}_{k\lambda}\sqrt{\frac{\hbar\omega_k}{2\varepsilon_0 V}} \left(c_{k\lambda}e^{-i\omega_k t + i\mathbf{k}\cdot\mathbf{r}} - c_{k\lambda}^\dagger e^{i\omega_k t - i\mathbf{k}\cdot\mathbf{r}} \right) , \tag{3.44}$$

$$\mathbf{B}(\mathbf{r}, t) = i\sum_{k\lambda} \mathbf{k} \times \mathbf{e}_{k\lambda}\sqrt{\frac{\hbar}{2\varepsilon_0 V\omega_k}} \left(c_{k\lambda}e^{-i\omega_k t + i\mathbf{k}\cdot\mathbf{r}} - c_{k\lambda}^\dagger e^{i\omega_k t - i\mathbf{k}\cdot\mathbf{r}} \right) . \tag{3.45}$$

Calculating now the energy of the radiation field using these quantum mechanical operators yields

$$H = \frac{1}{2}\int_{\text{cavity}} dV \left(\varepsilon_0 E_T(\mathbf{r}, t) \cdot E_T(\mathbf{r}, t) + \frac{1}{\mu_0}B(\mathbf{r}, t) \cdot B(\mathbf{r}, t) \right) \tag{3.46}$$

$$= \sum_{k\lambda} \hbar\omega_k \left(c_{k\lambda}^\dagger c_{k\lambda} + \frac{1}{2} \right) , \tag{3.47}$$

which is analogous to a collection of quantum harmonic oscillators. Each of these harmonic oscillators represents a different light mode, and their energies follow an equally spaced ladder, described in the previous chapter. The energy of a light mode harmonic oscillator is referred to in terms of the energy level that it occupies, or the number of *photons*.

3.3   Quantisation of atomic Hamiltonian

Similarly to a radiation field, we can quantise the electronic energy of an atom. Let $|i\rangle$ be an energy eigenstate with eigenvalue $\hbar\omega_i$, which leads to

$$H|i\rangle = \hbar\omega_i|i\rangle . \tag{3.48}$$

We can use the closure theorem

$$\sum_i |i\rangle\langle i| = 1 \tag{3.49}$$

and the orthonormality of the eigenstates to show that

$$\langle i|H|j\rangle = \hbar\omega_i\delta_{ij} , \tag{3.50}$$

where δ_{ij} is the Kronecker delta. The Hamiltonian in Eq. (3.48) is reduced to

$$H = \sum_i \hbar\omega_i|i\rangle\langle i| . \tag{3.51}$$

Suppose now that operator $|i\rangle\langle j|$ is applied to an arbitrary state $|k\rangle$. The orthonormality of the eigenstates leads to

$$|i\rangle\langle j|k\rangle = |i\rangle\delta_{jk} . \tag{3.52}$$

Operator $|i\rangle\langle j|$ therefore acts as a *projection* operator, which turns state $|j\rangle$ into state $|i\rangle$ and anything else into zero. For a two-level atom with levels $|0\rangle$ and $|1\rangle$, and energy difference $\hbar\omega_0$ between them, we can introduce operators

$$\sigma^+ = |1\rangle\langle 0| \quad \text{and} \quad \sigma^- = |1\rangle\langle 0| . \tag{3.53}$$

We see that σ^+ shifts the atom from its ground state to its excited state and σ^- does the reverse, with

$$\sigma^+|0\rangle = |1\rangle \quad \text{and} \quad \sigma^-|1\rangle = |0\rangle \tag{3.54}$$

and

$$\sigma^+|1\rangle = 0 \quad \text{and} \quad \sigma^-|0\rangle = 0 . \tag{3.55}$$

Other properties of the projection operators can be obtained from definitions, leading to

$$\sigma^-\sigma^+ = |0\rangle\langle 1|1\rangle\langle 0| = |0\rangle\langle 0| \tag{3.56}$$

and similarly

$$\sigma^+ \sigma^- = |1\rangle\langle 0|0\rangle\langle 1| = |1\rangle\langle 1| \,. \tag{3.57}$$

These operators represent probabilities of finding an atom in its ground and excited state, respectively. The closure theorem also implies that

$$\sigma^+ \sigma^- + \sigma^- \sigma^+ = 1 \,, \tag{3.58}$$

and the Hamiltonian in Eq. (3.51) takes the form

$$H = \hbar \omega_0 \sigma^+ \sigma^- \,. \tag{3.59}$$

3.4 Atom-field interaction and the Jaynes-Cummings model

In general, a free atom interacts with an infinite number of radiation modes. However, an optical cavity allows us to isolate only single mode for interaction with the atom. We consider a single mode in one dimension. In the Schroedinger picture, Eq. (3.44) loses its time dependence and becomes

$$E(x) = i\sqrt{\frac{\hbar \omega_k}{2\varepsilon_0 V}} \left(c e^{ikx} - c^\dagger e^{-ikx} \right) \,. \tag{3.60}$$

Since we are free to choose the phase of the field, we shift it by $\frac{\pi}{2}$ to obtain a simpler expression,

$$\begin{aligned} E(x) &= i\sqrt{\frac{\hbar \omega_k}{2\varepsilon_0 V}} \left(c e^{i\left(kx-\frac{\pi}{2}\right)} - c^\dagger e^{-i\left(kx-\frac{\pi}{2}\right)} \right) \\ &= \sqrt{\frac{\hbar \omega_k}{2\varepsilon_0 V}} \left(c e^{ikx} + c^\dagger e^{-ikx} \right) \,. \end{aligned} \tag{3.61}$$

Under the dipole approximation (cf. Gerry & Knight (2004)), the spatial variation of the field over the dimensions of the atom is considered negligible,

$$\frac{\lambda}{2\pi} = \frac{1}{k} \gg x_{\text{atom}} \tag{3.62}$$

where x_{atom} is a characteristic length scale of the atom. Under this condition,

$$e^{\pm ikx} \approx 1 \pm ikx \tag{3.63}$$

and the exponential in the Eq. (3.61) can be replaced by unity, yielding

$$E(x) = \sqrt{\frac{\hbar \omega_k}{2\varepsilon_0 V}} \left(c + c^\dagger \right) \,. \tag{3.64}$$

In an optical cavity, the electric field forms a standing wave, and its expression in Eq. (3.64) is modified to

$$E(x) = \sqrt{\frac{\hbar\omega_k}{2\varepsilon_0 V}}\left(c + c^\dagger\right)\sin(kx)\,, \tag{3.65}$$

with the energy given by Eq. (3.46) as

$$H = \hbar\omega c^\dagger c\,, \tag{3.66}$$

where we dropped the zero-point energy constant.

In the Coulomb gauge, the dipole atom-field interaction is represented by

$$H = \mathbf{D} \cdot \mathbf{E} = \sqrt{\frac{\hbar\omega_k}{2\varepsilon_0 V}}\,D\sin(kx)(c + c^\dagger)\,, \tag{3.67}$$

where D is the projection of the atomic dipole moment $\mathbf{D}$ in the direction of the cavity,

$$D = \mathbf{D} \cdot \hat{\mathbf{x}}\,, \tag{3.68}$$

with $\hat{\mathbf{x}}$ being the unit vector of the cavity axis. For a two-level atom, D can be written in terms of atomic operators Eq. (3.53), as

$$\begin{aligned} D &= |0\rangle\langle 0|D|1\rangle\langle 1| + |1\rangle\langle 1|D|0\rangle\langle 0|\,, \\ &= D_0|0\rangle\langle 1| + D_0|1\rangle\langle 0| = D_0\left(\sigma^- + \sigma^+\right)\,, \end{aligned} \tag{3.69}$$

where $D_0 = \langle 0|D|1\rangle = \langle 1|D|0\rangle$ is a constant. The interaction Hamiltonian (3.67) therefore becomes

$$H = \hbar G\left(\sigma^+ + \sigma^-\right)\left(c + c^\dagger\right)\,, \tag{3.70}$$

with

$$G = \sqrt{\frac{\omega_k}{2\hbar\varepsilon_0 V}}D_0\sin(kx)\,. \tag{3.71}$$

Furthermore, under the rotating wave approximation, non-energy conserving terms $\sigma^+ c^\dagger$ and $\sigma^- c$ are dropped, leading to Eq. (3.70) taking the form

$$H = \hbar G\left(\sigma^+ c + \sigma^- c^\dagger\right)\,. \tag{3.72}$$

Putting this interaction term together with the energy of the radiation mode (3.66) and the electronic energy of the interacting atom (3.59) yields the infamous Jaynes-Cummings model

$$H = \hbar\omega c^\dagger c + \hbar\omega_0\sigma^+\sigma^- + \hbar G\left(\sigma^+ c + \sigma^- c^\dagger\right)\,. \tag{3.73}$$

3.5   Conclusions

The Jaynes-Cummings model describes the interaction between a two-level atom and a single radiation mode. It was therefore chosen as a starting point for our treatment of a trapped atomic system in both cavity-mediated cooling and sonoluminescence. In this chapter, we described the theory behind each term in the Jaynes-Cummings model. We started with canonical quantisation of the free radiation field and showed how it can be represented by a bath of harmonic oscillators. Similarly, the electronic state of a two-level atom was quantised using the raising and lowering operators. Finally, the interaction term between the two-level atom and the radiation mode was developed. In later chapters, the Jaynes-Cummings model will be used as a core and modified according to the system being examined.

Chapter 4

Cooling of a single particle

The main purpose of this chapter is to introduce the methodology for treatment of cavity-mediated laser cooling and prepare the reader for the material that follows, where we study the process of cooling of a many-body system. Cooling of a single particle is well studied and effectively executed using the laser sideband technique (cf. Stenholm (1986)). However, it falls short when it comes to cooling particles with a complex level structure or cooling multiple particles simultaneously.

Cavity-mediated laser cooling has been proposed as an alternative technique and multiple indications of its effectiveness were later found (cf. Black *et al.* (2003); Chuah *et al.* (2013); Gibbons *et al.* (2008); Kampschulte *et al.* (2010); Maunz *et al.* (2004); McKeever *et al.* (2003); Nußmann *et al.* (2005); Vigneron (1995); Wolke *et al.* (2012)). In this and the next chapter, we show how use of an optical cavity can aid the problem of cooling multiple particles. The current chapter is dedicated to outlining the methodology for treating the cooling process and applying the model to a single atom.

In general, cooling is achieved by coupling atomic and motional degrees of freedom. Since the atom is trapped, it can be spatially localized to dimensions much smaller than an optical wavelength. This is referred to as *Lamb-Dicke limit*. Internal dynamics of a two-level atom can be appropriately described by the Jaynes-Cummings model. As the atom is strongly coupled to the cavity, the external laser facilitates the transition

$$|m, n\rangle \rightarrow |m - 1, n + 1\rangle \tag{4.1}$$

or

$$|m, n\rangle \rightarrow |m + 1, n + 1\rangle, \tag{4.2}$$
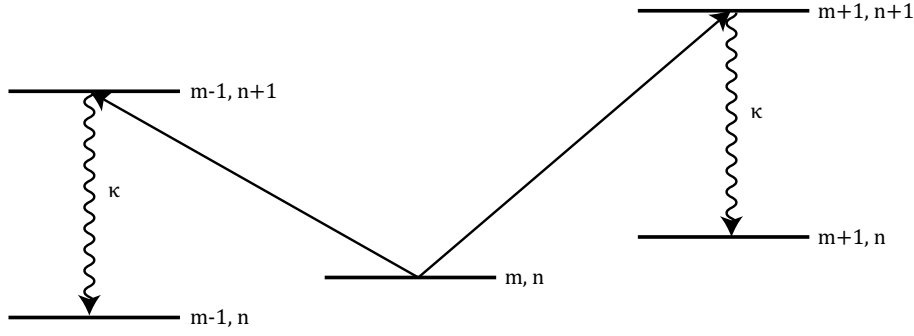
Figure 4.1: Diagrammatic representation of the cooling scheme. Here a generic state is denotes by $|m, n\rangle$, where m is the number of phonons and n is the number of cavity photons. During cooling, the atom is detuned in such way that its phonon is converted into a cavity photon (shown as middle-to-left process). On the other hand, under heating detunings, an extra phonon is created (shown as middle-to-right process). The cavity returns to its original state through the cavity decay κ.

depending on the detuning of the laser, as shown in Fig. 4.1. This is in contrast with the free space laser cooling, where the atom is excited instead of cavity. The cavity mode then relaxes into its original state via the decay channel,

$$|m \pm 1, n + 1\rangle \rightarrow |m \pm 1, n\rangle . \tag{4.3}$$

If the cooling laser is properly detuned to cooling resonances, then the atom will undergo the downward transition along the ladder of the vibrational energy states $|m\rangle$.

In our setup, we deal with a one-dimensional system, where the atom is confined in the direction of the cavity axis, as indicated in Fig. 4.2. Since we are in the Lamb-Dicke limit, we can localise the atom in different positions along the standing wave, and, for maximal effect, we choose the node of the standing wave. The atom is driven from the side by an external laser resonant to the electronic transition.

By applying the master equation to this setup, we can identify the parameter regimes that facilitate cooling of the confined atom. Moreover, we will show that there exists a triplet of resonances that are particularly beneficial for cooling, one of which includes the infamous red sideband from the free space laser sideband cooling. The other two have not been reported before and therefore constitute a new result. The three resonances are separated by the laser Rabi frequency and therefore
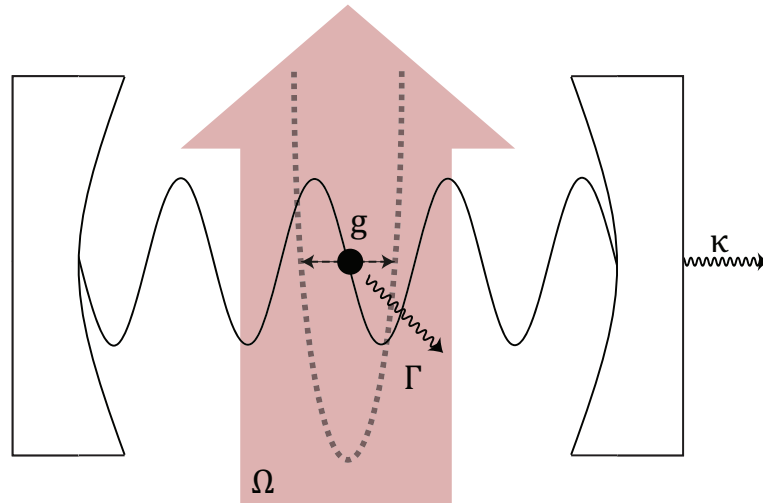
Figure 4.2: Schematic view of the experimental setup, consisting of a resonantly driven atom which is externally confined in the node of an optical resonator.

resemble the Mollow triplet. The results of this chapter were published in Kim & Beige (2013).

This chapter is structured as follows. In Section 4.1, we introduce the Hamiltonian for our system, which will be used in the master equation later on. In Section 4.2, we go into the interaction picture with respect to free energy, to show the emergence of the cooling resonances which will consitute the main result of this chapter. In Sections 4.3 and 4.4, we use the master equation to derive and study a set of differential equations, so-called rate equations, which describe the dynamics of our system. These equations again yield the cooling resonances, properties of which are very dependent on experimental parameters, such as trap frequency, cavity-laser detuning and so on. These dependencies are investigated in Section 4.5. Finally, conclusions are drawn in Section 4.6.

4.1   The Hamiltonian

The system that we are going to examine is shown in Fig. 4.2. It consists of vibrational energy of the trapped atomic particle H_{vib}, its free electronic energy H_{el}, the free energy of the cavity radiation field H_{cav}, interaction of the atom with the cavity field H_{int} and interaction of the atom with the driving laser H_{L}. Our model is developed as an extension to the Jaynes-Cummings model outlined in chapter 3, to which we

add the vibrational energy of the atom and its interaction with the driving laser.

When an atom of mass M is confined in a harmonic trap of frequency v, its motion is described by a harmonic oscillator,

$$H_{\text{vib}} = \frac{p^2}{2M} + \frac{1}{2}Mv^2x^2 \,, \tag{4.4}$$

where p and x are momentum and position of the atom, respectively, along the cavity axis. This energy can be quantised with discrete energy levels or phonons, as was shown in chapter 2, and the change of the phonon number is modelled by creation and annhilation operators b and $b^\dagger$,

$$b = \sqrt{\frac{Mv}{2\hbar}} \left(x + \frac{\text{i}}{Mv}p \right) \,,$$
$$b^\dagger = \sqrt{\frac{Mv}{2\hbar}} \left(x - \frac{\text{i}}{Mv}p \right) \,, \tag{4.5}$$

with the standard bosonic commutator relations,

$$[b, b^\dagger] = 1 \,. \tag{4.6}$$

The energy of the harmonic oscillator, and hence of the trapped atom, is given (up to a constant) by

$$H_{\text{vib}} = \hbar v \, b^\dagger b \,. \tag{4.7}$$

The cooling process therefore strives to minimize this vibrational energy by bringing the atom to the lowest possible state.

The Hamiltonian for the electronic energy of a two-level atom was described in Section 3.3. Given an atom with the ground state $|0\rangle$, the excited state $|1\rangle$ and the transition frequency ω_0, it has the form

$$H_{\text{el}} = \hbar\omega_0 \, \sigma^+\sigma^- \,, \tag{4.8}$$

where σ^+ and σ^- are electronic raising and lowering operators, respectively.

The cavity in our system is assumed to be populated only by a single mode of frequency ω, in which case its energy is given (up to a constant) by Eq. (3.66) as

$$H_{\text{cav}} = \hbar\omega \, c^\dagger c \,, \tag{4.9}$$

where $c^\dagger$ and c are creation and annihilation operators for this mode. These operators have the same commutator relations as the phonon operators,

$$[c, c^\dagger] = 1 \,. \tag{4.10}$$

The population of the mode will be referred to as cavity photons.

The atom-laser interaction is modelled semiclassically, where the quantised atom interacts with a classical electric field,

$$H_{\mathrm{L}} = D \cdot E_{\mathrm{L}} = \left(D_0 \sigma^- + D_0^* \sigma^- \right) \left(E_0 e^{-i\omega_{\mathrm{L}}t} + E_0^* e^{i\omega_{\mathrm{L}}t} \right), \tag{4.11}$$

where we used the result of Eq. (3.69). To maximize the effect, the laser is tuned in resonance to the electronic transition of the atom, so that

$$\omega_{\mathrm{L}} = \omega_0. \tag{4.12}$$

Lastly, the most important term of the Hamiltonian is the atom-cavity interaction H_{int}. This term is the origin of the cooling dynamics and, as we shall see, describes the coupling between phonon and photons of the system via atomic excitations. Recall from the Jaynes-Cummings model (cf. Section 3.4) that the strength of the interaction G in Eq. (3.71) is, in general, dependent on the position of the atom,

$$G = G(r) = g \sin\left(kr \right). \tag{4.13}$$

Overall, the absolute position of the atom r can be written as

$$r = R + x, \tag{4.14}$$

where R is the absolute position of the trap centre and x is the position operator, which represents the atomic deviation from the trap centre. We can fix the trap centre at the node of the cavity field, which allows us to write

$$G = G(x) = g \sin\left(kx \right). \tag{4.15}$$

Since the atom in our model is confined along the cavity radiation mode, we will have to take the position of the atom into account. In the strong confinement regime, oscillations of the atom about the centre of the trapping potential will be small, so that we can keep only the first term of the Taylor expansion of $G(x)$,

$$G(x) \approx gkx. \tag{4.16}$$

We can now express the atomic position operator in terms of atomic phonon operators b and $b^\dagger$ (cf. Eq. 4.5), arriving at the atom-phonon-photon interaction

$$H_{\mathrm{int}} = \eta\, g \left(b + b^\dagger \right) \left(c\sigma^+ + c^\dagger \sigma^- \right), \tag{4.17}$$

which represents the coupling between the vibrational motion of the atom, its electronic excitation and the light mode of the cavity. Here

$$\eta = \sqrt{\frac{\hbar k^2}{2Mv}} \tag{4.18}$$

is the so-called Lamb-Dicke parameter which signifies strength of the trapping potential. In the strong trapping regime, we have $\eta \ll 1$. As we shall see later, the term (4.17) is the essential source of cooling in our theoretical model.

Combining all terms together, we have the full Hamiltonian,

$$\begin{aligned}
H \;=\;& \hbar\omega_0\,\sigma^+\sigma^- + \hbar v\,b^\dagger b + \hbar\omega\,c^\dagger c \\
&+\left(D_0\sigma^- + D_0^*\sigma^+\right)\left(E_0 e^{-i\omega_0 t} + E_0^* e^{i\omega_0 t}\right) \\
&+\eta\,g\left(b + b^\dagger\right)c\sigma^+ + \text{H.c.}
\end{aligned} \tag{4.19}$$

Since our Hamiltonian is time-dependent, the standard procedure is to look at the system in a frame rotating with the driving laser frequency, in our case ω_0. Going into the interaction picture with respect to

$$H_0 \;=\; \hbar\omega_0(\sigma^+\sigma^- + c^\dagger c)\,, \tag{4.20}$$

we obtain the interaction Hamiltonian

$$\begin{aligned}
H_\text{I} \;=\;& \hbar v\,b^\dagger b + \hbar\delta\,c^\dagger c + \frac{1}{2}\hbar\Omega\left(\sigma^- + \sigma^+\right) \\
&+\hbar\eta g\left(b + b^\dagger\right)(\sigma^+ c + \sigma^- c^\dagger)\,.
\end{aligned} \tag{4.21}$$

Here we have applied the rotating wave approximation to the atom-laser interaction term. Terms rotating at frequencies of $2\omega_0$ oscillate very rapidly compared with the remaining terms and therefore can be dropped. We also introduced the cavity-laser frequency detuning,

$$\delta = \omega - \omega_0\,, \tag{4.22}$$

and the Rabi frequency

$$\Omega = \frac{2D_0^* E_0}{\hbar}\,, \tag{4.23}$$

which is associated with the strength of the semiclassical atom-laser interaction.

4.2 Second interaction picture

Before we proceed with the master equation approach, we can gain some insight by going into yet another interaction picture with respect to free energies. First, we diagonalise the laser driving operator

$$\Sigma_2 = \sigma^- + \sigma^+ , \tag{4.24}$$

where we find its eigenstates to be

$$|\lambda_\pm\rangle = \frac{1}{\sqrt{2}} \big(|0\rangle \pm |1\rangle\big) , \tag{4.25}$$

with the corresponding eigenvalues

$$\lambda_\pm = \pm 1 . \tag{4.26}$$

Using this notation, electronic transition operators can be written as

$$\sigma^\pm = \frac{1}{2} \big(|\lambda_+\rangle\langle\lambda_+| - |\lambda_-\rangle\langle\lambda_-| \pm |\lambda_+\rangle\langle\lambda_-| \mp |\lambda_-\rangle\langle\lambda_+| \big) . \tag{4.27}$$

Consequently, the Hamiltonian H_I in Eq. (4.21) can be written as

$$
\begin{aligned}
H_I &= \hbar v\, b^\dagger b + \hbar\delta\, c^\dagger c + \frac{1}{2}\hbar\Omega \big(|\lambda_+\rangle\langle\lambda_+| - |\lambda_-\rangle\langle\lambda_-|\big) \\
&\quad + \frac{1}{2}\hbar\eta g\, (b + b^\dagger)(c + c^\dagger)\big(|\lambda_+\rangle\langle\lambda_+| - |\lambda_-\rangle\langle\lambda_-| \big) , \\
&\quad + \frac{1}{2}\hbar\eta g\, (b + b^\dagger)(c - c^\dagger)\big(|\lambda_+\rangle\langle\lambda_-| - \text{H.c.} \big) .
\end{aligned}
\tag{4.28}
$$

Going into the interaction picture with respect to

$$\tilde{H}_0 = \hbar v\, b^\dagger b + \hbar\delta\, c^\dagger c + \frac{1}{2}\hbar\Omega \big(|\lambda_+\rangle\langle\lambda_+| - |\lambda_-\rangle\langle\lambda_-|\big) , \tag{4.29}$$

yields

$$
\begin{aligned}
\tilde{H}_I &= \frac{1}{2}\hbar\eta g\, \big[e^{-i(\delta+v)t}\, bc + e^{-i(\delta-v)t}\, bc^\dagger + \text{H.c.} \big] \\
&\qquad \times \big(|\lambda_+\rangle\langle\lambda_+| - |\lambda_-\rangle\langle\lambda_-| \big) \\
&\quad + \frac{1}{2}\hbar\eta g\, \big[e^{-i(\delta+v)t}\, bc - e^{-i(\delta-v)t}\, bc^\dagger - \text{H.c.} \big] \\
&\qquad \times \big(e^{i\Omega t}\, |\lambda_+\rangle\langle\lambda_-| - \text{H.c.} \big) .
\end{aligned}
\tag{4.30}
$$

We can therefore identify six resonances for four different operators, $bc^\dagger$, $b^\dagger c$, $b^\dagger c^\dagger$ and bc. Operators $bc^\dagger$ and $b^\dagger c$ are Hermitian conjugates and represent reverse operations of tranferring between states $|m+1, n\rangle$ and $|m, n+1\rangle$, where m and n represent
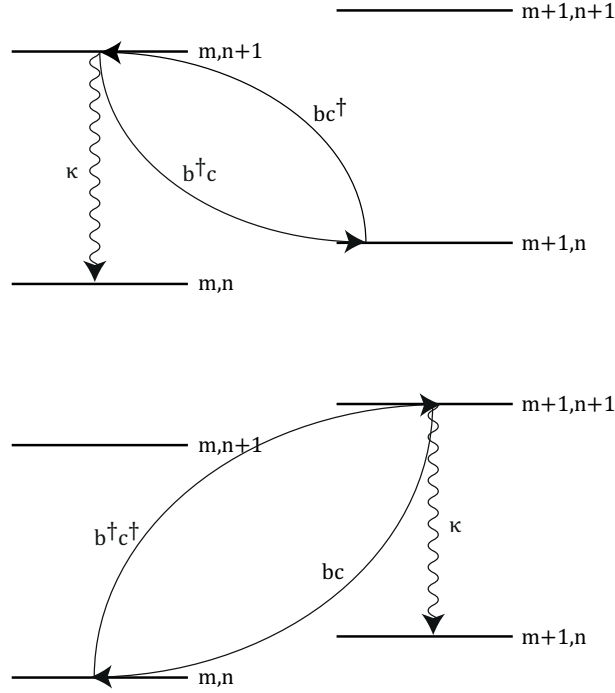
Figure 4.3: Role of operators $bc^\dagger$ and $b^\dagger c$ as cooling and heating operators. The Hermitian conjugates of these operators represent the process of annihilation of a cavity photon which competes with the cavity decay κ. The operators $bc^\dagger$ and $b^\dagger c$ therefore dominate over their respective Hermitian conjugates.

the number of phonons and the number of cavity photons, respectively. However, in addition to the operator $b^\dagger c$, a cavity photon can also disappear through the cavity decay channel κ, as indicated in Fig. 4.3 (top). This means that operator $bc^\dagger$ dominates over operator $b^\dagger c$ and, since it involves transitioning down the ladder of phonon states, we treat it as a cooling operator. Similarly, operator $b^\dagger c^\dagger$ dominates over operator bc and is treated as a heating operator, as shown in Fig. 4.3 (bottom).

Expanding Eq. (4.30), we obtain

$$
\begin{aligned}
\tilde{H}_\mathrm{I} &= \frac{1}{2}\hbar\eta g \left(e^{-\mathrm{i}(\delta-\nu)t}\, bc^\dagger + e^{\mathrm{i}(\delta+\nu)t}\, b^\dagger c^\dagger + \dots \right)\left(|\lambda_+\rangle\langle\lambda_+| - |\lambda_-\rangle\langle\lambda_-| \right) \\
&+ \frac{1}{2}\hbar\eta g \left(e^{-\mathrm{i}(\delta-\nu)t}e^{-\mathrm{i}\Omega t}\, |\lambda_-\rangle\langle\lambda_+|bc^\dagger - e^{-\mathrm{i}(\delta-\nu)t}e^{\mathrm{i}\Omega t}\, |\lambda_+\rangle\langle\lambda_-|bc^\dagger \right. \\
&\left. + e^{\mathrm{i}(\delta+\nu)t}e^{\mathrm{i}\Omega t}\, |\lambda_+\rangle\langle\lambda_-|b^\dagger c^\dagger - e^{\mathrm{i}(\delta+\nu)t}e^{-\mathrm{i}\Omega t}\, |\lambda_-\rangle\langle\lambda_+|b^\dagger c^\dagger + \dots \right). \quad (4.31)
\end{aligned}
$$

The coefficients of $bc^\dagger$ include

$$
e^{-\mathrm{i}(\delta-\nu)t} \quad \text{and} \quad e^{-\mathrm{i}(\delta-\nu\pm\Omega)t}, \qquad (4.32)
$$

while the coefficients of $b^\dagger c^\dagger$ include

$$e^{i(\delta+\nu)t} \quad \text{and} \quad e^{i(\delta+\nu\pm\Omega)t}. \tag{4.33}$$

The resonant condition occurs when the exponents vanish. This means that detunings

$$\delta_0 \equiv \nu \qquad\qquad \delta_\pm \equiv \nu \pm \Omega \tag{4.34}$$

comprise the cooling resonances for the cooling operator $bc^\dagger$ and detunings

$$\mu_0 \equiv -\nu \qquad\qquad \mu_\pm \equiv -\nu \pm \Omega \tag{4.35}$$

comprise the heating resonances for the heating operator $b^\dagger c^\dagger$. In the later chapters, we will see how these resonances emerge from the rate equations and their role in cavity-mediated cooling.

4.3   Master equation

The main difference between free-space sideband cooling and cavity-mediated laser cooling is that, in cavity-mediated laser cooling, the vibrational energy of the system is dissipated into free space via the light mode of the cavity, instead of the atomic excitation. This makes the spontaneous atomic decay rate Γ far less crucial in the cavity-mediated cooling. Instead, the cooling efficiency depends strongly on the spontaneous cavity decay rate κ in addition to the spontaneous atomic decay rate Γ. To model this, the quantum optical master equation reads (cf. Cirac *et al.* (1993))

$$\begin{aligned}
\dot{\rho} &= -\frac{i}{\hbar}[H_I, \rho] + \frac{1}{2}\kappa \left(2c\rho c^\dagger - c^\dagger c\rho - \rho c^\dagger c\right) \\
&\quad + \frac{1}{2}\Gamma \left(2\sigma^-\rho\sigma^+ - \sigma^+\sigma^-\rho - \rho\sigma^+\sigma^-\right).
\end{aligned} \tag{4.36}$$

The results of the previous section tell us what to expect as long as the spontaneous decay rates κ and Γ remain relatively small. To learn more about the cooling process and to study the effect of relatively large spontaneous decay rates, we employ the master equation to show that the time evolution of the expectation value of an arbitrary operator A is given by

$$\begin{aligned}
\langle \dot{A} \rangle &= -\frac{i}{\hbar}\langle [A, H_I] \rangle + \frac{1}{2}\kappa \left\langle 2c^\dagger A c - A c^\dagger c - c^\dagger c A \right\rangle \\
&\quad + \frac{1}{2}\Gamma \left\langle 2\sigma^+ A \sigma^- - A\sigma^+\sigma^- - \sigma^+\sigma^- A \right\rangle.
\end{aligned} \tag{4.37}$$

This expression will be used to derive a closed set of rate equations that govern the time evolution of the average vibrational energy of the system, or the mean phonon number

$$m \equiv \langle b^\dagger b \rangle. \tag{4.38}$$

The average vibrational energy of the system is the measure of the temperature of the atomic system.

4.4 The relevant expectation values

In order to obtain a closed set of cooling equations, we need to consider the expectation values of certain mixed operators X_{ijk} of the form

$$X_{ijk} \equiv B_i \Sigma_j C_k \tag{4.39}$$

with the B, Σ, and C operators defined as

$$
\begin{aligned}
(B_0, \Sigma_0, C_0) &\equiv (1, 1, 1), \\
(B_1, \Sigma_1, C_1) &\equiv (b^\dagger b, \sigma^+ \sigma^-, c^\dagger c), \\
(B_2, \Sigma_2, C_2) &\equiv (b + b^\dagger, \sigma^- + \sigma^+, c + c^\dagger), \\
(B_3, \Sigma_3, C_3) &\equiv i(b - b^\dagger, \sigma^- - \sigma^+, c - c^\dagger), \\
(B_4, C_4) &\equiv (b^2 + b^{\dagger 2}, c^2 + c^{\dagger 2}), \\
(B_5, C_5) &\equiv i(b^2 - b^{\dagger 2}, c^2 - c^{\dagger 2}).
\end{aligned} \tag{4.40}
$$

Using these operators, the Hamiltonian H_I in Eq. (4.21) becomes

$$H_I = \hbar v\, B_1 + \hbar \delta\, C_1 + \frac{1}{2} \hbar \Omega\, \Sigma_2 + \frac{1}{2} \hbar \eta g\, B_2 (\Sigma_2 C_2 + \Sigma_3 C_3). \tag{4.41}$$

In the following, we use this representation of the Hamiltonian, since the X operators obey relatively simple commutator relations. In particular, using commutator

relations for phonon, photon and electronic operators, one can show that

$$
\begin{aligned}
\left[\Sigma_1, \Sigma_2\right] &= i\Sigma_3 \,, \\
\left[\Sigma_1, \Sigma_3\right] &= -i\Sigma_2 \,, \\
\left[\Sigma_2, \Sigma_3\right] &= 2i\left(2\Sigma_1 - 1\right) \,, \\
\left[B_1, B_2\right] &= iB_3 \,, \\
\left[B_1, B_3\right] &= -iB_2 \,, \\
\left[B_2, B_3\right] &= -2i \,, \\
\left[C_1, C_2\right] &= iC_3 \,, \\
\left[C_1, C_3\right] &= -iC_2 \,, \\
\left[C_2, C_3\right] &= -2i \,.
\end{aligned}
\tag{4.42}
$$

Moreover, we denote expectation values of the X operators by

$$
x_{ijk} \quad \equiv \quad \langle X_{ijk} \rangle \,.
\tag{4.43}
$$

Since all the operators X_{ijk} are Hermitian, the variables x_{ijk} are all real. To distinguish terms in different orders in η more easily, we adopt the notation

$$
x_{ijk} \quad \equiv \quad x_{ijk}^{(0)} + x_{ijk}^{(1)} + \dots
\tag{4.44}
$$

while the mean phonon number m is written as

$$
m \quad \equiv \quad m^{(0)} + m^{(1)} + \dots
\tag{4.45}
$$

and so on. The superscripts indicate the scaling of the contribution of the respective variable in η.

4.4.1   Time evolution in zeroth order in η

First we have a look at the $\eta = 0$ case. This means, we assume that there is no coupling between phonon, photon, and electronic states. In the absence of cavity pumping, the cavity will remain in its vacuum state, with

$$
\langle C_k \rangle^{(0)} = 0
\tag{4.46}
$$

for all k. Analogously, or by using Eqs. (4.37) and (4.41), one can show that

$$
\dot{m}^{(0)} \quad = \quad 0 \,.
\tag{4.47}
$$

This tells us that there is no cooling in zeroth order in η. Moreover we find that

$$
\begin{aligned}
\langle \dot{B}_2 \rangle^{(0)} &= -v \langle B_3 \rangle^{(0)}, \\
\langle \dot{B}_3 \rangle^{(0)} &= v \langle B_2 \rangle^{(0)}, \\
\langle \dot{B}_4 \rangle^{(0)} &= -2v \langle B_5 \rangle^{(0)}, \\
\langle \dot{B}_5 \rangle^{(0)} &= 2v \langle B_4 \rangle^{(0)}.
\end{aligned}
\tag{4.48}
$$

When solving these rate equations, we find that the phonon coherences $\langle B_2 \rangle^{(0)}$ to $\langle B_5 \rangle^{(0)}$ oscillate around zero on time scales given by the phonon frequency v. When analysing the cavity-mediated cooling process on a much longer time scale, the above phonon coherences can be adiabatically eliminated from the system dynamics. Setting their time derivatives in Eq. (4.48) equal to zero yields

$$
\langle B_i \rangle^{(0)} \equiv 0, \qquad i = 2, \dots, 5.
\tag{4.49}
$$

Notice that we only use this equation to analyse the cooling dynamics of our system. In this case, Eq. (4.49) is well justified, since the effective cooling rate γ_c of the experimental setup, which we will consider here, scales as η^2.

Similarly, denoting

$$
s_j \equiv \langle \Sigma_j \rangle^{(0)}
\tag{4.50}
$$

for expectation values of the electronic states of the trapped particle, one can show that

$$
\begin{aligned}
\dot{s}_1 &= \frac{1}{2}\Omega s_3 - \Gamma s_1, \\
\dot{s}_2 &= -\frac{1}{2}\Gamma s_2, \\
\dot{s}_3 &= \Omega (1 - 2s_1) - \frac{1}{2}\Gamma s_3
\end{aligned}
\tag{4.51}
$$

in zeroth order in η. These expectation values reach a stationary state relatively quickly. When analysing processes on the time scale given by the cooling rate γ_c, these too can be adiabatically eliminated and approximated by their stationary state solutions,

$$
\begin{aligned}
s_1 &= \frac{\Omega^2}{\Gamma^2 + 2\Omega^2}, \\
s_2 &= 0, \\
s_3 &= \frac{2\Gamma\Omega}{\Gamma^2 + 2\Omega^2}.
\end{aligned}
\tag{4.52}
$$

Before using these results to derive an effective cooling equation for the mean phonon number m, we notice that

$$x_{ijk}^{(0)} = \langle B_i \rangle^{(0)} \langle \Sigma_j \rangle^{(0)} \langle C_k \rangle^{(0)} \tag{4.53}$$

when $\eta = 0$, since all three subsystems evolve independently in this case.

4.4.2 Time evolution in first order in η

Let us now have a closer look at the differential equations which describe the time evolution of m and the x_{ijk} variables in first order in η. Using Eqs. (4.37) and (4.41) we find that

$$\dot{m}^{(1)} = \frac{1}{2}\eta g \left(x_{322}^{(0)} + x_{333}^{(0)} \right) . \tag{4.54}$$

Unfortunately, Eq. (4.53) implies $x_{322}^{(0)} = x_{333}^{(0)} = 0$ which yields

$$\dot{m}^{(1)} = 0 . \tag{4.55}$$

As in other laser cooling schemes of atomic particles, the mean phonon number m changes only on the very slow time scale given by η^2. As we shall see below, we obtain a non-zero time derivative of m, when we calculate x_{322} and x_{333} up to first order in η. Therefore, we now have a closer look at these expectation values.

Taking the results in Eqs. (4.46), (4.49), (4.52), and (4.53) into account, one can show that

$$\dot{x}_{202}^{(1)} = -v\,x_{302}^{(1)} - \delta\,x_{203}^{(1)} - \eta g \left(1 + 2m^{(0)}\right) s_3 - \frac{1}{2}\gamma_0\,x_{202}^{(1)} ,$$

$$\dot{x}_{203}^{(1)} = -v\,x_{303}^{(1)} + \delta\,x_{202}^{(1)} + \eta g \left(1 + 2m^{(0)}\right) s_2 - \frac{1}{2}\gamma_0\,x_{203}^{(1)}$$

$$\dot{x}_{302}^{(1)} = v\,x_{202}^{(1)} - \delta\,x_{303}^{(1)} + \eta g\,s_2 - \frac{1}{2}\gamma_0\,x_{302}^{(1)}$$

$$\dot{x}_{303}^{(1)} = v\,x_{203}^{(1)} + \delta\,x_{302}^{(1)} + \eta g\,s_3 - \frac{1}{2}\gamma_0\,x_{303}^{(1)} , \tag{4.56}$$

and

$$\dot{x}_{212}^{(1)} = -v\,x_{312}^{(1)} - \delta\,x_{213}^{(1)} + \frac{1}{2}\Omega\,x_{232}^{(1)} - \frac{1}{2}\gamma_2\,x_{212}^{(1)} ,$$

$$\dot{x}_{213}^{(1)} = -v\,x_{313}^{(1)} + \delta\,x_{212}^{(1)} + \frac{1}{2}\Omega\,x_{233}^{(1)} - \frac{1}{2}\gamma_2\,x_{213}^{(1)} ,$$

$$\dot{x}_{312} = v\,x_{212}^{(1)} - \delta\,x_{313}^{(1)} + \frac{1}{2}\Omega\,x_{332}^{(1)} - \frac{1}{2}\gamma_2\,x_{312}^{(1)} ,$$

$$\dot{x}_{313}^{(1)} = v\,x_{213}^{(1)} + \delta\,x_{312}^{(1)} + \frac{1}{2}\Omega\,x_{333}^{(1)} - \frac{1}{2}\gamma_2\,x_{313}^{(1)} . \tag{4.57}$$

Moreover, one can show that

$$
\begin{aligned}
\dot{x}_{222}^{(1)} &= -\nu\, x_{322}^{(1)} - \delta\, x_{223}^{(1)} - \frac{1}{2}\gamma_1\, x_{222}^{(1)}\,, \\
\dot{x}_{223}^{(1)} &= -\nu\, x_{323}^{(1)} + \delta\, x_{222}^{(1)} + 2\eta g\left(1 + 2m^{(0)}\right) s_1 - \frac{1}{2}\gamma_1\, x_{223}^{(1)}\,, \\
\dot{x}_{322}^{(1)} &= \nu\, x_{222}^{(1)} - \delta\, x_{323}^{(1)} + 2\eta g\, s_1 - \frac{1}{2}\gamma_1\, x_{322}^{(1)}\,, \\
\dot{x}_{323}^{(1)} &= \nu\, x_{223}^{(1)} + \delta\, x_{322}^{(1)} - \frac{1}{2}\gamma_1\, x_{323}^{(1)}\,,
\end{aligned}
\tag{4.58}
$$

and

$$
\begin{aligned}
\dot{x}_{232}^{(1)} &= -\nu\, x_{332}^{(1)} - \delta\, x_{233}^{(1)} + \Omega\left(x_{202}^{(1)} - 2x_{212}^{(1)}\right) - 2\eta g\left(1 + 2m^{(0)}\right) s_1 - \frac{1}{2}\gamma_1\, x_{232}^{(1)}\,, \\
\dot{x}_{233}^{(1)} &= -\nu\, x_{333}^{(1)} + \delta\, x_{232}^{(1)} + \Omega\left(x_{203}^{(1)} - 2x_{213}^{(1)}\right) - \frac{1}{2}\gamma_1\, x_{233}^{(1)}\,, \\
\dot{x}_{332}^{(1)} &= \nu\, x_{232}^{(1)} - \delta\, x_{333}^{(1)} + \Omega\left(x_{302}^{(1)} - 2x_{312}^{(1)}\right) - \frac{1}{2}\gamma_1\, x_{332}^{(1)}\,, \\
\dot{x}_{333}^{(1)} &= \nu\, x_{233}^{(1)} + \delta\, x_{332}^{(1)} + \Omega\left(x_{303}^{(1)} - 2x_{313}^{(1)}\right) + 2\eta g\, s_1 - \frac{1}{2}\gamma_1\, x_{333}^{(1)}\,.
\end{aligned}
\tag{4.59}
$$

Here the effective spontaneous decay rates γ_n are defined as

$$
\gamma_n \equiv \kappa + n\,\Gamma\,.
\tag{4.60}
$$

Combined with the differential equation for the time evolution of the mean phonon number m, these equations constitute a closed set of rate equations in second order in η.

4.4.3 An effective cooling equation

The previous two subsections have shown that there is no time evolution of the mean phonon number m in zeroth and first order in η (cf. Eqs. (4.47) and (4.55)). Going an order higher in η and using again Eqs. (4.37) and (4.41) yields

$$
\dot{m}^{(2)} = \frac{1}{2}\eta g\left(x_{322}^{(1)} + x_{333}^{(1)}\right)\,.
\tag{4.61}
$$

We now assume that the atom-phonon-photon interaction constant ηg is either much smaller than the atom-cavity detuning δ, the cavity decay rate κ, or the phonon frequency ν,

$$
\eta g \ll \delta,\ \kappa,\ \text{or}\ \nu\,.
\tag{4.62}
$$

This condition guarantees that the mean phonon number m evolves on a much slower time scale than all other expectation values, which are involved in the cooling pro-

cess. This allows us to calculate the coherences $x_{ijk}^{(1)}$ in Eqs. (4.56)-(4.59) via an adiabatic elimination. Doing so and setting their derivatives equal to zero, we find that

$$
\begin{aligned}
\dot{m}^{(2)} &= \left(1 + m^{(0)}\right) \frac{2\eta^2 g^2 \Omega^2}{\Gamma^2 + 2\Omega^2} \left(\frac{\gamma_1}{\gamma_1^2 + \xi_+^2} \right. \\
&\quad \left. + \frac{\left(\gamma_0 \gamma_1 \gamma_2 + \gamma_{-1} \xi_+^2\right)\left(\gamma_2^2 + \xi_+^2\right) + 4\Omega^2 \left(\gamma_0 \gamma_2^2 + \gamma_4 \xi_+^2\right)}{\left(\gamma_0^2 + \xi_+^2\right)\left[\left(\gamma_1^2 + \xi_+^2\right)\left(\gamma_2^2 + \xi_+^2\right) + 8\Omega^2 \left(\gamma_1 \gamma_2 - \xi_+^2\right) + 16\Omega^4\right]} \right) \\
&\quad - m^{(0)} \frac{2\eta^2 g^2 \Omega^2}{\Gamma^2 + 2\Omega^2} \left(\frac{\gamma_1}{\gamma_1^2 + \xi_-^2} \right. \\
&\quad \left. + \frac{\left(\gamma_0 \gamma_1 \gamma_2 + \gamma_{-1} \xi_-^2\right)\left(\gamma_2^2 + \xi_-^2\right) + 4\Omega^2 \left(\gamma_0 \gamma_2^2 + \gamma_4 \xi_-^2\right)}{\left(\gamma_0^2 + \xi_-^2\right)\left[\left(\gamma_1^2 + \xi_-^2\right)\left(\gamma_2^2 + \xi_-^2\right) + 8\Omega^2 \left(\gamma_1 \gamma_2 - \xi_-^2\right) + 16\Omega^4\right]} \right)
\end{aligned}
\tag{4.63}
$$

with the parameter $\xi_{\pm}$ defined as

$$
\xi_{\pm} \equiv 2(\delta \pm v) \tag{4.64}
$$

and with the γ_n defined as in Eq. (4.60).

Setting the time derivative $\dot{m}^{(2)}$ in Eq. (4.63) equal to zero yields an analytical expression for the stationary state phonon number m_{ss} of the proposed cooling process in zeroth order in η. Unfortunately, this expression is relatively complex and looking at it does not yield much insight into the considered cavity-mediated laser cooling process. In the following, we therefore only notice that the time evolution of the mean phonon number m is to a very good approximation given by a differential equations of the form

$$
\dot{m} = -\gamma_{\mathrm{c}} m + c, \tag{4.65}
$$

where γ_{c} is an effective cooling rate and where c is a constant. Taking Eqs. (4.47) and (4.55) into account and comparing Eq. (4.65) with Eq. (4.63) confirms that both γ_{c} and c scale as η^2. The comparison also yields analytical expressions for $\gamma_{\mathrm{c}}^{(2)}$ and $c^{(2)}$. In the following, we discuss the dependence of $\gamma_{\mathrm{c}}^{(2)}$ and of the stationary state phonon number $m_{\mathrm{ss}}^{(0)}$,

$$
m_{\mathrm{ss}}^{(0)} = \frac{c^{(2)}}{\gamma_{\mathrm{c}}^{(2)}}, \tag{4.66}
$$

on the different experimental parameters of the atom-cavity system in Fig. 4.2.

4.4.4 Confirmation of the expected cooling and heating resonances

Before doing so, let us have a closer look at Eq. (4.63). Suppose that the laser driving is so weak that all the Ω^2 terms in Eq. (4.63) become negligible. In this case, we find

that

$$m_{\text{ss}}^{(0)} \quad = \quad \frac{\kappa^2 + 4(\delta - \nu)^2}{16\delta\nu} \,.$$ (4.67)

This stationary state phonon number is exactly the same as the stationary state phonon number for laser sideband cooling of a trapped particle in free space (cf. Blake *et al.* (2011b); Leibfried *et al.* (2003); Wineland & Dehmelt (1975)) but with Γ replaced by κ. For relatively small cavity decay rates κ, it assumes its minimum when $\delta = \delta_0$ with δ_0 defined as in Eq. (4.34). Looking only at the case of weak laser driving, one might indeed conclude that there is only a single cooling resonance and a very close analogy between laser sideband and cavity-mediated laser cooling. Instead, this work illustrates that atom-phonon-cavity systems can exhibit a much richer inner dynamics than systems with only atom-phonon interactions.

Another interesting parameter regime is the one where $\Omega, \xi_\pm \gg \kappa, \Gamma$. In this case, Eq. (4.63) simplifies to

$$\dot{m}^{(2)} \quad = \quad \eta^2 g^2 \left(\frac{\gamma_1}{\xi_+^2} + \frac{\gamma_{-1}\xi_+^2 + 4\gamma_4\Omega^2}{\xi_+^4 - 8\Omega^2\xi_+^2 + 16\Omega^4} \right) \left(1 + m^{(0)} \right)$$

$$-\eta^2 g^2 \left(\frac{\gamma_1}{\xi_-^2} + \frac{\gamma_{-1}\xi_-^2 + 4\gamma_4\Omega^2}{\xi_-^4 - 8\Omega^2\xi_-^2 + 16\Omega^4} \right) m^{(0)} \,.$$ (4.68)

The corresponding stationary state phonon number $m_{\text{ss}}^{(0)}$ equals zero when $\xi_-^2 = 4\Omega^2$, ie. when δ equals either δ_- or δ_+ in Eq. (4.34). This simple analysis confirms the presence of the two additional laser-Rabi frequency dependent cooling resonances $\delta_\pm$. However, notice that the above constraint $\xi_- \gg \kappa, \Gamma$ excludes the case where $\delta = \nu$. Hence this simple calculation returns only two of the three cooling resonances.

We now return to Eq. (4.63) and use it to calculate the stationary state phonon number $m_{\text{ss}}^{(0)}$ for the experimental setup in Fig. 4.2 for concrete experimental parameters. Fig. 4.4 shows $m_{\text{ss}}^{(0)}$ as a function of the atom-cavity detuning δ for a relatively wide range of parameters. To illustrate that the predictions in Section 4.2 apply, even for relatively large spontaneous decay rates, we choose κ and Γ to be of about the same order of magnitude as the phonon frequency ν and the atom-cavity detuning δ. For relatively large laser Rabi frequencies Ω, we indeed observe three distinct cooling resonances with sharp local minima of the stationary state phonon number m_{ss}. These are the atom-cavity detunings δ_0 and $\delta_\pm$ which we defined in Eq. (4.34). In contrast to this and in good agreement with the discussion in Section 4.2, the stationary state phonon number $m_{\text{ss}}^{(0)}$ increases significantly, when δ approaches one of

the three heating resonances μ_0 and $\mu_\pm$ in Eqs. (4.35). Only, when Ω becomes much smaller than ν, then the cooling resonances and the heating resonances, respectively, become all the same. In this case, cooling occurs only for $\delta = \nu$ and extreme heating occurs for $\delta = -\nu$.

4.5 A comparison of the three cooling resonances

The emergence of the three resonances, δ_0, δ_+ and δ_-, shows that cavity-mediated laser cooling could exhibit more complicated dynamics than free space sideband laser cooling. The δ_0 resonance is the widely used red sideband in the free space cooling and was often shown to be the most optimal resonance in terms of both the stationary state phonon number and the cooling rate. However, for a wide range of experimental parameters, such as the trapping frequency or the laser Rabi frequency, a lower stationary state phonon number can be reached when using the δ_+ resonance. In these cases, we believe that driving the system on the δ_+ resonance could be more beneficial if the lowest possible temperature is the goal of the study.

The difference between the δ_0 and the δ_+ resonance is due to the fact that the δ_0 resonance is accompanied by the electronic $|0\rangle \rightarrow |1\rangle$ or a $|1\rangle \rightarrow |0\rangle$ transition, while the δ_+ resonance is accompanied by the $|\lambda_+\rangle \rightarrow |\lambda_-\rangle$ transition. The creation of the $|\lambda_+\rangle$ states by the cooling laser is suspected to be more dominant for a range of parameters and therefore yields a lower stationary state phonon number. On the other hand, the $|\lambda_-\rangle$ states remain less populated, and the δ_- resonance always shows worse performance.

To find out how to best cool a trapped particle when using the experimental setup in Fig. 4.2, we now compare the stationary state phonon numbers $m_{ss}^{(0)}$ and the effective cooling rates $\gamma_c^{(2)}$ of the three cooling resonances δ_0 and $\delta_\pm$ with each other. When comparing the expressions for $\dot{m}^{(2)}$ in Eqs. (4.63) and (4.65), we find that $\gamma_c^{(2)}$ becomes independent of η and g when dividing it by $(\eta g)^2$. The following results therefore apply for any values of these two parameters, as long as they fulfill the condition which we specified in Eq. (4.62).

Dependence on the laser Rabi frequency

Fig. 4.5 shows the stationary state phonon number $m_{ss}^{(0)}$ and the cooling rate $\gamma_c^{(2)}$ as a function of the laser Rabi frequency Ω. As suggested by Eq. (4.63), we find that there is no effective cooling, when the laser Rabi frequency Ω becomes very small. In the
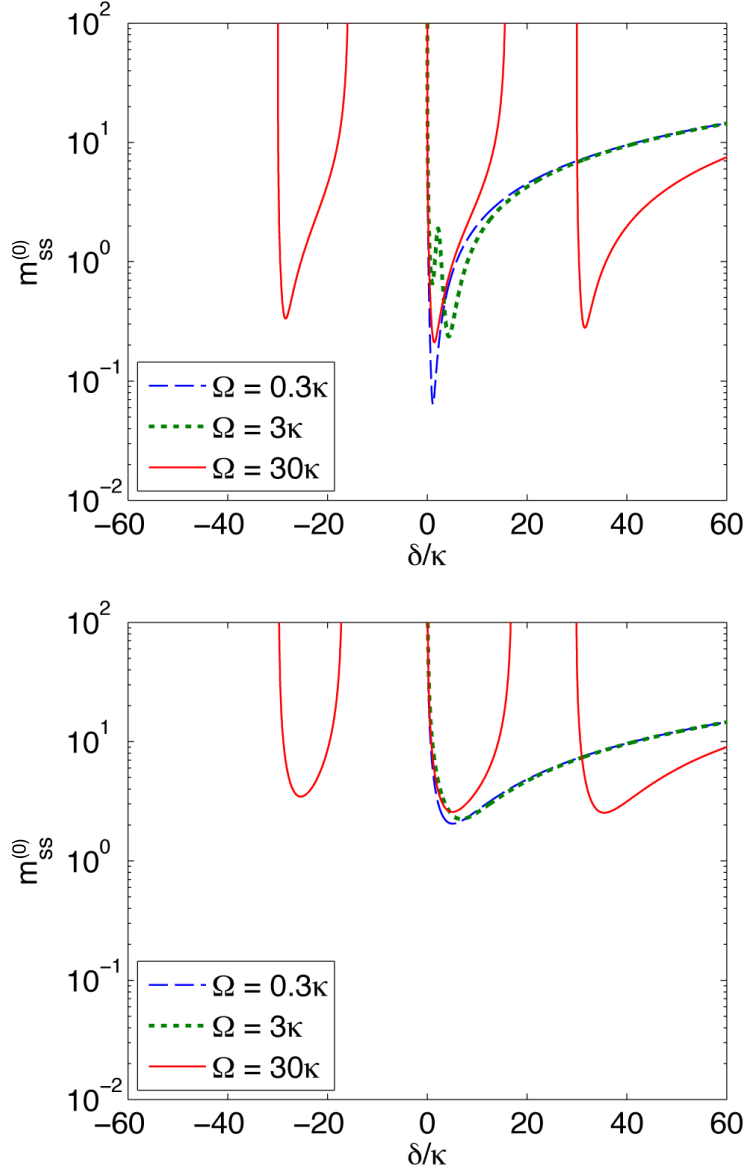
Figure 4.4: Logarithmic plot of the stationary state phonon number $m_{ss}^{(0)}$ as a function of the atom-cavity detuning δ for three different Rabi frequencies Ω and $\nu = \Gamma$, while $\kappa = \Gamma$ (upper figure) and $\kappa = 10\,\Gamma$ (lower figure). This figure has been obtained from Eq. (4.63) by setting $\dot{m}^{(2)}$ equal to zero and clearly illustrates the presence of the cooling and heating resonances which we identified in Eqs. (4.34) and (4.35).

limit $\Omega \to 0$, the cooling rate $\gamma_c^{(2)}$ tends for all three cooling resonances to zero. Although the stationary state phonon number $m_{ss}^{(0)}$ might be relatively small, this case is of no interest, since the stationary state is reached only after a very long time. When Ω increases, also the cooling rate $\gamma_c^{(2)}$ increases rapidly. Naively one might expect that increasing the laser Rabi frequency Ω further and further also increases the cooling rate further. However, this is not the case and, as shown in Fig. 4.5, the cooling process saturates relatively quickly and the stationary state phonon number remains more or less constant for very large Ω.

When comparing all three cooling resonances, we see that the atom-cavity detuning δ_- yields the highest values of $m_{ss}^{(0)}$ and is therefore of no practical interest. One reason for this can be found in Eqs. (4.34) and (4.35). For $\delta = \delta_-$, there is always a heating resonance relatively close by, which compensates some of the effects of the resonant cooling transition. Another reason for the relatively high values of $m_{ss}^{(0)}$ for $\delta = \delta_-$ is that the applied laser field creates a relatively large population in the state $|\lambda_+\rangle$ of the trapped particle, while the state $|\lambda_-\rangle$ remains less populated (cf. Eq. (4.52)). As one can see from Eq. (4.30), for $\delta = \delta_-$, the resonant annihilation of a phonon and the creation of a cavity photon is accompanied by an atomic transition from the state $|\lambda_-\rangle$ into $|\lambda_+\rangle$. When the average population in the state $|\lambda_-\rangle$ is relatively low, the atom is not well prepared to assist the cooling process when $\delta = \delta_-$.

In contrast to this, the system is in general well detuned from all heating transitions, when the atom-cavity detuning equals either δ_0 or δ_+. Moreover, for $\delta = \delta_+$ and for $\delta = \delta_0$, resonant cooling transitions are accompanied by a $|\lambda_+\rangle \to |\lambda_-\rangle$ and by a $|0\rangle \to |1\rangle$ or a $|1\rangle \to |0\rangle$ transition, respectively. Since the average population in the state $|\lambda_+\rangle$ and in the atomic states $|0\rangle$ and $|1\rangle$, respectively, is relatively large (cf. Eq. (4.52)), the laser driving prepares the trapped particle well to facilitate the annihilation of a phonon and to assist the cooling process when $\delta = \delta_+$ or $\delta = \delta_0$. Indeed, Fig. 4.5 shows that the atom-cavity detuning δ_+ yields the lowest stationary state photon number $m_{ss}^{(0)}$ for a relatively wide range of laser Rabi frequencies Ω. For the concrete parameters in Fig. 4.5, this applies when Ω lies roughly between 2 and 7 Γ. For larger values of Ω, we obtain the lowest stationary state phonon number when choosing $\delta = \delta_0$ (sideband cooling case).
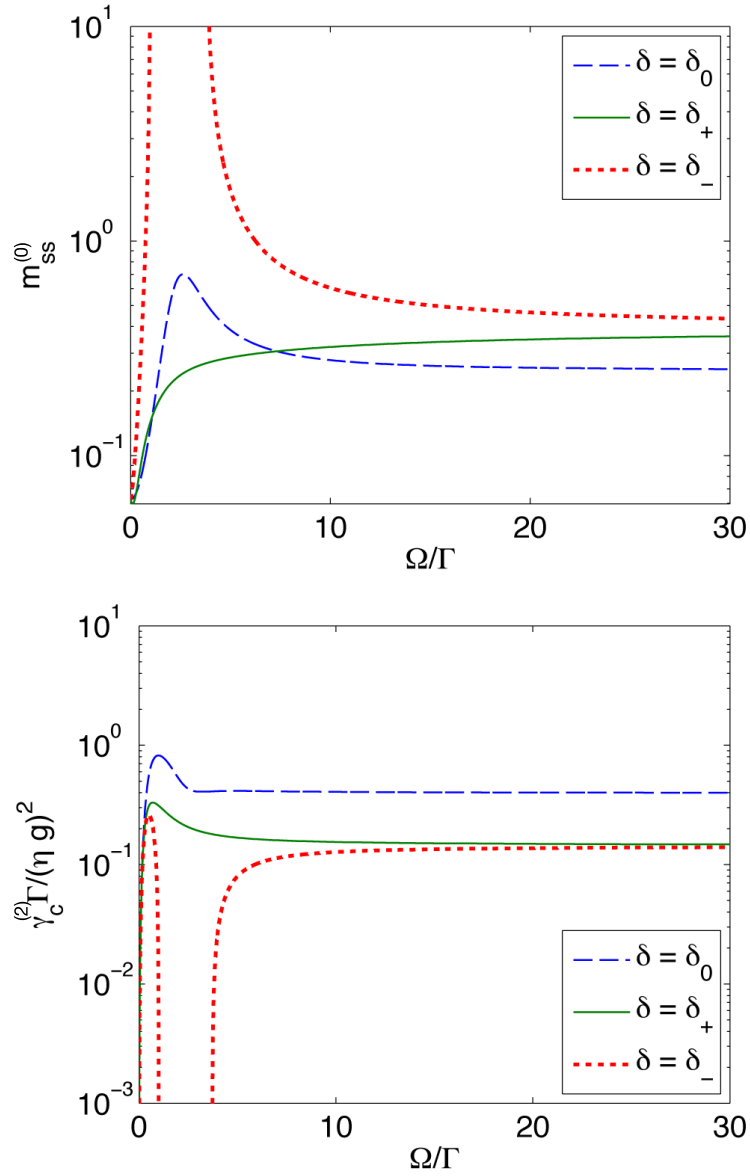
Figure 4.5: Logarithmic plot of the stationary state phonon number $m_{ss}^{(0)}$ and the cooling rate $\gamma_c^{(2)}$ as a function of the laser Rabi frequency Ω, while $\nu = \kappa = \Gamma$.

Dependence on the phonon frequency

Let us now have a closer look at the dependence of the cooling process on the phonon frequency ν. To do so, we consider a relatively small and a relatively large value of Ω, while keeping all other system parameters comparable to previous experimental parameters. As suggested by Fig. 4.5, we choose $\Omega = 3\,\Gamma$ (cf. Fig. 4.6) and $\Omega = 30\,\Gamma$ (cf. Fig. 4.7). In Fig. 4.7, we can easily identify two phonon frequencies ν for which certain cooling resonances (eg. δ_-) becomes identical to one of the heating resonances in Eq. (4.35). When this applies, the cooling rate $\gamma_c^{(2)}$ becomes very small (in some cases it even becomes negative which implies heating) and $m_{ss}^{(0)}$ tends to infinity. Moreover, in both figures, the atom-cavity detuning δ_- yields the highest stationary state phonon numbers and is therefore of less practical interest than δ_0 and δ_+. For relatively small phonon frequencies ν, the lowest stationary state phonon number is achieved, when the atom-cavity detuning equals δ_+. For very strongly confined particles, it is better to choose $\delta = \delta_0$ (sideband cooling case). As one would expect, we notice that higher phonon frequencies allow to cool the trapped particle to significantly lower temperatures.

Dependence on the spontaneous cavity decay rate

Finally, we discuss the dependence of $m_{ss}^{(0)}$ and $\gamma_c^{(2)}$ on the spontaneous cavity decay rate κ. As in the previous subsection, we choose $\Omega = 3\,\Gamma$ (cf. Fig. 4.8) and $\Omega = 30\,\Gamma$ (cf. Fig. 4.9). For a relatively wide range of experimental parameters, we find that the detuning δ_+ yields the lowest stationary state phonon number (cf. Figs. 4.8 and 4.9). This is especially the case, when the spontaneous cavity decay rate κ is relatively large. Although this is not illustrated here, we would like to add that the cooling transitions become over-damped when κ becomes too large. In this case, the cooling becomes very inefficient and the stationary state phonon number $m_{ss}^{(0)}$ increases rapidly.

4.6   Conclusions

In this chapter, we analysed cavity-mediated laser cooling for a single atom with external confinement in the direction of the cavity axis (cf. Fig. 4.2). The Hamiltonian H_I of this system contains an atom-phonon-photon interaction term, which gives rise to three sharp resonances with a minimum stationary state phonon number. For a wide range of experimental parameters, one should choose the atom-cavity detuning δ equal to δ_+ in Eq. (4.34) in order to minimise the stationary state phonon
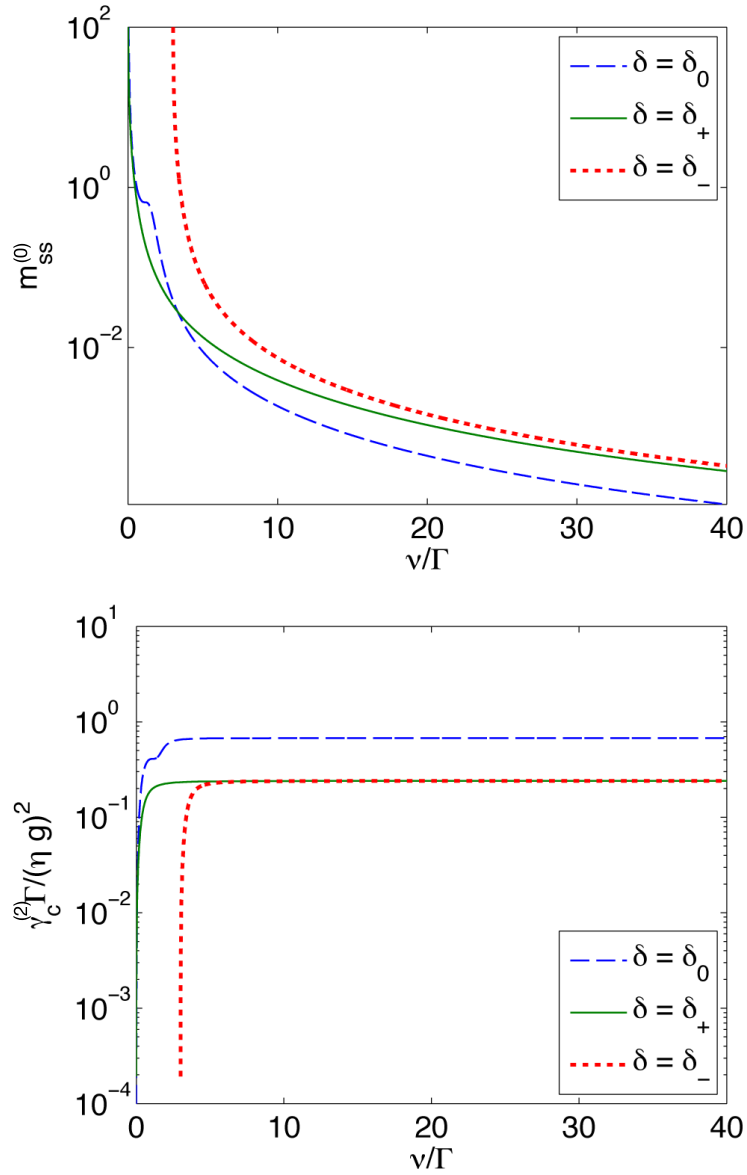
Figure 4.6: Logarithmic plot of the stationary state phonon number $m_{ss}^{(0)}$ and the cooling rate $\gamma_c^{(2)}$ as a function of the phonon frequency ν for $\Omega = 3\,\Gamma$ and $\kappa = \Gamma$.
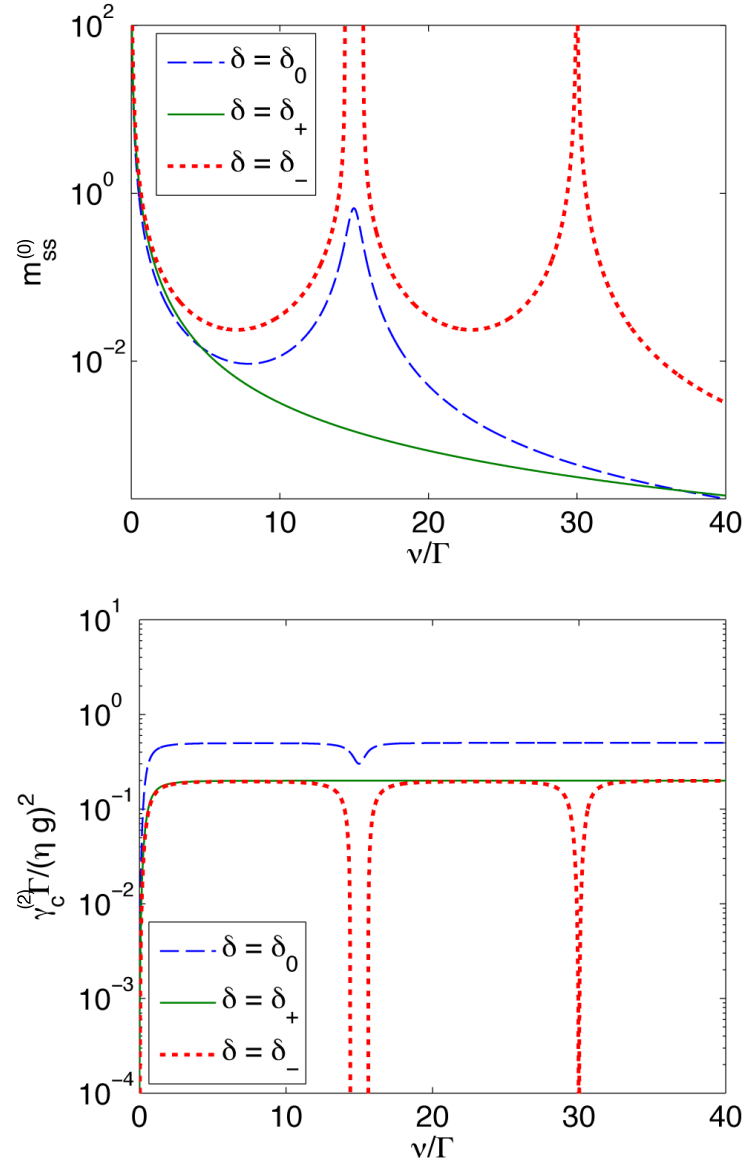
Figure 4.7: Logarithmic plot of the stationary state phonon number $m_{ss}^{(0)}$ and the cooling rate $\gamma_c^{(2)}$ as a function of the phonon frequency ν for $\Omega = 30\,\Gamma$ and $\kappa = \Gamma$.
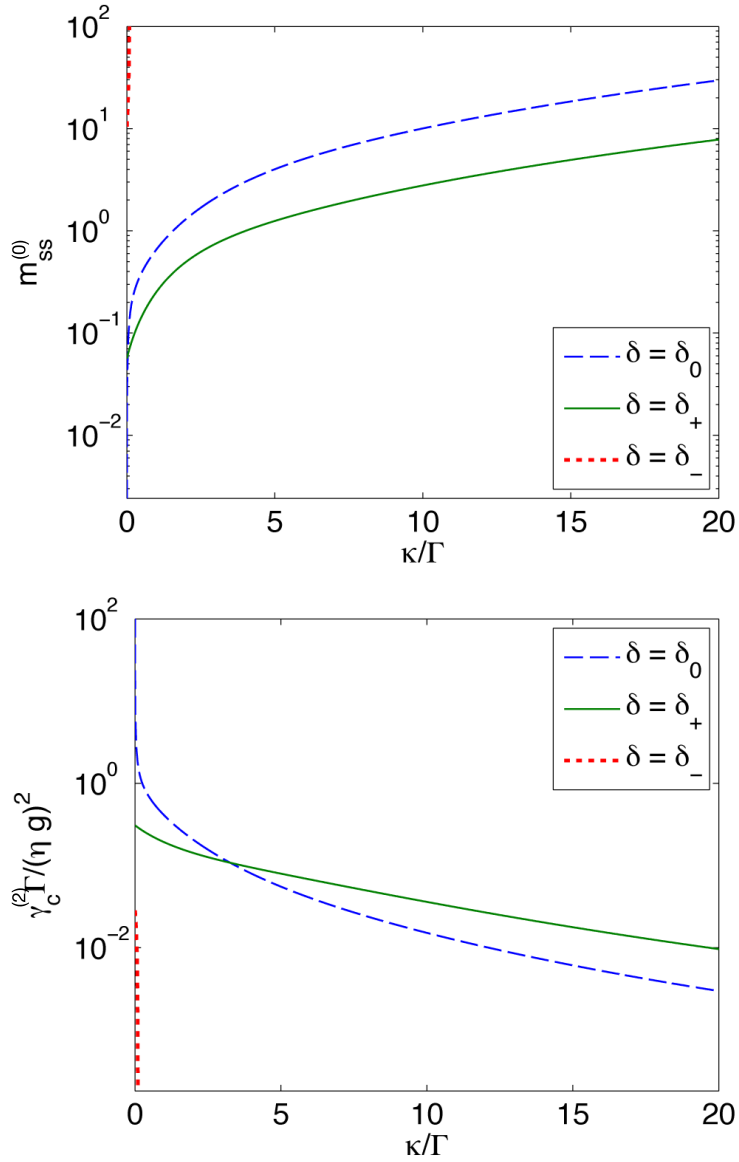
Figure 4.8: Logarithmic plot of the stationary state phonon number $m_{ss}^{(0)}$ and the cooling rate $\gamma_c^{(2)}$ as a function of the spontaneous cavity decay rate κ for $\Omega = 3\,\Gamma$ and $\nu = \Gamma$.
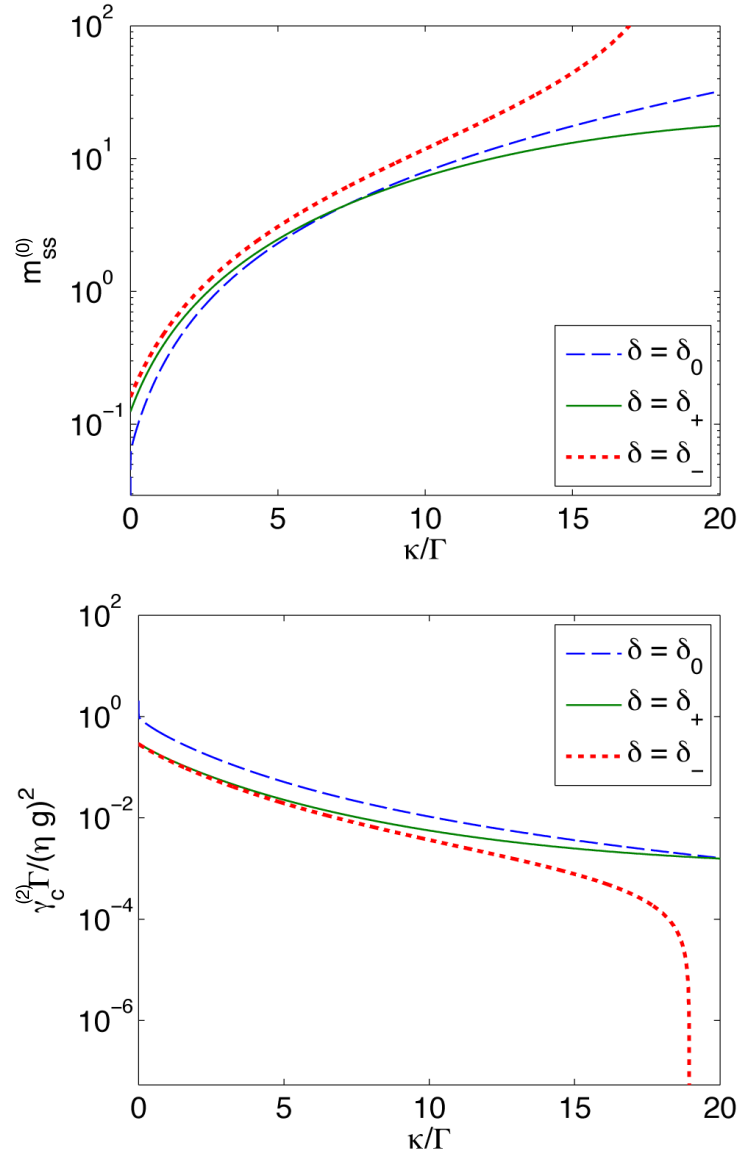
Figure 4.9: Logarithmic plot of the stationary state phonon number $m_{ss}^{(0)}$ and the cooling rate $\gamma_c^{(2)}$ as a function of the spontaneous cavity decay rate κ for $\Omega = 30\,\Gamma$ and $v = \Gamma$.

number m_{ss} (cf. Figs. 4.5–4.9). This resonance depends on the laser Rabi frequency Ω and is different from the usually considered resonance δ_0 for laser-sideband cooling.

To obtain an effective cooling rate γ_c and an analytical expression for the stationary state phonon number m_{ss} for the experimental setup which we consider in this chapter (cf. Eq. (4.63)), we proceed as in Blake *et al.* (2011a,b, 2012). Starting from the standard quantum optical master equation, we derive linear differential equations — so-called rate or cooling equations — for the time evolution of different expectation values. When taking a large enough number of expectation values into account, we obtain a closed set of equations, which can be used to analyse the time evolution of the mean phonon number m on a time scale given by η^2. The only assumption made in our calculations is that the atom-cavity coupling constant g multiplied with the Lamb-Dicke η is much smaller than at least one other experimental parameters (cf. Eq. (4.62)). The condition in Eq. (4.62) guarantees that the mean phonon number m evolves on a much slower time scale than all the other relevant expectation values and allows us to obtain Eq. (4.63) via an adiabatic elimination.

Achieving very low stationary state phonon numbers for a single trapped particle requires a relatively large phonon frequency v, while very large spontaneous decay rates κ and Γ need to be avoided. Achieving relatively large cooling rates moreover requires a relatively large atom-cavity coupling constant g, since γ_c is proportional to $(\eta g)^2/\Gamma$. To overcome this problem, it might be interesting to study the cooling process of the experimental setup in Fig. 4.2 when it contains many trapped particles.

Chapter 5

Cooling of a many-body system

The cooling dynamics of many-body systems is much richer and complicated than that of a single particle. As mentioned earlier, laser sideband cooling is not very efficient for cooling multiple atoms simultaneously and an optical cavity became one of the proposed techniques to aid this process. However, non-cavity methods have also been reported (cf. e.g. Morigi & Eschner (2001)). In general, even non-interacting atoms in a cavity exhibit very rich behaviour, involving self-trapping and self-organisation (cf. Baumann *et al.* (2010); Domokos & Ritsch (2002)). In this chapter, we address the problem of cooling a large number of atomic particles collectively and show how an optical cavity can be used to facilitate this process. We investigate a one-dimensional non-interacting atomic gas strongly confined in the direction of the cavity axis and driven by a resonant laser. The experimental setup is very similar to the setup described in Chapter 4 and is shown in Fig. 5.1. The single trapped atom that was treated earlier is now replaced by a homogeneous atomic gas of N particles.

By applying the optical master equation to our system, we find that the stationary state of the mean phonon number is reduced during the cooling process by the amount governed by a certain phonon coherence ζ, which itself is destroyed in the process. Moreover, we find that the cooling process is collective, where the cooling rate scales positively with the number of atoms in the system. The phonon coherence ζ is associated with the phonon exchange between the particles and, under the assumption of non-interacting atoms, can be expressed in terms of mean deviation of the particles from the trap centre. Using the thermodynamical framework of canonical density operator, we demonstrate that thermalising the atomic system in an anharmonic, asymmetric potential is an effective method for reviving the phonon coherence ζ without increasing the mean phonon number. Thermal states therefore
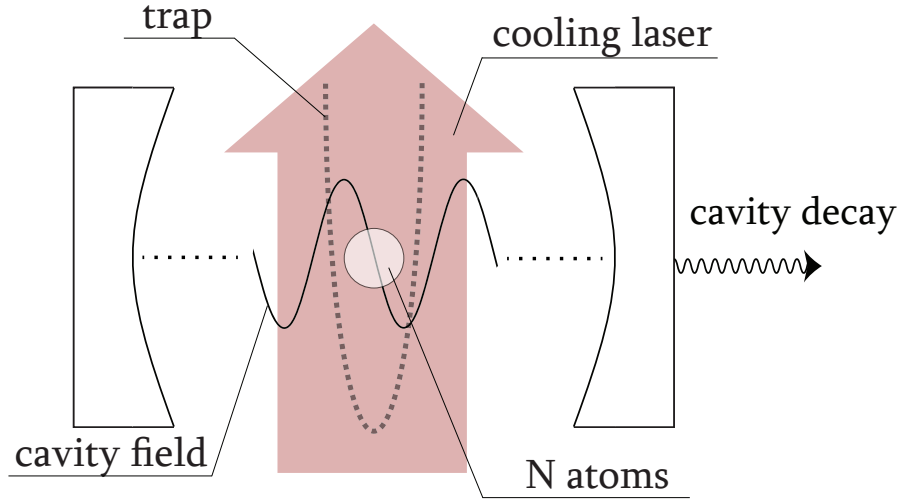
Figure 5.1: Schematic view of the experimental setup, consisting of a resonantly driven atomic gas which is externally confined at the node of an optical resonator.

provide practical pathways for continuous cooling without compromising the temperature of the system. The entire process is split into two stages, where the cooling pulses are alternated with periods of thermalisation, and shown in Fig. (5.2). Doing so, the system is expected to reach very low temperatures very fast, due to the collective cooling rate during cooling pulses.

5.1   Theoretical background

Armed with the model of the single particle cavity cooling, we can now use the same methodology to study a many-body system. For a non-interacting gas of N atoms, the Hamiltonian has a similar form as in Eq. (4.19), with the operator subsitutions

$$b \to \sum_i b_i \, ,$$
$$b^\dagger \to \sum_i b_i^\dagger \, ,$$
$$\sigma^- \to \sum_i \sigma_i^- \, ,$$
$$\sigma^+ \to \sum_i \sigma_i^+ \, . \tag{5.1}$$
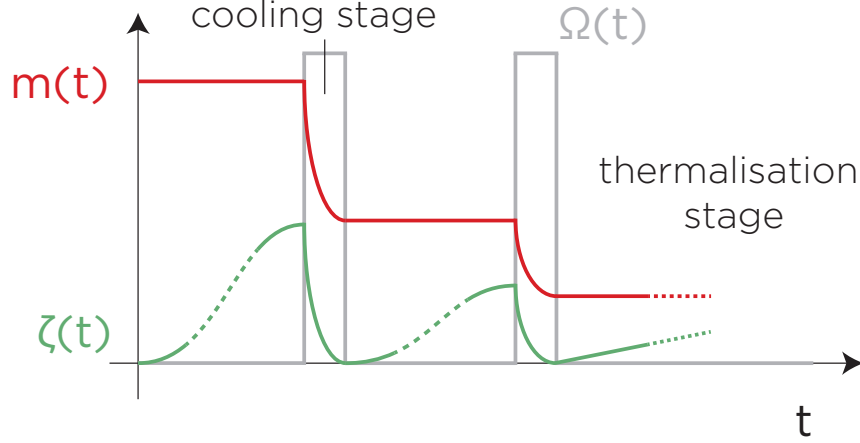
Figure 5.2: Timeline of the proposed cooling process which consists of cooling stages interspersed with displacement stages. During the first stage, a short laser pulse with Rabi frequency Ω is applied, which translates a collective phonon coherence ζ into a reduction of the mean number of phonons m of the trapped particles. The purpose of the second stage is the build up of ζ without increasing m. When repeating both stages many times, the particles are expected to reach a very low temperature.

Here, the behaviour of each atom i is described by a separate operator with index i, where operators with different indices commute, since the atoms do not interact with each other. In addition, we assume that each particle experiences the same trapping potential, which leads to the vibrational Hamiltonian of the form

$$H_{\text{vib}} = \sum_{i=1}^{N} \hbar \nu \, b_i^\dagger b_i \,, \tag{5.2}$$

up to a constant.

Similarly, the electronic energy of the system is described by the electronic Hamiltonian,

$$H_{\text{el}} = \sum_{i=1}^{N} \hbar \omega_0 \, \sigma_i^+ \sigma_i^- \,, \tag{5.3}$$

with $\sigma_i^+ = |1\rangle_{ii}\langle 0|$ and $\sigma_i^- = |0\rangle_{ii}\langle 1|$. The states $|0\rangle_i$ and $|1\rangle_i$ denote the ground and the excited state of atom i and have the same properties as for the single atom.

The single-mode cavity is the same as in the previous chapter, and the Hamiltonian for its energy remains unchanged,

$$H_{\text{cav}} = \hbar \omega \, c^\dagger c \,. \tag{5.4}$$

Each atom will interact with the cavity mode independently from the other atoms, with the interaction term written as

$$H_{\text{int}} = \sum_{i=1}^{N} \hbar G_i(x)\, c\sigma_i^+ + \text{H.c.}\,, \tag{5.5}$$

where $G_i(x)$ is interaction strength constant for atom i. Similarly, each atom will interact with the resonant driving laser independently from the other atoms,

$$H_{\text{L}} = \sum_{i=1}^{N} \frac{1}{2}\hbar\Omega\, \sigma_i^+\, e^{-i\omega_0 t} + \text{H.c.}\,. \tag{5.6}$$

Therefore, replacing the single trapped atom with a non-interacting atomic gas is equivalent to replacing the phonon and electronic operators in Eq. (4.19) with their indexed counterparts and summing over all N particles. The full Hamiltonian becomes

$$
\begin{aligned}
H \;=\;& \hbar\omega\, c^\dagger c + \sum_{i=1}^{N} \Big(\hbar\nu\, b_i^\dagger b_i + \hbar\omega_0\, \sigma_i^+ \sigma_i^- + \hbar G_i(x)\, c\sigma_i^+ \\
& + \frac{1}{2}\hbar\Omega\, \sigma_i^+\, e^{-i\omega_0 t} + \text{H.c.} \Big)
\end{aligned}
\tag{5.7}
$$

in the usual dipole and rotating wave approximation. Assuming the strong confinement regime, all of the atoms will be located at the node of the cavity field. This leads to $G_i(x)$ having the similar form as in chapter 4, and in the interaction picture the Hamiltonian becomes

$$
\begin{aligned}
H_{\text{I}} \;=\;& \hbar\delta\, c^\dagger c + \sum_{i=1}^{N} \hbar\nu\, b_i^\dagger b_i + \sum_{i=1}^{N} \frac{1}{2}\hbar\Omega\, (\sigma_i^- + \sigma_i^+) \\
& + \sum_{i=1}^{N} \hbar\eta g\, (b_i + b_i^\dagger)(\sigma_i^+ c + \sigma_i^- c^\dagger)\,,
\end{aligned}
\tag{5.8}
$$

where

$$\delta = \omega - \omega_0 \tag{5.9}$$

is the cavity-laser detuning. The crucial atom-phonon-photon interaction is expressed by the last term of the Hamiltonian and shows the existing cross-talk of the non-interactive particles via the cavity mode. As we will see later, the atom-phonon-photon interaction is essential for collective cooling of the atomic gas.

As mentioned earlier, the entire cooling process is composed of two different stages. During the first stage, the atomic gas is coupled to an optical cavity while

being driven by an external laser and its dynamics can be described by the Hamiltonian (5.8) above. Since the system is open, spontaneous photon emission is taken into account by the quantum optical many-body master equation

$$
\begin{aligned}
\dot{\rho}_\mathrm{I} \;=\; & -\frac{\mathrm{i}}{\hbar}\left[H_\mathrm{I}, \rho_\mathrm{I}\right] + \frac{1}{2}\kappa\left(2c\rho_\mathrm{I}c^\dagger - c^\dagger c\rho_\mathrm{I} - \rho_\mathrm{I}c^\dagger c\right) \\
& + \frac{1}{2}\Gamma\sum_i\left(2\sigma_i^-\rho_\mathrm{I}\sigma_i^+ - \sigma_i^+\sigma_i^-\rho_\mathrm{I} - \rho_\mathrm{I}\sigma_i^+\sigma_i^-\right),
\end{aligned}
\tag{5.10}
$$

where ρ_I denotes the density matrix of the atom-phonon-photon system in the interaction picture, κ is the cavity decay rate and Γ is the atomic decay rate.

5.2 Cooling stage

Let us first outline several conditions that will be used in the analysis of the cooling dynamics. Since we are especially interested in the cooling of a relatively large gas of atoms, the number of atoms N will be large,

$$
N \;\gg\; 1.
\tag{5.11}
$$

As we shall see, the terms which dominate the time evolution of the relevant expectation value are either zeroth or first order in η, while assuming that terms which scale as $N\eta$ are zeroth-order terms. In the following, we analyse both of these time scales separately. The calculations in the next subsections are valid as long as

$$
\nu,\ \Omega,\ \Gamma,\ \kappa \;\gg\; \eta g.
\tag{5.12}
$$

To see that this is indeed the case, we need to have a closer look at the rate equations in the following two subsections.

5.2.1 The relevant expectation values

Analogous to the previous chapter, we first introduce the expectation values of certain operators necessary to obtain a closed set of cooling equations, including one for the time evolution of the average mean phonon number. These operators have the form

$$
X^{(i,j)}_{abc} \equiv B^{(i)}_a \Sigma^{(j)}_b C_c
\tag{5.13}
$$

with the B, Σ, and C operators defined such that

$$
\begin{aligned}
(B_0^{(i)}, \Sigma_0^{(i)}, C_0) &\equiv (1, 1, 1), \\
(B_1^{(i)}, \Sigma_1^{(i)}, C_1) &\equiv (b_i^\dagger b_i, \sigma_i^+ \sigma_i^-, c^\dagger c), \\
(B_2^{(i)}, \Sigma_2^{(i)}, C_2) &\equiv (b_i + b_i^\dagger, \sigma_i^- + \sigma_i^+, c + c^\dagger), \\
(B_3^{(i)}, \Sigma_3^{(i)}, C_3) &\equiv \mathrm{i}(b_i - b_i^\dagger, \sigma_i^- - \sigma_i^+, c - c^\dagger),
\end{aligned} \tag{5.14}
$$

while

$$
\begin{aligned}
B_4^{(i)} &\equiv b_i^2 + b_i^{\dagger 2}, \\
B_5^{(i)} &\equiv \mathrm{i}(b_i^2 - b_i^{\dagger 2}).
\end{aligned} \tag{5.15}
$$

These operators follow simple commutators relations,

$$
\begin{aligned}
\left[\Sigma_1^{(i)}, \Sigma_2^{(i)}\right] &= \mathrm{i}\Sigma_3^{(i)}, \\
\left[\Sigma_1^{(i)}, \Sigma_3^{(i)}\right] &= -\mathrm{i}\Sigma_2^{(i)}, \\
\left[\Sigma_2^{(i)}, \Sigma_3^{(i)}\right] &= -2\mathrm{i}\left(1 - 2\Sigma_1^{(i)}\right), \\
\left[B_1^{(i)}, B_2^{(i)}\right] &= \mathrm{i}B_3^{(i)}, \\
\left[B_1^{(i)}, B_3^{(i)}\right] &= -\mathrm{i}B_2^{(i)}, \\
\left[B_2^{(i)}, B_3^{(i)}\right] &= -2\mathrm{i}, \\
[C_1, C_2] &= \mathrm{i}C_3, \\
[C_1, C_3] &= -\mathrm{i}C_2, \\
[C_2, C_3] &= -2\mathrm{i},
\end{aligned} \tag{5.16}
$$

while

$$
\left[A_1^{(i)}, A_2^{(j)}\right] = 0 \tag{5.17}
$$

for arbitrary operators $A_1^{(i)}$ and $A_2^{(j)}$ with $i \neq j$.

In the following, we denote the expectation values of the $X_{abc}^{(i,j)}$ operators by

$$
x_{abc}^{(i,j)} \equiv \langle X_{abc}^{(i,j)} \rangle. \tag{5.18}
$$

As we shall see below, we also need to take phonon coherences of the form

$$
y_{ab}^{(i,j)} \equiv \langle B_a^{(i)} B_b^{(j)} \rangle \tag{5.19}
$$

into account. Since the operators $X_{abc}^{(i,j)}$ and $B_a^{(i)} B_b^{(j)}$ are all Hermitian, the variables $x_{abc}^{(i,j)}$ and $y_{ab}^{(i,j)}$ are all real. Notice also that for $i = j$, they become single-particle expectation values from chapter 4.

The quantity we are interested in is the average mean phonon number m, redefined now as

$$m \equiv \frac{1}{N} \sum_{i=1}^{N} m_i \,, \tag{5.20}$$

with

$$m_i = \langle b_i^\dagger b_i \rangle \,. \tag{5.21}$$

In addition, we consider in the following the single-particle averaged expectation values x_{abc},

$$x_{abc} \equiv \frac{1}{N} \sum_{i=1}^{N} x_{abc}^{(i,i)} \,, \tag{5.22}$$

and the two-particle averaged correlations $\tilde{x}_{abc}$ and y_{ab},

$$
\begin{aligned}
\tilde{x}_{abc} &\equiv \frac{1}{N(N-1)} \sum_{i=1}^{N} \sum_{j \neq i} x_{abc}^{(i,j)} \,, \\
y_{ab} &\equiv \frac{1}{N(N-1)} \sum_{i=1}^{N} \sum_{j \neq i} y_{ab}^{(i,j)} \,.
\end{aligned}
\tag{5.23}
$$

Using the definitions above, it can be easily shown that, for example,

$$x_{a0c} = \tilde{x}_{a0c} \quad \text{and} \quad y_{ab} = y_{ba} \,, \tag{5.24}$$

for all a, b and c.

The normalisation of the definitions has been chosen such that they are effectively single-particle measures and to a good approximation independent of the exact number N.

Using the notation that we introduced, the relevant Hamiltonian H_I in Eq. (5.8) can be rewritten as

$$
\begin{aligned}
H_\mathrm{I} &= \hbar \delta\, C_1 + \sum_{i=1}^{N} \hbar v B_1^{(i)} + \sum_{i=1}^{N} \frac{1}{2} \hbar \Omega \Sigma_2^{(i)} \\
&\quad + \sum_{i=1}^{N} \frac{1}{2} \hbar \eta g B_2^{(i)} \left(\Sigma_2^{(i)} C_2 + \Sigma_3^{(i)} C_3 \right) \,.
\end{aligned}
\tag{5.25}
$$

5.2.2 Time evolution of m and y's

Using Eq. (5.10), one can show that the time evolution of the expectation values of an arbitrary operator A_I in the interaction picture is given by

$$
\begin{aligned}
\langle \dot{A}_I \rangle \;=\;& -\frac{i}{\hbar} \langle [A_I, H_I] \rangle \\
& + \frac{1}{2} \Gamma \sum_i \left\langle 2\sigma_i^+ A_I \sigma_i^- - A_I \sigma_i^+ \sigma_i^- - \sigma_i^+ \sigma_i^- A_I \right\rangle \\
& + \frac{1}{2} \kappa \left\langle 2c^\dagger A_I c - A_I c^\dagger c - c^\dagger c A_I \right\rangle .
\end{aligned}
\tag{5.26}
$$

We now have a closer look at the time evolution of the relevant expectation values of the atom-cavity-phonon system in first order in η. Using Eq. (5.26), one can show that the average mean phonon number evolves according to

$$
\dot{m} \;=\; \tfrac{1}{2} \eta g \left(x_{322} + x_{333} \right) .
\tag{5.27}
$$

Taking into account that Eq. (5.24) implies $y_{23} = y_{32}$, we obtain the following time derivatives of the two-particle phonon coherences y_{ab},

$$
\begin{aligned}
\dot{y}_{22} \;=\;& -2\nu\, y_{23} , \\
\dot{y}_{23} \;=\;& \dot{y}_{32} = \nu \left(y_{22} - y_{33} \right) + \eta g \left(\tilde{x}_{222} + \tilde{x}_{233} \right) , \\
\dot{y}_{33} \;=\;& 2\nu\, y_{23} + 2\eta g \left(\tilde{x}_{322} + \tilde{x}_{333} \right)
\end{aligned}
\tag{5.28}
$$

without neglecting any terms. As pointed out in the beginning of this section (cf. Eq. (5.12)), our analysis assumes that the phonon frequency ν is much larger than the reduced cavity coupling ηg. Separating the time evolution of the above expectation values on these two time scales, we now introduce the new variables

$$
\begin{aligned}
\zeta \;\equiv\;& \frac{1}{4} \left(y_{22} + y_{33} \right) \\
y_- \;\equiv\;& \frac{1}{4} \left(y_{22} - y_{33} \right) .
\end{aligned}
\tag{5.29}
$$

From Eq. (5.28) we see that the time derivative of y_- and of y_{23} equal

$$
\begin{aligned}
\dot{y}_- \;=\;& -\nu\, y_{23} - \frac{1}{2} \eta g \left(\tilde{x}_{322} + \tilde{x}_{333} \right) , \\
\dot{y}_{23} \;=\;& \nu\, y_- + \eta g \left(\tilde{x}_{222} + \tilde{x}_{233} \right) .
\end{aligned}
\tag{5.30}
$$

Solving these equations via an adiabatic elimination, one immediately sees that

$$
y_- = y_{23} = \mathcal{O}\left(\frac{\eta g}{\nu} \right)
\tag{5.31}
$$

to a very good approximation. This means that both two-particle phonon coherences oscillate rapidly in time around a relatively small value and remain negligible during the cooling stage.

In the following we are only interested in the time evolution of the slowly evolving variables ζ and m. Proceeding as above and combining again Eqs. (5.28) and (5.29), we moreover obtain the differential equation

$$\dot{\zeta} = \frac{1}{2}\eta g \left(\tilde{x}_{322} + \tilde{x}_{333} \right) . \tag{5.32}$$

This means, the average mean phonon number m (cf. Eq. (5.27)) and the phonon coherence ζ both evolve on the relatively slow time scale given by η.

As we shall see below, the phonon coherence ζ plays a crucial role in cooling of the many-body system. Let us emphasize that ζ can only be defined when there are at least two particles in the trap. This is why the cooling process which we describe here is qualitatively different from cavity-mediated laser-cooling of a single particle.

5.2.3 Time evolution of the x-coherences

To analyse the dynamics for m and ζ, we now need to have a closer look at the expectation values x_{322}, x_{333}, $\tilde{x}_{322}$, and $\tilde{x}_{333}$. Starting with the single-particle expectation values x_{322} and x_{333}, these are equal to zero in zeroth order in η. However, when there are many particles, such that $N \gg 1$, then ηN is effectively a term in zeroth order in η. Taking this into account and neglecting higher order terms, we can use Eq. (5.26) together with Eq. (5.25) to show that the expectation values x_{abc} evolve according to

$$\begin{aligned}
\dot{x}_{202} &= -vx_{302} - \delta x_{203} - N\eta g z_{2203} - \frac{1}{2}\gamma_0 x_{202} , \\
\dot{x}_{203} &= -vx_{303} + \delta x_{202} + N\eta g z_{2202} - \frac{1}{2}\gamma_0 x_{203} , \\
\dot{x}_{302} &= vx_{202} - \delta x_{303} - N\eta g z_{3203} - \frac{1}{2}\gamma_0 x_{302} , \\
\dot{x}_{303} &= vx_{203} + \delta x_{302} + N\eta g z_{3202} - \frac{1}{2}\gamma_0 x_{303} ,
\end{aligned} \tag{5.33}$$

and

$$\begin{aligned}
\dot{x}_{212} &= -vx_{312} - \delta x_{213} + \frac{1}{2}\Omega x_{232} - N\eta g z_{2213} - \frac{1}{2}\gamma_2 x_{212} , \\
\dot{x}_{213} &= -vx_{313} + \delta x_{212} + \frac{1}{2}\Omega x_{233} + N\eta g z_{2212} - \frac{1}{2}\gamma_2 x_{213} , \\
\dot{x}_{312} &= vx_{212} - \delta x_{313} + \frac{1}{2}\Omega x_{332} - N\eta g z_{3213} - \frac{1}{2}\gamma_2 x_{312} , \\
\dot{x}_{313} &= vx_{213} + \delta x_{312} + \frac{1}{2}\Omega x_{333} + N\eta g z_{3212} - \frac{1}{2}\gamma_2 x_{313} .
\end{aligned} \tag{5.34}$$

Moreover, we have

$$
\begin{aligned}
\dot{x}_{222} &= -\nu x_{322} - \delta x_{223} - N\eta g z_{2223} - \frac{1}{2}\gamma_1 x_{222}, \\
\dot{x}_{223} &= -\nu x_{323} + \delta x_{222} + N\eta g z_{2222} - \frac{1}{2}\gamma_1 x_{223}, \\
\dot{x}_{322} &= \nu x_{222} - \delta x_{323} - N\eta g z_{3223} - \frac{1}{2}\gamma_1 x_{322}, \\
\dot{x}_{323} &= \nu x_{223} + \delta x_{322} + N\eta g z_{3222} - \frac{1}{2}\gamma_1 x_{323}.
\end{aligned}
\tag{5.35}
$$

and

$$
\begin{aligned}
\dot{x}_{232} &= -\nu x_{332} - \delta x_{233} + \Omega\left(x_{202} - 2x_{212}\right) - N\eta g z_{2233} - \frac{1}{2}\gamma_1 x_{232}, \\
\dot{x}_{233} &= -\nu x_{333} + \delta x_{232} + \Omega\left(x_{203} - 2x_{213}\right) + N\eta g z_{2232} - \frac{1}{2}\gamma_1 x_{233}, \\
\dot{x}_{332} &= \nu x_{232} - \delta x_{333} + \Omega\left(x_{302} - 2x_{312}\right) - N\eta g z_{3233} - \frac{1}{2}\gamma_1 x_{332}, \\
\dot{x}_{333} &= \nu x_{233} + \delta x_{332} + \Omega\left(x_{303} - 2x_{313}\right) + N\eta g z_{3232} - \frac{1}{2}\gamma_1 x_{333}.
\end{aligned}
\tag{5.36}
$$

Here we used a short hand notation

$$
\gamma_n \equiv \kappa + n\Gamma
\tag{5.37}
$$

for combined spontaneous photon decay rates and defined the two-particle expectation values z_{abcd} such that

$$
z_{abcd} \equiv \frac{1}{N(N-1)} \sum_{i=1}^{N} \sum_{j \neq i} \langle B_a^{(i)} B_b^{(j)} \Sigma_c^{(i)} \Sigma_d^{(j)} \rangle.
\tag{5.38}
$$

Again, these are normalised by the number $N(N-1)$ of particle pairs in the trap. This means, these correlations are not expected to depend strongly on N, as long as N is sufficiently large.

Calculating $\tilde{x}_{abc}$, we find that these evolve in the same way as the x_{abc} expectation values with the same indices but with the x_{abc} and z_{abcd} on the right hand side of Eqs. (5.33)–(5.36) replaced by $\tilde{x}_{abc}$ and $\tilde{z}_{abcd}$, respectively. Here $\tilde{z}_{abcd}$ has been defined such that

$$
\tilde{z}_{abcd} \equiv \frac{1}{N(N-1)(N-2)} \sum_{i=1}^{N} \sum_{j \neq i} \sum_{k \neq i,j} \langle B_a^{(i)} B_b^{(k)} \Sigma_c^{(j)} \Sigma_d^{(k)} \rangle.
\tag{5.39}
$$

As we shall see in the next subsection, these correlations are essentially the same as the two-particle correlations z_{abcd} in Eq. (5.38).

5.2.4   Time evolution of the z-coherences

When deriving the rate equations for the above z-coherences, we do not get any terms which scale as $N\eta g$. The reason for this is that these are particle-only expectation values. The corresponding operators do not contain any cavity photon operators. Effectively, the z-coherences evolve as if the interaction Hamiltonian H_{I} in Eq. (5.8) does not contain any interaction between the atoms, phonons and cavity photons in the system. All three subsystems evolve independently. Moreover, due to the presence of the spontaneous atomic decay rate Γ, the electronic states of the trapped particles evolve rapidly, i.e. on the time scale given by $1/\Omega$ and $1/\Gamma$, into a stationary state. Taking this into account, we find that

$$z_{abcd} = \tilde{z}_{abcd} = y_{ab}\, s_c^{\mathrm{ss}} s_d^{\mathrm{ss}}\,, \tag{5.40}$$

where the s_a^{ss} are the stationary state values of the expectation values for the operators Σ_a,

$$s_a \;\equiv\; \langle \Sigma_a^{(i)} \rangle\,, \tag{5.41}$$

which are the same for all particles. To calculate the s_a, we use Eq. (5.26) and obtain the rate equations

$$\dot{s}_1 = \frac{1}{2}\Omega\, s_3 - \Gamma\, s_1\,,$$
$$\dot{s}_2 = -\frac{1}{2}\Gamma\, s_2\,,$$
$$\dot{s}_3 = \Omega\,(1 - 2s_1) - \frac{1}{2}\Gamma\, s_3\,. \tag{5.42}$$

The stationary state values of the expectation values s_a are obtained by setting the right hand sides of these three equations equals to zero. Doing so, we find that

$$\begin{aligned}
s_1^{\mathrm{ss}} &= \frac{\Omega^2}{\Gamma^2 + 2\Omega^2}\,, \\
s_2^{\mathrm{ss}} &= 0\,, \\
s_3^{\mathrm{ss}} &= \frac{2\Gamma\Omega}{\Gamma^2 + 2\Omega^2}\,.
\end{aligned} \tag{5.43}$$

In Section 5.2.2, we have seen that y_- and y_{23} oscillate rapidly around zero. Hence, there are only a few non-zero two-particle coherences which have to be taken into account. Taking the definitions of ζ and y_- into account, we are left with

$$\begin{aligned}
z_{22cd} &= \tilde{z}_{22cd} = 2\zeta\, s_c^{\mathrm{ss}} s_d^{\mathrm{ss}}\,, \\
z_{32cd} &= \tilde{z}_{32cd} = 0\,,
\end{aligned} \tag{5.44}$$

with c and d being either equal to 0, 1 or 3.

5.2.5 Adiabatic elimination of the x-coherences

The main purpose of this subsection is to obtain an effective cooling equation for the cooling stage. To do so, we calculate the x- and the $\tilde{x}$-expectation values via an adiabatic elimination. Doing so is well justified by the time scale separation, which we introduced in Eq. (5.12). But before doing so, we notice that the results in the previous section imply that the x- and the $\tilde{x}$-expectation values obey exactly the same rate equations. When calculating these two-particle coherences with the help of adiabatic elimination, we hence find that

$$x_{abc} = \tilde{x}_{abc} \,. \tag{5.45}$$

As shown earlier, the same applied for the s-expectation values (cf. Eq. (5.44)). This allows us to neglect all tildes from now on.

Performing the adiabatic elimination, setting the right hand sides of Eq. (5.35) equal to zero, and using the results of the previous subsection, we find that

$$
\begin{aligned}
x_{322} &= 0 \,, \\
x_{333} &= -\frac{2}{\eta g} A_N \zeta \,,
\end{aligned}
\tag{5.46}
$$

with A_N given by

$$A_N = \frac{N(8\eta g\Omega\Gamma)^2 \nu\kappa\delta}{\left(\kappa^4 + 16(\delta^2 - \nu^2)^2 + 8\kappa^2(\delta^2 + \nu^2)\right)(\Gamma^2 + 2\Omega^2)^2} \,. \tag{5.47}$$

As we will see later, ζ cannot be negative for non-interacting particles and cooling therefore occur for positive values of A_N. As one would intuitively expect, this applies whenever δ is positive.

Although the cavity-mediated laser-cooling process which we analyse in here is different from single-particle laser-cooling schemes, there is a common resonance. For $\delta = \nu$, the above effective cooling rate A_N assumes its maximum and simplifies to

$$A_N = \frac{N(8\eta g\Omega\Gamma\nu)^2}{\kappa(\kappa^2 + 16\nu^2)(\Gamma^2 + 2\Omega^2)^2} \,. \tag{5.48}$$

This means, for the cooling process which we analyse in here, we observe exactly the same detuning as in laser sideband cooling. As expected, the cooling process is most efficient, when the conversion of phonon into a cavity photon becomes resonant.

The factor N in Eqs. (5.47) and (5.48) shows that the time evolution of the mean phonon number m is collectively enhanced compared to the single-particle case. If

N is sufficiently large, the cooling happens on a very short time scale. This cooling process takes advantage of the simultaneous coupling of all N trapped particles to the same cavity photon mode.

5.2.6 Final state of the cooling stage

Substituting Eqs. (5.46) into Eq. (5.32) and combining the rate equations for the slowly evolving variables in Eqs. (5.27) and (5.32) with Eq. (5.45), we obtain

$$\dot{m} = \dot{\zeta} = -A_N \zeta \,. \tag{5.49}$$

with A_N defined as in the previous subsection. For cooling, we assume that the parameter A_N is always positive, which means that any initial ζ coherence is damped away to zero during cooling. Taking this into account and solving Eq. (5.49) for times t which are much larger than $1/A_N$, we find that

$$m(t) = m(0) - \zeta(0) \,,$$
$$\zeta(t) = 0 \,. \tag{5.50}$$

The time independence of the right hand sides of these two equations on t shows that the average mean phonon number m and the average phonon coherence ζ both assume a quasi-stationary state at the end of the cooling stage.

The reduction of the average mean phonon number m hence only occurs if the phonon coherence ζ is positive at the beginning of the cooling process. Both average mean phonon number m and the phonon coherence ζ then experience exponential reduction during the cooling process with A_N being the corresponding damping rate. Since the damping rate scales as N, this process happens in general on a relatively fast time scale. However, as soon as ζ reaches zero, the cooling stops. The important issue is therefore to find a way for keeping ζ positive throughout the cooling process.

5.3 Thermalisation stage

As shown earlier, the phonon coherence ζ is destroyed during the cooling stage. However, since the damping rate A_N can be very large due to the large number of atomic particles N, the duration of the cooling stage can be kept very short. In this section, we demonstrate how decoupling the trapped atomic system from the cavity and letting it evolve into a thermal state in an anharmonic, asymmetric potential can revive the phonon coherence ζ without compromising the temperature of the atomic

gas. During the second stage, the atoms are displaced away from the trap centre and we can show that this results in a positive thermal average value for the ζ.

5.3.1   Theoretical model

Substituting definitions in Eqs. (5.15) and (5.19) into Eq. (5.23), and combining it with Eq. (5.29) shows that

$$\zeta = \frac{1}{N(N-1)} \sum_{i=1}^{N} \sum_{j \neq i} \langle b_i^\dagger b_j \rangle . \tag{5.51}$$

Going back to the position-momentum space with variable substitutions, defined in chapter 2,

$$\begin{aligned}
b_i &\equiv \sqrt{\frac{M\nu}{2\hbar}}\, x_i + \mathrm{i}\,\sqrt{\frac{1}{2\hbar M\nu}}\, p_i \,, \\
b_i^\dagger &\equiv \sqrt{\frac{M\nu}{2\hbar}}\, x_i - \mathrm{i}\,\sqrt{\frac{1}{2\hbar M\nu}}\, p_i \,,
\end{aligned} \tag{5.52}$$

we observe that

$$\zeta = \frac{1}{N(N-1)} \sum_{i=1}^{N} \sum_{j \neq i} \left(\frac{M\nu}{2\hbar} \langle x_i x_j \rangle + \frac{1}{2\hbar M\nu} \langle p_i p_j \rangle \right) . \tag{5.53}$$

Since there are no interactions between the particles and their confinement is so strong that there is effectively no flux of atoms out of the trap, the particles move independently and their motion can be described by product states with

$$\begin{aligned}
\langle x_i x_j \rangle &= \langle x_i \rangle \langle x_j \rangle = \langle x_i \rangle^2 \,, \\
\langle p_i p_j \rangle &= \langle p_i \rangle \langle p_j \rangle = 0 \,.
\end{aligned} \tag{5.54}$$

Combining this observation with the Eq. (5.53) yields

$$\zeta = \frac{M\nu}{2\hbar} \langle x \rangle^2 \,, \tag{5.55}$$

where $\langle x \rangle$ is the mean distance of the atoms from the trap center. Variable ζ is now independent of N and it suffices only to consider a single non-interacting particle.

The main aim of the thermalisation stage is to build a non-zero displacement of the atoms from the trap centre. For this purpose, we consider a slightly anharmonic, asymmetric trap. Moreover, we decouple the atomic system from the optical cavity and switch off the cooling laser, so that the vibrational state of the system would evolve independently. To give a concrete example of a physical process which results

in a positive phonon expectation value ζ, we assume now that every atom relaxes into a thermal equilibrium with respect to the surrounding atoms via slow coherent and incoherent processes. At the end of this thermalisation, the density matrix of the confined particles equals

$$\rho = \frac{1}{Z} e^{-\beta H_{\text{vib}}}, \tag{5.56}$$

where

$$Z = \text{Tr}\left(e^{-\beta H_{\text{vib}}}\right) \tag{5.57}$$

is a partition function. The thermal parameter β in this equation depends only on the temperature of the system, i.e. the mean energy $\langle H_{\text{vib}}\rangle$ of the trapped atoms at the end of the cooling stage.

To show that this state indeed corresponds to a positive phonon expectation value ζ and to get a feeling for how ζ depends on the mean phonon number m of the trapped particles, we assume that each non-interacting particle obeys the Hamiltonian of the form,

$$H_{\text{vib}} = \hbar v \left(b^\dagger b + \frac{1}{2} \right) + \hbar \mu \left(b + b^\dagger \right)^3, \tag{5.58}$$

where μ is a constant that measures the magnitude of anharmonicity.

5.3.2 Thermal averages of the trapped atomic gas

In order to obtain an analytical expression for ζ, we assume that

$$\mu \ll v, \tag{5.59}$$

and carry out calculations up to second order in μ/v. Denoting $H_{\text{vib}} = H_1 + H_2$, with

$$\begin{aligned} H_1 &\equiv \hbar v \left(b^\dagger b + \tfrac{1}{2} \right), \\ H_2 &\equiv \hbar \mu \left(b + b^\dagger \right)^3, \end{aligned} \tag{5.60}$$

we can use the Baker-Campbell-Hausdorff formula and Taylor expansion to show that

$$\rho = \frac{1}{Z} e^{-\beta H_1} \left(1 - \beta H_2 - \tfrac{1}{2}\beta^2 \left[H_1, H_2 \right] \right) + \dots. \tag{5.61}$$

Combining Eqs. (5.52) and (5.55), we can show that

$$
\begin{aligned}
\zeta &= \frac{M\nu}{2\hbar} \langle x \rangle^2 \\
&= \frac{1}{4} \langle b + b^\dagger \rangle^2 \\
&= \frac{1}{4} \left[\mathrm{Tr} \left(\frac{1}{Z} \mathrm{e}^{-\beta H_1} \left(1 - \beta H_2 - \tfrac{1}{2}\beta^2 [H_1, H_2] \right) \left(b + b^\dagger \right) \right) \right]^2 .
\end{aligned}
\tag{5.62}
$$

where b and $b^\dagger$ are single-particle destruction and creation operators, respectively. Performing the trace operation in the number state basis, this phonon variable simplifies to

$$
\zeta = \left(\frac{3}{2} \beta \hbar \mu \right)^2 \left(2 (k_1 + m_1) + 1 + \frac{1}{2} \beta \hbar \nu (2m_1 + 1) \right)^2 ,
\tag{5.63}
$$

where the expectation values

$$
m_1 \equiv \langle b^\dagger b \rangle
\tag{5.64}
$$

and

$$
k_1 \equiv \langle \left(b^\dagger b \right)^2 \rangle
\tag{5.65}
$$

belong to the thermal state of a single harmonic oscillator with Hamiltonian H_1. These are well-known and are given by (cf. Blaise & Henri-Rousseau (2011))

$$
m_1 = \frac{1}{\mathrm{e}^{\beta \hbar \nu} - 1} \quad \text{and} \quad k_1 = \frac{\mathrm{e}^{\beta \hbar \nu} + 1}{\left(\mathrm{e}^{\beta \hbar \nu} - 1 \right)^2}
\tag{5.66}
$$

for $\mathrm{e}^{-\beta \hbar \nu} < 1$. Combining these two expressions with the Eq. (5.63) yields the explicit dependence of ζ on m,

$$
\zeta = \left[\frac{3\mu}{2\nu} (2m + 1) \ln \left(1 + \frac{1}{m} \right) \left(2m + 1 + \frac{1}{2} \ln \left(1 + \frac{1}{m} \right) \right) \right]^2 .
\tag{5.67}
$$

Fig. 5.3 compares Eq. (5.67) with the numerically obtained dependence of ζ on the mean phonon number m of the trapped particles. As expected, ζ is non-zero and positive unless m tends to zero (as m reaches zero, the assumptions of Eq. (5.61) break down and the analytical expression (5.67) for ζ is no longer valid). Moreover, ζ increases rapidly as the vibrational energy of the particles increases. The hotter the atoms, the further away they accumulate from the trap center.

The expression (5.67) shows that letting the atomic gas thermalise during the thermalisation stage increases the value of the phonon coherence ζ and therefore revives it after being damped away during the cooling stage. The vibrational energy of the atomic system remains unchanged during thermalisation, since the system is isolated and there is no net flux of particles. We can alternate cooling and thermalisation stages, as shown on Fig. (5.2), to cool the atomic gas to very low temperatures.
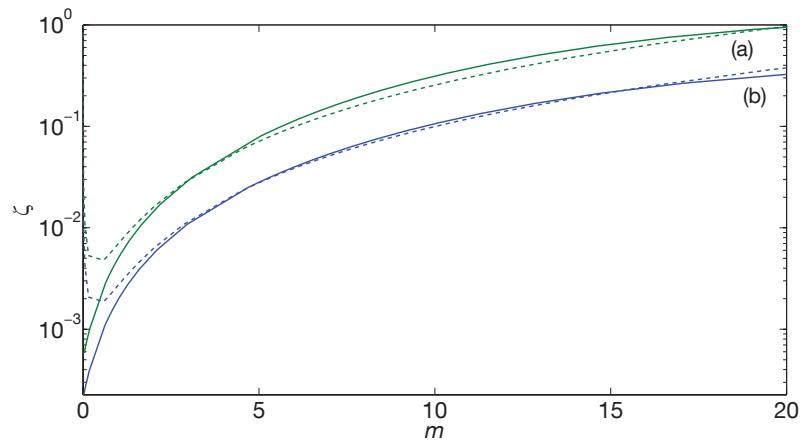
Figure 5.3: Logarithmic plot of the dependence of the phonon variable ζ on the mean phonon number m for $\mu = 0.008\,v$ (a) and $\mu = 0.005\,v$ (b). The dashed lines show the analytical result in Eq. (5.67). The solid lines are the result of a numerical analysis of the thermal states in Eq. (5.56) for different β.

5.4   Conclusions

In this chapter, we developed a two-stage model for cooling of an atomic gas of non-interacting particles. Each atom is strongly coupled to a common cavity radiation mode, which enables a cross-talk between them and is confined in a common trapping potential. When driven by a cooling laser, the average mean phonon number is expected to decrease exponentially, where its total change is dependent on the phonon coherence ζ, which represents phonon exchange between the atoms.

As outlined in this chapter, m and ζ experience a high damping rate, proportional to the number of atoms in the system (cf. Eq. (5.49)), during the cooling stage. To be able to nevertheless take advantage of the collective effects, we propose to proceed as suggested in Fig. 5.2 and to alternate short cooling pulses with relatively long thermalisation stages.

During the cooling stage, the atomic gas reaches the stationary state which depends on the phonon coherence ζ, which itself is damped away to zero. To revive the phonon coherence ζ without compromising the temperature of the system, we propose decoupling the gas for the cavity radiation field by switching off the cooling laser and thermalising it in an anharmonic, asymmetric trapping potential. We show that during each thermalisation stage the atoms accumulate ζ without increasing their vibrational energy. If ζ is continuously restored to its thermal state value, the cooling process described above continues until the particles reach a very low temperature.

This is illustrated in Fig. 5.4 which shows how the mean phonon number m would evolve, if ζ would remain at its thermal-state level (cf. e.g. Eq. (5.67)).
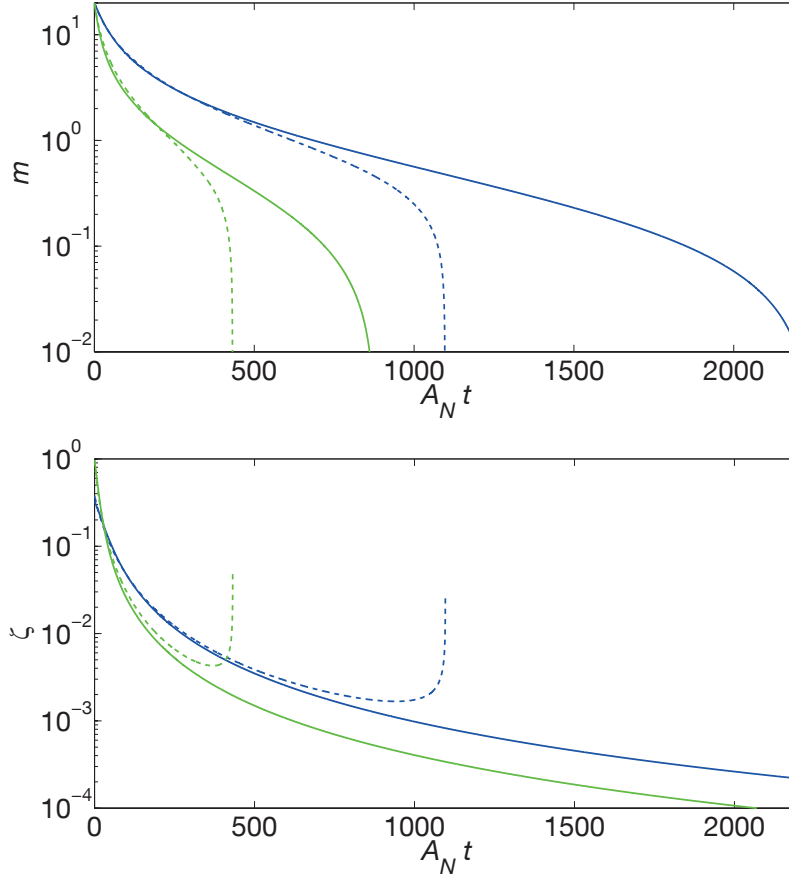
Figure 5.4: Time evolution of m and ζ for $m(0) = 20$, $\mu = 0.008\,\nu$ (green), and $\mu = 0.005\,\nu$ (blue), if intermittent thermalisation stages (which are not shown here) keep ζ effectively at its thermal state value. The dashed lines are based on Eq. (5.67), while the solid lines use a more exact numerical solution for $\zeta(m)$.

Overall, the proposed two-stage process is expected to cool the many-body system to very low temperature. Since the cooling rate is collective, the duration of the cooling pulses can be kept very short. The consequent thermalisation stages prepare the system for the next cooling pulse by reviving the phonon coherence ζ. Only when the vibrational energy of the particles tends to zero (cf. Fig. 5.3), ζ becomes too small and the cooling of the particles slows down. Eventually heating mechanisms which are not taken into account in this model dominate the dynamics of the atoms and limit their final temperature.

Chapter 6

Quantum sonoluminescence

In this chapter, we apply the two-stage collective model developed earlier to describe the mechanism of sonoluminescence. Sonoluminescence is a phenomenon of strong light emission from a gas bubble that is acoustically suspended and periodically driven in a liquid by ultrasonic frequencies (cf. Brenner *et al.* (2002)). A typical single-bubble sonoluminescence cycle is shown in Fig. 6.1. As the bubble expands, it reaches a critical radius, after which point the bubble rapidly collapses. The collapse is accompanied by the sudden emission of light which is indicative of very high temperatures inside the bubble. Afterwards, the bubble oscillates around its equilibrium radius until it regains its stability.

Sonoluminescence was first reported in Gaitan (1990) and Gaitan & Crum (1990). Afterwards, Barber & Putterman (1991) measured the width of the light pulse to be less than 50 ps. Such result suggested that in the single-bubble sonoluminescence, the light emission is decoupled from the bubble dynamics. While the radius of the bubble can be explained by the classical Rayleigh-Plesset equation, the mechanism of the light emission remains unclear. The discover of sharp emission lines in the optical regime (cf. Brenner *et al.* (2002); Flannigan & Suslick (2007); Suslick & Flannigan (2008)) indicate the population of highly excited energy eigenstates and the presence of a dense plasma. In addition, a sensitive dependence of the light emission on the type of gas within the cavity was found (cf. Brenner *et al.* (2002); Hiller *et al.* (1994)). A valid theoretical model needs to be able to account for both of these phenomena, which cannot yet be explained classically.

In this chapter, we develop a two-stage quantum toy model to treat the dynamics of the atomic gas inside the bubble. The atomic system trapped inside the cavitating bubble is treated similarly to the atomic gas in the previous chapter, while the electromagnetic field inside the bubble is quantised in the same way as cavity ra-

ditation field. Since the evolution of the bubble exhibits distinct phases of growth and collapse, we model these phases in terms of thermal states and strong-coupling states, as was described in chapter 5. During the thermalisation stage, the atomic gas thermalises with energy being redistributed amongst the particles. The atomic system is decoupled from the radiation field inside the bubble and evolves independently. However, during the collapse, the bubble becomes opaque and the atomic gas strongly couples to the single standing-wave mode of the bubble. Given the resemblance of this system to the atom-cavity-phonon system seen earlier, we treat it in a similar way, while studying heating instead of cooling. The latter stage is referred to as the heating stage.

As we will see later, our quantum two-stage model describes heating mechanisms present in sonoluminescence and explains the observed temperature changes, as well as main attributes of the phenomenon, such as dependence on atomic structures, radius of the bubble and presence of plasma. Using our model, we identify additional heating due to quantum effects and explain final temperatures in sonoluminescence experiments.

6.1   Introduction

Fig. 6.1 shows a typical single-bubble sonoluminescence cycle and indicates the relevant time scales. The collapse phase begins at point A, when the bubble becomes thermally isolated from the surroundings. This is accompanied by rapid heating and a light flash between points *B* and *C*.

When the bubble reaches its minimum radius, we assume that the electromagnetic field inside becomes quantised. This means, the atomic particles suddenly behave as if placed inside an optical cavity. The walls of the cavity are formed by the walls of the collapsing bubble. As before, we quantise the motion of the atomic system inside the bubble. During the expansion phase, however, the particles constantly remain in a thermal state which only depends on their current temperature. If the particles are sufficiently hot and a plasma is formed, collisions result in correlations between the particles. During a subsequent collapse phase, these correlations can fuel a cavity-mediated collective heating process, similarly to what has been seen in the previous chapter. As shown in chapters 4 and 5, the interplay between the electronic and vibrational degrees of freedom of the trapped particles combined with the spontaneous emission of photons can result in significant changes of the temperature of a quantum system. If repeated over many cycles, such a heating mechanism
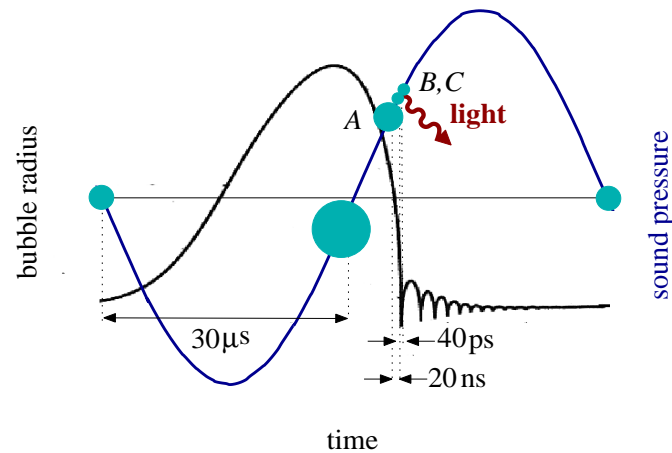
Figure 6.1: Time dependence of the driving sound pressure and of the bubble radius in a typical single-bubble sonoluminescence cycle. Point A marks the beginning of the collapse phase in which the bubble becomes thermally isolated from the liquid. At point B, the temperature within the bubble is significantly increased and a strong light flash occurs. Point C denotes the beginning of the expansion phase in which the bubble oscillates around its equilibrium radius until it regains its stability.

could have a significant effect.

6.2   Theoretical model

In this section, we introduce a quantum optical model for the description of the atomic particles trapped inside a sonoluminescing bubble which applies during the thermalisation and during the bubble collapse phase. Several degrees of freedom need to be taken into account. Once the atoms are tightly confined, their motion becomes quantised and the vibrational states of the particles play a crucial role in their dynamics. Moreover, there are the electronic degrees of freedom of the trapped particles. At high enough temperatures, the atoms might be either in their electronic ground state or in a highly excited state. For simplicity, only two atomic state are considered. During the thermalisation stage, the dynamics of the system is dominated by collisions.

During the collapse phase, the bubble radius becomes comparable to the wavelength of the corresponding atomic transition. If the bubble walls become opaque and the water dipole molecules arrange as if part of a metallic surface, the electro-

magnetic field inside the bubble too becomes quantised. The atomic particles couple effectively to a standing-wave radiation mode. Consequently, the dynamics of the system is dominated by the sudden presence of an optical cavity with a mode frequency close to the atomic transition frequency. The result is an atom-cavity-phonon coupling with the spontaneous emission of photons at a relatively high rate. During this stage, the collisions between the particles become negligible.

6.2.1 Thermalisation stage

During the thermalisation stage, the total Hamiltonian of the atom-phonon-photon system can be written as

$$H = H_{\text{el}} + H_{\text{vib}} + H_{\text{col}} \tag{6.1}$$

in the Schroedinger picture. The first two terms in this equation are the free energy of the vibrational and the electronic states of the trapped particles. The third term models elastic collisions between the particles inside the bubble. Spontaneous emission from the atoms remains negligible. In this regime, the system evolves thermally and thermodynamical models can be used to describe its behaviour. In the following, we have a closer look at the terms in Eq. (6.1).

Electronic degrees of freedom

If we denote the ground state of atom i by $|0\rangle_i$ and its excited state by $|1\rangle_i$, respectively, the atomic Hamiltonian H_{el} can be written as

$$H_{\text{el}} = \sum_{i=1}^{N} \hbar\omega_0\, \sigma_i^+ \sigma_i^- , \tag{6.2}$$

where $\hbar\omega_0$ is the energy difference between electronic states. Moreover, $\sigma_i^+ \equiv |1\rangle_{ii}\langle 0|$ and $\sigma_i^- \equiv |0\rangle_{ii}\langle 1|$ are atomic raising and lowering operators with the commutator relation

$$[\sigma_i^+, \sigma_i^-] = 2\sigma_{3i} , \tag{6.3}$$

where σ_{3i} is as usual the Pauli operator defined by

$$\sigma_{3i} = \frac{1}{2} \left(|1\rangle_{ii}\langle 1| - |0\rangle_{ii}\langle 0| \right) . \tag{6.4}$$

Vibrational degrees of freedom

The presence of the bubble walls confines the position of the atomic particles in general so strongly that they do remain inside the bubble at all times. When the bubble radius approaches its minimum, the situation of the atomic particles becomes similar to the situation of ions inside an ion trap: their vibrational degrees of freedom need to be quantised. Approximating the trapping potential by a harmonic oscillator, the Hamiltonian for the vibrational energy of the atoms can simply be written as

$$H_{\text{vib}} \quad = \quad \sum_{i=1}^{N} \frac{p_i^2}{2M} + \frac{1}{2} M v^2 x_i^2 \,, \tag{6.5}$$

where M is the mass of a single atom and v denotes the respective trap frequency. Moreover, p_i is the momentum of particle i in the direction of the cavity axis and x_i denotes the distance of particle i from the centre of the trap.

To write the above Hamiltonian H_{vib} in a more compact form, we now introduce the single-particle phonon destruction and creation operators b_i and $b_i^\dagger$ with the bosonic commutator relation

$$[b_i, b_i^\dagger] \quad = \quad 1 \tag{6.6}$$

such that

$$\begin{aligned} p_i &= \text{i} \sqrt{\frac{\hbar M v}{2}} \left(b_i^\dagger - b_i \right) \,, \\ x_i &= \sqrt{\frac{\hbar}{2 M v}} \left(b_i + b_i^\dagger \right) \,. \end{aligned} \tag{6.7}$$

When substituting these operators into equation into Eq. (6.5), it simplifies to

$$H_{\text{vib}} \quad = \quad \sum_{i=1}^{N} \hbar v \left(b_i^\dagger b_i + \frac{1}{2} \right) \,. \tag{6.8}$$

The assumption of only a single harmonic trapping potential is valid as long as the particles are well localised around their equilibrium position. During the bubble collapse phase, it is known that the atoms form a so-called van der Waals crystal. They are not only trapped by the presence of the bubble walls but also by complex interactions with their surrounding particles. We therefore think that the above description of the motion of the particles is well justified.

Atomic collisions

The onset of sonoluminescence requires that the bubble is hot enough for the particles inside the bubble to form a plasma. This means, although strongly confined,

collisions between particles which result into an exchange of phonons and electronic excitations are no longer negligible. To take this into account, we assume in the following that we have elastic collisions between the particles. An additional term in the Hamiltonian H_{col} which describes these to a very good approximation is given by

$$H_{\mathrm{col}} \;=\; \sum_{\langle i,j \rangle} \hbar \Omega_{\mathrm{vib}} \, b_i^\dagger b_j + \hbar \Omega_{\mathrm{el}} \, \sigma_i^+ \sigma_j^- \;. \tag{6.9}$$

In the following, this Hamiltonian is taken into account during the thermalisation stage of the sonoluminescing bubble. On the other hand, Ω_{vib} and Ω_{el} remain negligible during the heating stage, as long as they are much smaller than the effective heating rate of the trapped particles. The sum in the above Hamiltonian is over all pairs $\langle i, j \rangle$ of next neighbours. In one dimension, their number scales as the number of atoms N in the trap.

6.2.2   Heating stage

During the heating stage, the Hamiltonian in Eq. (6.1) no longer applies. Additional terms due to the sudden presence of an almost resonant optical cavity have to be taken into account. The total Hamiltonian of the atom-phonon-photon system in the Schroedinger picture is now of the form

$$H \;=\; H_{\mathrm{el}} + H_{\mathrm{vib}} + H_{\mathrm{cav}} + H_{\mathrm{int}} \tag{6.10}$$

with H_{el} and H_{vib} being the same free energies as in the previous subsection. Now we are interested in a much shorter time scale on which collisions between the particles remain negligible. Instead the possible transfer of energy from the atoms into the cavity field, which changes the vibrational degrees of freedom of the system, has to be taken into account. The term H_{cav} describes the free energy of the quantised cavity field. The final term in Eq. (6.10) represents the atom-cavity-photon interaction. These two terms are explained below.

Cavity degrees of freedom

In the following, we describe the energy of the electromagnetic field between the bubble walls by the single-mode cavity Hamiltonian

$$H_{\mathrm{cav}} \;=\; \hbar \omega \, c^\dagger c \,, \tag{6.11}$$

where ω denotes the frequency of the photon mode. This frequency depends on the radius of the bubble which constantly changes in time. Moreover c is the cavity photon annihilation operator with

$$[c, c^\dagger] = 1. \tag{6.12}$$

The photon mode which we are interested in is the one with frequency ω that is the closest to the atomic transition frequency ω_0 in Eq. (6.2). Such mode is the cavity photon mode whose wavelength equals the bubble diameter, and its frequency ω will therefore will be dependent on the radius of the bubble λ.

Atom-phonon-photon interactions

In addition to the cavity energy, we need to account for the possible conversion of atomic excitation into cavity photons and vice versa. As before, we write the corresponding interaction Hamiltonian H_{int} in the usual dipole and rotating wave approximation,

$$H_{\text{int}} = \sum_{i=1}^{N} \hbar g \sin\left(kr_i\right) \sigma_i^+ c + \text{H.c.}, \tag{6.13}$$

where r_i denotes the absolute position of particle i within the resonator. Hence r_i is the sum of the equilibrium position R_i of the respective particle and its displacement x_i from the trap center such that

$$r_i = R_i + x_i. \tag{6.14}$$

Moreover g denotes the atom-cavity coupling constant and k is the wave vector of the standing-wave cavity field mode. Without restrictions, we can assume that g is real by absorbing any potential phase factor into the definition of the respective σ_i^- operator.

Suppose, the atomic particles accumulate predominantly in the center of the bubble during the bubble collapse phase. Then the equilibrium positions R_i of the confined particles coincide with the center of the bubble, which coincides with the node of the resonator field. Taking this into account, we find that

$$g \sin\left(kr_i\right) = \eta g \left(b_i + b_i^\dagger\right) + \mathcal{O}(\eta^3) \tag{6.15}$$

to a very good approximation, where the Lamb-Dicke parameter η is a measure for the strength of the external trapping potential defined earlier. For strongly confined particles, we have

$$\eta \ll 1 \tag{6.16}$$

and higher order terms in η become negligible.

Spontaneous photon emission

Taking the results of the previous subsections into account when substituting Eq. (6.15) into Eq. (6.13) and introducing the interaction picture with respect to the free Hamiltonian

$$H_0 = H_{\mathrm{el}} + \hbar\omega_0\, c^\dagger c\,, \tag{6.17}$$

we finally obtain the interaction Hamiltonian

$$H_{\mathrm{I}} = -\hbar\Delta\, c^\dagger c + \sum_{i=1}^{N} \hbar v\, b_i^\dagger b_i + \sum_{i=1}^{N} \hbar\eta g\, (b_i + b_i^\dagger)\, \sigma_i^+ c + \text{H.c.} \tag{6.18}$$

with the detuning Δ defined as the difference between the atomic and the cavity frequency,

$$\Delta \equiv \omega_0 - \omega\,. \tag{6.19}$$

A closer look at Eq. (6.18) shows that the presence of the cavity again results in an atom-phonon-photon interaction. As we shall see below, this interaction has the potential to significantly heat the atomic particles, even on a very short time scale.

In the following, we assume that the atomic particles are in general well shielded from the free radiation field surrounding the sonoluminescing bubble. During the thermalisation stage, the atomic density is relatively high and almost all atoms are fully surrounded by other particles. During the heating stage, the atomic particles are moreover surrounded by cavity mirrors so that there is effectively no coupling to the free radiation field outside the bubble. We therefore neglect direct spontaneous emission from the excited atomic states. The possible spontaneous photon emission of cavity photons into the surrounding liquid during the heating stage is in the following taken into account by the quantum optical master equation

$$\dot{\rho}_{\mathrm{I}} = -\frac{\mathrm{i}}{\hbar}\,[H_{\mathrm{I}}, \rho_{\mathrm{I}}] + \kappa\,\left(c\rho_{\mathrm{I}}c^\dagger - \tfrac{1}{2}c^\dagger c\rho_{\mathrm{I}} - \tfrac{1}{2}\rho_{\mathrm{I}}c^\dagger c\right)\,, \tag{6.20}$$

where κ is the cavity decay rate and where ρ_{I} denotes the density matrix of the atom-phonon-photon system in the interaction picture.

6.2.3 Notation

To simplify the following calculation, we now proceed as in chapter 5 and define the B, Σ, and C operators

$$
\begin{aligned}
\left(B_0^{(i)}, \Sigma_0^{(i)}, C_0 \right) &\equiv (1, 1, 1) \,, \\
\left(B_1^{(i)}, \Sigma_1^{(i)}, C_1 \right) &\equiv \left(b_i^\dagger b_i, \sigma_i^+ \sigma_i^-, c^\dagger c \right) \,, \\
\left(B_2^{(i)}, \Sigma_2^{(i)}, C_2 \right) &\equiv \left(b_i + b_i^\dagger, \sigma_i^- + \sigma_i^+, c + c^\dagger \right) \,, \\
\left(B_3^{(i)}, \Sigma_3^{(i)}, C_3 \right) &\equiv \mathrm{i} \left(b_i - b_i^\dagger, \sigma_i^- - \sigma_i^+, c - c^\dagger \right) \,.
\end{aligned}
\tag{6.21}
$$

To calculate the time derivatives of expectation values, we need to derive commutators of their respective operators and of all the operators in the Hamiltonian. Using Eqs. (6.3), (6.6), and (6.12) one can show that

$$
\begin{aligned}
\left[\Sigma_1^{(i)}, \Sigma_2^{(i)} \right] &= \mathrm{i}\Sigma_3^{(i)} \,, \\
\left[\Sigma_1^{(i)}, \Sigma_3^{(i)} \right] &= -\mathrm{i}\Sigma_2^{(i)} \,, \\
\left[\Sigma_2^{(i)}, \Sigma_3^{(i)} \right] &= -2\mathrm{i}\left(1 - 2\Sigma_1^{(i)} \right) \,, \\
\left[B_1^{(i)}, B_2^{(i)} \right] &= \mathrm{i}B_3^{(i)} \,, \\
\left[B_1^{(i)}, B_3^{(i)} \right] &= -\mathrm{i}B_2^{(i)} \,, \\
\left[B_2^{(i)}, B_3^{(i)} \right] &= -2\mathrm{i} \,, \\
\left[C_1, C_2 \right] &= \mathrm{i}C_3 \,, \\
\left[C_1, C_3 \right] &= -\mathrm{i}C_2 \,, \\
\left[C_2, C_3 \right] &= -2\mathrm{i} \,,
\end{aligned}
\tag{6.22}
$$

while

$$
\left[A_1^{(i)}, A_2^{(j)} \right] = 0
\tag{6.23}
$$

for arbitrary operators $A_1^{(i)}$ and $A_2^{(j)}$ with $i \neq j$. Since the operators in Eq. (6.21) obey relatively straight-forward commutator relations, we now introduce the short-hand-notation

$$
\begin{aligned}
M_{\mathrm{vib}} &\equiv \frac{1}{4}\hbar\Omega_{\mathrm{vib}} \sum_{\langle i,j \rangle} \left(B_2^{(i)} B_2^{(j)} + B_3^{(i)} B_3^{(j)} \right) \\
M_{\mathrm{el}} &\equiv \frac{1}{4}\hbar\Omega_{\mathrm{el}} \sum_{\langle i,j \rangle} \left(\Sigma_2^{(i)} \Sigma_2^{(j)} + \Sigma_3^{(i)} \Sigma_3^{(j)} \right)
\end{aligned}
\tag{6.24}
$$

and write the interaction Hamiltonian H_I in Eq. (6.18) in the following as

$$H_I = \sum_{i=1}^{N} \frac{1}{2} \hbar \eta g \, B_2^{(i)} \left(\Sigma_2^{(i)} C_2 + \Sigma_3^{(i)} C_3 \right) + \sum_{i=1}^{N} \hbar v \, B_1^{(i)} - \hbar \Delta \, C_1 \quad (6.25)$$

to simplify the derivation of effective rate equations for the heating stage.

6.3   Thermalisation stage

In this chapter, we distinguish between two different stages in the dynamics of a sonoluminescing bubble. As long as the bubble radius is relatively large and the walls of the bubble remain transparent, there is effectively no cavity field and the atomic particles evolve on a relatively slow time scale. We refer to this stage in the following as the *thermalisation stage*. Indeed, it has been found that the time evolution of the bubble is very well described by the laws of classical thermodynamics. This only changes, when the bubble radius collapses. We refer to this stage in the following as the *heating stage* and analyse its dynamics in detail in Section 6.4. But before doing so, let us have a look at the thermalisation stage.

In this section, we assume that the time evolution of the electronic and the vibrational degrees of freedom of the particles inside the bubble is governed by thermal processes. For simplicity, we assume that there is effectively no exchange of energy with the surrounding liquid. The energy within the bubble is simply redistributed among the different degrees of freedom, while each particle reaches a thermal equilibrium state with respect to the surrounding particles. Since there are no interactions between phonons and atomic excitations, the density matrix ρ of the atomic particles at the end of the thermalisation stage can be written as

$$\rho = \rho_{\text{vib}} \otimes \rho_{\text{el}} . \quad (6.26)$$

As we shall see in the next section, heating of the atomic particles inside the bubble requires the presence of certain non-zero expectation values. In the remainer of this section, we calculate those expectation values for the density matrix in Eq. (6.26).

6.3.1   Relevant expectation values

These include the mean phonon number averaged over all particles which is given by

$$m \equiv \frac{1}{N} \sum_{i=1}^{N} \langle B_1^{(i)} \rangle . \quad (6.27)$$

Here m is normalised such that it does not change considerably, when atomic particles are either removed from or added to the trap. Another phonon expectation value which plays a crucial role during the heating stage is the phonon coherence

$$\zeta \;\equiv\; \frac{1}{N(N-1)} \sum_{i=1}^{N} \sum_{j \neq i} \langle b_i^\dagger b_j \rangle \,. \tag{6.28}$$

Both operators, the one corresponding to m and the one corresponding to ζ, commute with the free energy of the phonons given by H_{vib}. As we shall see below, they hence evolve on a relatively slow time scale during the heating stage.

Moreover, we shall see in the next section, that the mean population in excited atomic states plays a crucial role in the heating dynamics of the atomic particles inside the sonoluminescing bubble. In analogy to m in Eq. (6.27), we hence now define

$$s \;\equiv\; \frac{1}{N} \sum_{i=1}^{N} \langle \Sigma_1^{(i)} \rangle \,. \tag{6.29}$$

Moreover we need to consider the expectation values

$$\mu_{ab} \;\equiv\; \frac{1}{N(N-1)} \sum_{i=1}^{N} \sum_{j \neq i} \langle \Sigma_a^{(i)} \Sigma_b^{(j)} \rangle \tag{6.30}$$

with $a, b = 2, 3$ and with $\mu_{ab} \equiv \mu_{ba}$ by definition.

6.3.2 Electronic degrees of freedom

In the following, we neglect spontaneous emission from the excited states of the atomic particles. Instead we assume that the processes which excite the atoms due to thermal interactions dominate the time evolution of the particles. In this case, the density matrix ρ_{el} of the thermal state of the electronic degrees of freedom of the trapped particles equals

$$\rho_{\mathrm{el}} \;=\; \frac{1}{Z_{\mathrm{el}}} \, \mathrm{e}^{-\beta H} \tag{6.31}$$

with $Z_{\mathrm{el}} = \mathrm{Tr}\left(\mathrm{e}^{-\beta H} \right)$ being a partition function and with the relevant interaction Hamiltonian given by

$$H \;=\; H_{\mathrm{el}} + M_{\mathrm{el}} \,. \tag{6.32}$$

Using Eq. (6.2) and setting $\Omega_{\mathrm{el}} = 0$, yields

$$\rho_{\mathrm{el}} \;=\; \frac{|0\rangle \langle 0| + \mathrm{e}^{-\beta \hbar \omega_0} |1\rangle \langle 1|}{1 + \mathrm{e}^{-\beta \hbar \omega_0}} \tag{6.33}$$

which implies

$$s = \frac{e^{-\beta\hbar\omega_0}}{1 + e^{-\beta\hbar\omega_0}} \tag{6.34}$$

in zeroth order in Ω_{el}. The constant β in this equation is the same as in Eq. (6.40). For relatively hot particles, a non-negligible amount of population accumulates in the excited atomic state.

To calculate μ_{22} and μ_{33} with collisions taken into account, we split the Hamiltonian into the non-interacting and interacting part,

$$H = H_{el} + M_{el} = \hbar\omega_0 \sum_i \sigma_i^+ \sigma_i^- + \hbar\Omega_{el} \sum_{\langle i,j \rangle} \sigma_i^+ \sigma_j^- . \tag{6.35}$$

Using the Taylor expansion and the Baker-Campbell-Hausdorff formula, we can show that

$$e^{-\beta H} = e^{-\beta(H_{el}+M_{el})} = e^{-\beta H_{el}} \left(1 - \beta M_{el} - \frac{1}{2}\beta^2 [H_{el}, M_{el}] \right) + \dots . \tag{6.36}$$

The commutator on the right vanishes and we can write

$$\mu_{22} = \frac{1}{N(N-1)} \frac{1}{Z} \sum_{i=1}^{N} \sum_{j\neq i} \mathrm{tr}\left(e^{-\beta H_{el}} (1 - \beta M_{el}) (\sigma_i^- + \sigma_i^+)(\sigma_j^- + \sigma_j^+) \right) . \tag{6.37}$$

Taking the trace in the basis of atomic states $|0\rangle$ and $|1\rangle$ means that only a few terms remain,

$$\mu_{22} = -\frac{\beta\hbar\Omega_{el}}{N(N-1)} \sum_{i=1}^{N} \sum_{j\neq i} \langle \sigma_i^+ \sigma_i^- \sigma_j^- \sigma_j^+ \rangle$$

$$= \beta\hbar\Omega_{el} \left(s^2 - s \right) = \mu_{33} \tag{6.38}$$

In addition to these, we find that

$$\mu_{23} = \mu_{32} = 0 . \tag{6.39}$$

6.3.3 Vibrational degrees of freedom

The density matrix ρ_{vib} of the thermal state of the vibrational degrees of freedom of the trapped particles equals

$$\rho_{vib} = \frac{1}{Z_{vib}} e^{-\beta H} , \tag{6.40}$$

where the Hamiltonian H describes the motional degrees of freedom. Using the notation introduced in Section 6.2.3, it equals

$$H = H_{\text{vib}} + M_{\text{vib}}. \tag{6.41}$$

Moreover, $Z_{\text{vib}} = \text{Tr}\left(e^{-\beta H}\right)$ is a partition function and β is the thermal parameter which depends on the total energy of the trapped atoms at the beginning of the thermalisation stage. In the absence of any collisions ($\Omega_{\text{vib}} = 0$), the expectation value for the mean number of excitations in this thermal state of a single harmonic oscillator with Hamiltonian H_{vib} is well known and equals (cf. Blaise & Henri-Rousseau (2011))

$$m = \frac{1}{e^{\beta\hbar\nu} - 1} \tag{6.42}$$

for $e^{\beta\hbar\nu} < 1$. To calculate ζ for the case where $\Omega_{\text{vib}} = 0$, we notice that there are no interactions between the particles and that there is no flux of particles out of the trap. Hence the above thermal state is a product state with

$$\langle x_i x_j \rangle = \langle x_i \rangle \langle x_j \rangle \tag{6.43}$$

and

$$\langle p_i p_j \rangle = \langle p_i \rangle \langle p_j \rangle = 0 \tag{6.44}$$

for all particles i and j. Combining this observation with Eqs. (6.7) and (6.28) yields

$$\zeta = \frac{M\nu}{2\hbar} \langle x \rangle^2 \tag{6.45}$$

without any approximations, where $\langle x \rangle$ is the mean distance of the atoms from the trap center. Hence $\zeta = 0$ for a perfectly symmetric trap when $\Omega_{\text{vib}} = 0$.

However, this no longer applies for $\Omega_{\text{vib}} \neq 0$. Using Eq. (6.41) together with Eq. (6.36), we can calculate the expectation value ζ as

$$\zeta = -\frac{\beta\hbar\Omega_{\text{vib}}}{N(N-1)} \sum_{i=1}^{N} \sum_{j\neq i} \langle b_i^\dagger b_i (b_j^\dagger b_j + 1) \rangle$$

$$= -\beta\hbar\Omega_{\text{vib}} m(m+1). \tag{6.46}$$

As we will see later, evolution of this coherence during the heating stage translates into the change in temperature, and Eq. (6.46) shows that it only vanishes for $m = 0$.

6.3.4 Cavity degrees of freedom

During the thermalisation phase, the bubble walls remain transparent and there is no need to quantise the light inside the bubble. At the end of the thermalisation phase, when the walls of the bubble become opaque, this situation changes. However, we can safely assume that the cavity field is at this stage in its vacuum state, although the characteristic frequencies of the atoms and the cavity are of comparable size. Instead of thermalising, the cavity field interacts with the atoms, as described in the next section.

6.4 Heating stage

The heating phase begins, when the walls of the sonoluminescing bubble become opaque. This is when the electromagnetic field inside the bubble becomes quantised and the interaction between the atoms, the phonons and the cavity photons inside the bubble is no longer negligible. To describe their dynamics, we make in the following extensive use of Eqs. (6.18) and (6.20). For example, Eq. (6.20) can be used to show that any expectation value of a time-independent observable A_I in the interaction picture evolves according to the differential equation

$$\langle \dot{A}_I \rangle \;=\; -\frac{i}{\hbar} \left\langle [A_I, H_I] \right\rangle + \kappa \left\langle c^\dagger A_I c - \tfrac{1}{2} A_I c^\dagger c - \tfrac{1}{2} c^\dagger c A_I \right\rangle . \tag{6.47}$$

In the following, we refer to equations of this form as rate equations.

The calculations in the following section rely on several quantum optical standard approximations. For example, we assume that

$$\nu, \kappa \;\gg\; \eta g . \tag{6.48}$$

Another approximation which we use below is the so-called Lamb-Dicke approximation based on Eq. (6.16). Moreover we are especially interested in the heating of a relatively large cloud of atomic particles,

$$N \;\gg\; 1 . \tag{6.49}$$

Subsequently, we only take terms which dominate the heating process into account. As we shall see below, these terms scale as $N\eta^2$.

6.4.1 Additional expectation values

As we shall see below, to obtain a closed set of rate equations, including one for the mean phonon number m, we need to consider the time evolution of the single-

particle expectation values x_{abc} and the two-particle expectation values $\tilde{x}_{abc}$ given by

$$
\begin{aligned}
x_{abc} &\equiv \frac{1}{N} \sum_{i=1}^{N} \left\langle B_a^{(i)} \Sigma_b^{(i)} C_c \right\rangle, \\
\tilde{x}_{abc} &\equiv \frac{1}{N(N-1)} \sum_{i=1}^{N} \sum_{j\neq i} \left\langle B_a^{(i)} \Sigma_b^{(j)} C_c \right\rangle, \\
\hat{x}_{abcd} &\equiv \frac{1}{N(N-1)} \sum_{i=1}^{N} \sum_{j\neq i} \left\langle B_a^{(i)} \Sigma_b^{(i)} \Sigma_c^{(j)} C_d \right\rangle.
\end{aligned}
\tag{6.50}
$$

All of the above expectation values correspond to operators which contain a non-trivial cavity photon component. They hence evolve on the relatively fast time scales given by the cavity decay rate κ and the collective cavity coupling constant $N\eta g$. In addition we need to consider the two and three particle atom-phonon expectation values y_{abcd}, $\tilde{y}_{abcd}$, and $\hat{y}_{abcde}$ defined as

$$
\begin{aligned}
y_{abcd} &\equiv \frac{1}{N(N-1)} \sum_{i=1}^{N} \sum_{j\neq i} \langle B_a^{(i)} B_b^{(j)} \Sigma_c^{(i)} \Sigma_d^{(j)} \rangle, \\
\tilde{y}_{abcd} &\equiv \frac{1}{N(N-1)(N-2)} \sum_{i=1}^{N} \sum_{j\neq i} \sum_{k\neq i,j} \langle B_a^{(i)} B_b^{(k)} \Sigma_c^{(j)} \Sigma_d^{(k)} \rangle, \\
\hat{y}_{abcde} &\equiv \frac{1}{N(N-1)(N-2)} \sum_{i=1}^{N} \sum_{j\neq i} \sum_{k\neq i,j} \langle B_a^{(i)} B_b^{(k)} \Sigma_c^{(i)} \Sigma_d^{(j)} \Sigma_e^{(k)} \rangle.
\end{aligned}
\tag{6.51}
$$

The normalisation of the right hand sides of these equations has again been chosen such that they are effectively single-particle measures and therefore in general independent of the exact number N of atoms in the trap.

6.4.2 Time evolution in first order in η

The purpose of this section is to analyse the time evolution of the average mean phonon number m during the heating stage. Before doing so, we emphasize again that we are only interested in very tightly confined particles (cf. Eq. (6.48)). Hence the expectation values of phonon operators evolve in general on the time scale given by the phonon frequency ν. This means, they oscillate effectively around zero and can be neglected. The only exception are the variables defined in Eqs. (6.27) and (6.28). Using Eqs. (6.25) and (6.47) and neglecting collisions between the particles, one can show that m and ζ both evolve on a relatively slow time scale. Their time

derivatives are given by

$$\dot{m} = \frac{1}{2}\eta g \, (x_{322} + x_{333}) \,,$$

$$\dot{\zeta} = \frac{1}{2}\eta g \, (\tilde{x}_{322} + \tilde{x}_{333}) \tag{6.52}$$

without any approximations other than $\Omega_{\text{vib}} = \Omega_{\text{el}} = 0$. In addition, we need to have a closer look at the atomic variables defined in Section 6.3.1. Proceeding as above, one can show that these evolve according to

$$\dot{\mu}_{22} = -2\eta g \, \tilde{x}_{223} + 4\eta g \, \hat{x}_{2123} \,,$$

$$\dot{\mu}_{23} = \eta g \, (\tilde{x}_{222} - \tilde{x}_{233}) - 2\eta g \, (\hat{x}_{2122} - \hat{x}_{2133}) \,,$$

$$\dot{\mu}_{33} = 2\eta g \, \tilde{x}_{232} + 4\eta g \, \hat{x}_{2132} \,, \tag{6.53}$$

again without any approximations other than neglecting collisions. To analyse the dynamics of the above rate equations, we now have a closer look at the rate equations of the x-expectation values and their tilde counterparts.

6.4.3   Relevant time evolution in zeroth order in η

All of the single-particle x-expectation values are equal to zero in zeroth order in η. However, when the number of confined particles N is large (cf. Eq. (6.49)), then ηN is effectively a term in zeroth order in η. Taking this into account, one can show that the expectation values x_{abc} with $a, c = 2, 3$ evolve according to

$$\dot{x}_{2b2} = -\nu \, x_{3b2} + \Delta \, x_{2b3} - N\eta g \, y_{22b3} - \frac{1}{2}\kappa \, x_{2b2} \,,$$

$$\dot{x}_{2b3} = -\nu \, x_{3b3} - \Delta \, x_{2b2} + N\eta g \, y_{22b2} - \frac{1}{2}\kappa \, x_{2b3} \,,$$

$$\dot{x}_{3b2} = \nu \, x_{2b2} + \Delta \, x_{3b3} - N\eta g \, y_{32b3} - \frac{1}{2}\kappa \, x_{3b2} \,,$$

$$\dot{x}_{3b3} = \nu \, x_{2b3} - \Delta \, x_{3b2} + N\eta g \, y_{32b2} - \frac{1}{2}\kappa \, x_{3b3} \tag{6.54}$$

in zeroth order in η. Here we discarded all relatively small terms which scale as ηg due to the time scale separation introduced earlier in Eq. (6.48). Analogously, one can show that

$$\dot{\tilde{x}}_{2b2} = -\nu \, \tilde{x}_{3b2} + \Delta \, \tilde{x}_{2b3} - N\eta g \, \tilde{y}_{22b3} - \frac{1}{2}\kappa \, \tilde{x}_{2b2} \,,$$

$$\dot{\tilde{x}}_{2b3} = -\nu \, \tilde{x}_{3b3} - \Delta \, \tilde{x}_{2b2} + N\eta g \, \tilde{y}_{22b2} - \frac{1}{2}\kappa \, \tilde{x}_{2b3} \,,$$

$$\dot{\tilde{x}}_{3b2} = \nu \, \tilde{x}_{2b2} + \Delta \, \tilde{x}_{3b3} - N\eta g \, \tilde{y}_{32b3} - \frac{1}{2}\kappa \, \tilde{x}_{3b2} \,,$$

$$\dot{\tilde{x}}_{3b3} = \nu \, \tilde{x}_{2b3} - \Delta \, \tilde{x}_{3b2} + N\eta g \, \tilde{y}_{32b2} - \frac{1}{2}\kappa \, \tilde{x}_{3b3} \tag{6.55}$$

in zeroth order in η. These equations are the same as in Eq. (6.54) but with the x-variables replaced by $\tilde{x}$-expectation values and the y-variables replaced by their respective three-particle expectation values $\tilde{y}$. Analogously, one can show that the x_{abcd}-expectation values evolve according to the differential equations

$$
\begin{aligned}
\dot{\hat{x}}_{2122} &= -\nu\,\hat{x}_{3122} + \Delta\,\hat{x}_{2123} - N\eta g\,\hat{y}_{22122} - \frac{1}{2}\kappa\,\hat{x}_{2122}\,,\\
\dot{\hat{x}}_{2123} &= -\nu\,\hat{x}_{3123} - \Delta\,\hat{x}_{2122} + N\eta g\,\hat{y}_{22123} - \frac{1}{2}\kappa\,\hat{x}_{2123}\,,\\
\dot{\hat{x}}_{2132} &= -\nu\,\hat{x}_{3132} + \Delta\,\hat{x}_{2133} - N\eta g\,\hat{y}_{22132} - \frac{1}{2}\kappa\,\hat{x}_{2132}\,,\\
\dot{\hat{x}}_{2133} &= -\nu\,\hat{x}_{3133} - \Delta\,\hat{x}_{2132} + N\eta g\,\hat{y}_{22133} - \frac{1}{2}\kappa\,\hat{x}_{2133}\,,
\end{aligned}
\tag{6.56}
$$

while

$$
\begin{aligned}
\dot{\hat{x}}_{3122} &= \nu\,\hat{x}_{2122} + \Delta\,\hat{x}_{3123} - N\eta g\,\hat{y}_{32122} - \frac{1}{2}\kappa\,\hat{x}_{3122}\,,\\
\dot{\hat{x}}_{3123} &= \nu\,\hat{x}_{2123} - \Delta\,\hat{x}_{3122} + N\eta g\,\hat{y}_{32123} - \frac{1}{2}\kappa\,\hat{x}_{3123}\,,\\
\dot{\hat{x}}_{3132} &= \nu\,\hat{x}_{2132} + \Delta\,\hat{x}_{3133} - N\eta g\,\hat{y}_{32132} - \frac{1}{2}\kappa\,\hat{x}_{3132}\,,\\
\dot{\hat{x}}_{3133} &= \nu\,\hat{x}_{2133} - \Delta\,\hat{x}_{3132} + N\eta g\,\hat{y}_{32133} - \frac{1}{2}\kappa\,\hat{x}_{3133}\,.
\end{aligned}
\tag{6.57}
$$

We now need to have a closer look at the y-expectation values in Eqs. (6.54)–(6.57).

As long as we are only interested in the time evolution of the mean phonon number m on the relatively slow time scale given by ηg, the dynamics of the x-expectation values needs to be analysed only in zeroth order in η. Doing so, we notice that none of the time derivatives of the y expectation values scales as $N\eta g$. The interactions between the different particles during the heating stage play no role in their time evolution. Hence, the y-expectation values in Eq. (6.51) are to a very good approximation given by

$$
\begin{aligned}
y_{abcd} &= \frac{1}{N(N-1)}\sum_{i=1}^{N}\sum_{j\neq i}\langle B_a^{(i)}B_b^{(j)}\rangle\langle \Sigma_c^{(i)}\Sigma_d^{(j)}\rangle\\[4pt]
\tilde{y}_{abcd} &= \frac{1}{N(N-1)(N-2)}\sum_{i=1}^{N}\sum_{j\neq i}\sum_{k\neq i,j}\langle B_a^{(i)}B_b^{(k)}\rangle\langle \Sigma_c^{(j)}\Sigma_d^{(k)}\rangle,\\[4pt]
\hat{y}_{abcde} &= \frac{1}{N(N-1)(N-2)}\sum_{i=1}^{N}\sum_{j\neq i}\sum_{k\neq i,j}\langle B_a^{(i)}B_b^{(k)}\rangle\langle \Sigma_c^{(i)}\rangle\langle \Sigma_d^{(j)}\Sigma_e^{(k)}\rangle.
\end{aligned}
\tag{6.58}
$$

6.4.4   Weak-excitations regime

The two-particle correlations in the above equations come from the thermal state which has previously been created during the thermalisation stage. In the following, we assume that the expectation value of $\Sigma_1^{(i)}$, i.e. the variable s, is in general very small ($s \ll 1$). Moreover, one can show that most phonon expectation values evolve rapidly on the time scale given by the phonon frequency v with m and ζ being the only exceptions. Taking this into account and replacing the above expectation values by their respective particle averages, we find that

$$y_{22cd} = \tilde{y}_{22cd} = 2\zeta\,\mu_{cd}\,,$$

$$y_{32cd} = \tilde{y}_{32cd} = \hat{y}_{221de} = \hat{y}_{321de} = 0\,. \tag{6.59}$$

Moreover, due to the above mentioned time scale separation, the rate equations of the x-coherences can be solved via an adiabatic evolution. This yields

$$x_{2b2} = \frac{4N\eta g}{K}\left[2\Delta(\kappa^2 - 4v^2 + 4\Delta^2)\mu_{b2} - \kappa(\kappa^2 + 4v^2 + 4\Delta^2)\mu_{b3}\right]\zeta\,,$$

$$x_{2b3} = \frac{4N\eta g}{K}\left[\kappa(\kappa^2 + 4v^2 + 4\Delta^2)\mu_{b2} + 2\Delta(\kappa^2 - 4v^2 + 4\Delta^2)\mu_{b3}\right]\zeta\,,$$

$$x_{3b2} = \frac{8N\eta gv}{K}\left[4\kappa\Delta\,\mu_{b2} - (\kappa^2 + 4v^2 - 4\Delta^2)\mu_{b3}\right]\zeta\,,$$

$$x_{3b3} = \frac{8N\eta gv}{K}\left[(\kappa^2 + 4v^2 - 4\Delta^2)\mu_{b2} + 4\kappa\Delta\,\mu_{b3}\right]\zeta \tag{6.60}$$

with the constant K defined as

$$K \equiv \kappa^4 + 16(\Delta^2 - v^2)^2 + 8\kappa^2(\Delta^2 + v^2)\,. \tag{6.61}$$

Exactly the same equations apply for the respective $\tilde{x}$-xpectation values. Moreover, we find that

$$\hat{x}_{21cd} = 0 \tag{6.62}$$

to a very good approximation. Substituting these x-variables into Eqs. (6.52) and (6.53) yields a closed set of five effective heating equations.

6.4.5   Effective heating equations

We get effective heating equations, when substituting the results of the adiabatic elimination in the previous subsection into Eqs. (6.52) and (6.53). These are given by

$$\dot{m} = \dot{\zeta} = \frac{16N\eta^2 g^2 v\kappa\Delta}{K}\left(\mu_{22} + \mu_{33}\right)\zeta \tag{6.63}$$

and

$$\dot{\mu}_{22} = -\frac{8N\eta^2 g^2}{K}\left[\kappa(\kappa^2 + 4v^2 + 4\Delta^2)\mu_{22} - 2\Delta(\kappa^2 - 4v^2 + 4\Delta^2)\mu_{23}\right]\zeta,$$

$$\dot{\mu}_{23} = \frac{8N\eta^2 g^2}{K}\left[\Delta(\kappa^2 - 4v^2 + 4\Delta^2)\left(\mu_{22} - \mu_{33}\right) - \kappa(\kappa^2 + 4v^2 + 4\Delta^2)\mu_{23}\right]\zeta,$$

$$\dot{\mu}_{33} = -\frac{8N\eta^2 g^2}{K}\left[-2\Delta(\kappa^2 - 4v^2 + 4\Delta^2)\mu_{23} + \kappa(\kappa^2 + 4v^2 + 4\Delta^2)\mu_{33}\right]\zeta, \quad (6.64)$$

since μ_{23} and μ_{32} are exactly the same.

When having a closer look at the above equations, we notice that μ_{23} does not evolve in time, as long as $\mu_{23} = 0$ and $\mu_{22} = \mu_{33}$. Since this is the case at the beginning of the heating stage, as was outlined in the previous section, the above equations simplify effectively to only three equations

$$\dot{m} = \dot{\zeta},$$
$$\dot{\zeta} = \frac{16N\eta^2 g^2 \kappa}{K} v\Delta\,\mu\zeta,$$
$$\dot{\mu} = -\frac{16N\eta^2 g^2 \kappa}{K}(\kappa^2 + 4v^2 + 4\Delta^2)\,\mu\zeta, \quad (6.65)$$

after introducing the new variable μ as

$$\mu \equiv \mu_{22} + \mu_{33}. \quad (6.66)$$

As long as the detuning Δ (cf. Eq. (6.19)) is positive, and μ and ζ both have the same sign, as it is in general the case during the phase of the bubble collapse, the average mean phonon number m and the phonon expectation value ζ increase rapidly in time at the expense of the electronic expectation value μ. As mentioned already in the introduction, the thermalisation stage creates a resource, namely μ, which fuels a collectively-enhanced heating process during the bubble collapse phase.

The analysis of Eqs. (6.65) shows that

$$\dot{m} = \dot{\zeta}$$
$$\dot{\zeta} = C_1 \left(C_0 - C_2\zeta\right)\zeta,$$
$$\dot{\mu} = -C_1\Delta(C_0 - \mu)\mu \quad (6.67)$$

where

$$C_1 = \frac{16N\eta^2 g^2 \kappa v}{K}, \quad C_2 = \frac{\kappa^2 + 4v^2 + 4\Delta^2}{v}, \quad (6.68)$$

which are positive, and

$$C_0 = \Delta\mu_0 + C_2\zeta_0. \quad (6.69)$$

Eqs. (6.67) have the solutions

$$\zeta(t) = \frac{C_0 \zeta_0}{e^{-C_0 C_1 v t}(C_0 - C_2 \zeta_0) + C_2 \zeta_0},$$

$$\mu(t) = \frac{C_0 \mu_0}{e^{C_0 C_1 \Delta t}(C_0 - \mu_0) + \mu_0}, \tag{6.70}$$

where

$$\zeta_0 = \zeta(0),$$

$$\mu_0 = \zeta(0) \tag{6.71}$$

are the initial values of the atomic coherences at the beginning of the heating stage. We immediately see that for $\zeta_0 = 0$, the coherence $\zeta(t)$ remains zero during the entire process, and it follows from Eq. (6.67) that $\dot{m} = 0$, and no heating occurs. For $\zeta_0 \neq 0$, the coherence $\zeta(t)$ approaches the stationary state

$$\lim_{t \to \infty} \zeta(t) = \zeta_0 + \frac{\Delta \mu_0}{C_2}, \tag{6.72}$$

which means that the total change in ζ, and hence in m, is

$$\mathrm{d}m = \mathrm{d}\zeta = \frac{\Delta v \mu_0}{\kappa^2 + 4v^2 + 4\Delta^2}. \tag{6.73}$$

Therefore, we need both atomic coherences to maintain the heating process. Solutions in Eqs. (6.70) are plotted in Fig. 6.2 which shows that the evolution of $\zeta(t)$ is strongly dependent on the evolution of $\mu(t)$. As the electronic coherence $\mu(t)$ decays to zero, the growth of $\zeta(t)$ stops and heating no longer occurs.

6.5 Discussion

As mentioned earlier, the model in the chapter is a toy model and provides the quantum description of the heating mechanism of sonoluminescence. Fig. 6.2 shows that the system of time-dependent differential equations in Eq. (6.67) describes an increasing average mean phonon number of the atomic system and that this increase is strongly dependent on existence of electronic excitations of the atoms, which are characterised by $\mu(t)$.

In addition, we would like to remark on how luminous intensity of the single bubble sonoluminescence translates into temperature of different atomic systems. Eq. (6.42) relates the average mean phonon number m to the eigenfrequency of the
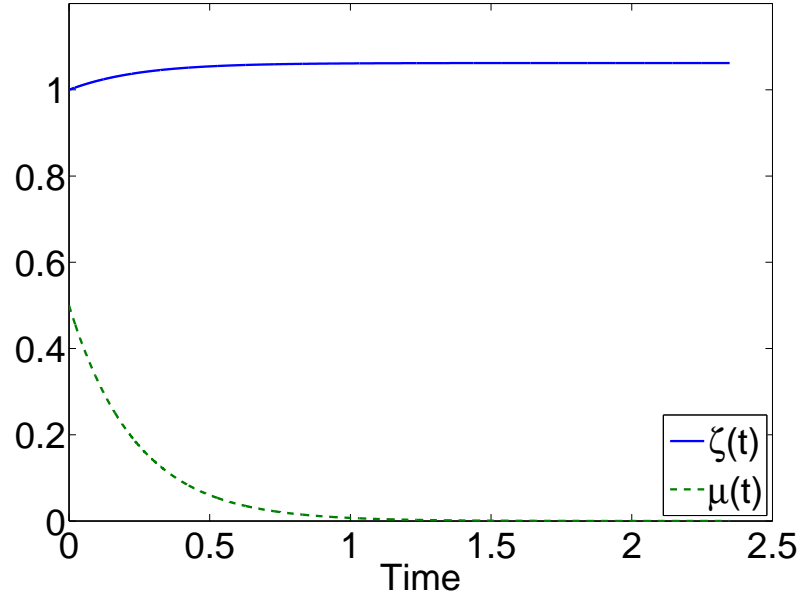
Figure 6.2: The evolution of the phonon coherence $\zeta(t)$ and the electronic coherence $\mu(t)$ during the heating stage, as described by Eqs. (6.70). Eqs. (6.67) show, that the change in the average mean phonon number is equal to the change in the phonon coherence $\zeta(t)$. Both are fueled by the electronic coherence $\mu(t)$, which vanishes during the heating stage, at which point the heating stops.

atomic motion v. The eigenfrequency is given in terms of atomic position deviation x as

$$v = \frac{\hbar}{2Mx^2} \, . \tag{6.74}$$

Assuming that the particles occupy a fraction f of the total bubble volume, the position x is related to the dimensions of the bubble as

$$Nx^3 = \frac{4}{3}f\pi\lambda^3 \, , \tag{6.75}$$

where λ is the radius of the bubble. Therefore, the increase in the average mean phonon number dm in Eq. (6.73) can be linked to change in temperature dT via Eq. (6.42), which results in

$$\frac{\Delta v\mu_0}{\kappa^2 + 4v^2 + 4\Delta^2} = \frac{1}{e^{\frac{\hbar v}{kB(T_0 + dT)}} - 1} - \frac{1}{e^{\frac{\hbar v}{T_0}} - 1} \, , \tag{6.76}$$

where T_0 is the initial temperature, v follows Eq. (6.74) and μ_0 follows Eq. (6.38). Assuming the number of excited atoms Ns follows the luminous intensity of the radiating bubble, we can solve Eq. (6.76) for the temperature increase dT. Fig. 6.3 shows that our model predicts the temperature difference to be higher for already brighter, and hence hotter, noble gases, which occurs as we go down the periodic table.
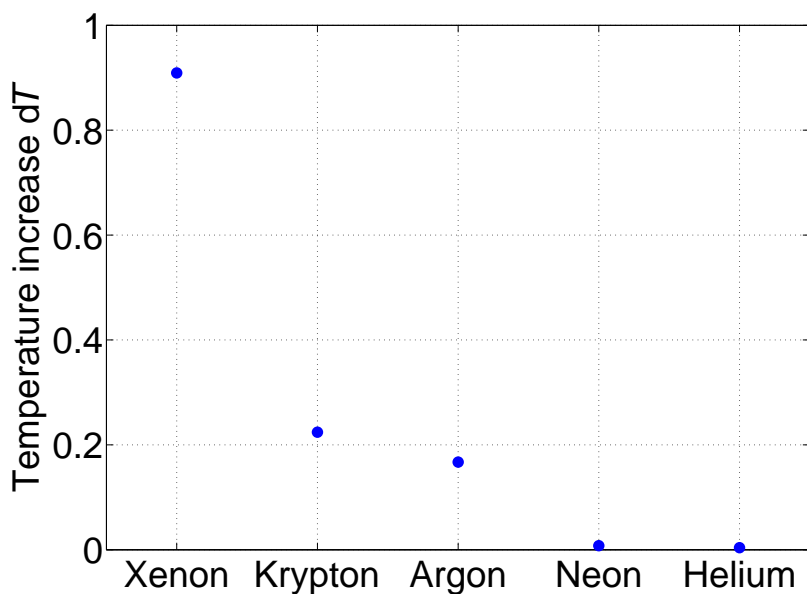
Figure 6.3: Dependence of the temperature rise on the atomic species in the radiating bubble. Noble gases with large atomic masses produce light with higher intensity and undergo stronger heating.

6.6 Conclusions

In this chapter, we identified major heating properties of sonoluminescence of single cavitating bubbles. We showed how a two-stage quantum model, which implements processes of thermalisation and quantum optical approaches, can explain the collective heating effect of sonoluminescence. The collective heating occurs during the collapse phase of the bubble lifecycle, which is preceded by a growth phase, during which the radius of the bubble gradually increases. In our model, we showed that strong collective heating strongly depends on atomic coherences which are generated beforehand by the thermalisation of the growth phase. Therefore, the thermalisation stage and the heating stage are closely connected and both are necessary to explain

the sonoluminescence cycle. In addition, we demonstrated how creation of plasma is necessary for heating by taking atomic collisions into account and how the final temperature is dependent on the atomic species present in the bubble. Overall, our many-body toy model identifies main additional heating mechanisms of sonoluminescence and provides a relatively simple theoretical description.

Chapter 7

Conclusions

In this thesis, we developed and analysed a quantum-mechanical model for collective cooling and heating of a many-body atomic system. Our model consists of a two-stage process, where we employ quantum-optical models together with the framework of thermodynamics. The entire process is split into a thermalisation stage, where necessary coherences between multiple particles are being created, and a cooling or heating stage, where the coherences mentioned above fuel the cooling or heating process and create a new stationary state. The symbiosis of the two stages results in suitable description of collective dynamics of the many-body atomic system.

The cooling stage of the full framework was first applied to a single atom confined within an optical resonator. The quantum-optical cooling model is based on applying the master equation to the atomic system strongly coupled to a single-mode optical cavity. The Jaynes-Cummings model serves as the foundation of the theoretical picture used to describe the atomic system. The rate equations obtained using the master equation were solved to show that the single-atom system reaches a stationary state where the final temperature is minimised for three distinct resonances.

The triplet of resonances consist of the well-known red sideband of free space laser cooling as well as two additional resonances separated from the red sideband by the laser Rabi frequency, and therefore resembles the free space Mollow triplet. It was shown that for a wide range of experimental parameters, one of the newly found resonances yields the lowest mean phonon number stationary state of all three. Therefore, driving the system on that resonance instead of the red sideband can provide a better alternative if the lowest possible mean phonon number is the goal of the experiment. These findings have been published in Kim & Beige (2013).

The full two-stage model was first applied to a one-dimensional atomic gas confined in a single-mode resonator. We found that alternating cooling pulses with peri-

ods of thermalisation can result in very low temperatures of the atomic gas. The stationary state of the cooling stage was shown to be strongly dependent on the phonon coherence ζ which is associated with the phonon exchange between the atoms. The phonon coherence ζ itself would decay to zero during the cooling stage. The cooling rate during the cooling stage was shown to be collective, i.e. increasing with the number of particle in the atomic gas. Therefore, to take advantage of the collective cooling rate, we proposed to introduce an additional thermalisation stage which would revive the phonon coherence without compromising the temperature of the atomic gas and prepare the system for the next cooling stage.

The full two-stage model therefore consists of combining both stages in succession for successfull collective cooling of the many-body atomic gas. Since the cooling rate is collective, the duration of the cooling pulses can be kept very short. Overall, when alternating cooling and thermalisation stages, the system is expected to reach very low temperatures.

We then applied our two-stage model to describe the mechanism of sonoluminescence. The collapse of the bubble during sonoluminescence occurs after a period of bubble radius growth and is accompanied by rapid temperature increase of the gas within the bubble. During the collapse, the bubble wall becomes opaque and the radiation field inside strongly resembles that of an optical cavity. We treated the atomic system trapped inside the bubble as being heated in an optical cavity, while the collapse was being modeled using the quantum optical approach. Alternating now thermalisation stages with heating stages results in description of growth and collapse phases of the bubble lifecycle. We show how the thermalisation stage creates atomic coherences necessary to explain the heating mechanism of the heating stage and how it accounts for the creation of plasma. We also identify heating resonances of the atomic gas inside the cavitating bubble and show how its temperature grows during the collapse, as well as how the type of the atomic species influences this growth.

Overall, we show how our two-stage model combines quantum mechanical models together with the framework of thermodynamics to describe the observed phenomena within many-body collective cooling and single-bubble sonoluminescence. Alternating two physically distinct stages could provide a viable approach when treating vibrational and electronic energies of many-body atomic systems.

References

ARFKEN, G., WEBER, H. & HARRIS, F. (2012). *Mathematical Methods for Physicists: A Comprehensive Guide*. Elsevier. 21

BARBER, B.P. & PUTTERMAN, S.J. (1991). Observation of synchronous picosecond sonoluminescence. *Nature*, **352**, 318–320. 7, 73

BAUMANN, K., GUERLIN, C., BRENNECKE, F. & ESSLINGER, T. (2010). Dicke quantum phase transition with a superfluid gas in an optical cavity. *Nature*, **464**, 1301–1306. 55

BEIGE, A., KNIGHT, P.L. & VITIELLO, G. (2005). Cooling many particles at once. *New Journal of Physics*, **7**, 96. 5, 6

BIENERT, M. & MORIGI, G. (2012). Cavity cooling of a trapped atom using electromagnetically induced transparency. *New Journal of Physics*, **14**, 023002. 6

BLACK, A.T., CHAN, H.W. & VULETIĆ, V. (2003). Observation of collective friction forces due to spatial self-organization of atoms: from rayleigh to bragg scattering. *Physical review letters*, **91**, 203001. 6, 29

BLAISE, P. & HENRI-ROUSSEAU, O. (2011). *Quantum Oscillators*. Wiley. 14, 70, 85

BLAKE, T., KURCZ, A. & BEIGE, A. (2011a). Comparing cavity and ordinary laser cooling within the lamb–dicke regime. *Journal of Modern Optics*, **58**, 1317–1328. 6, 54

BLAKE, T., KURCZ, A., SALEEM, N.S. & BEIGE, A. (2011b). Laser cooling of a trapped particle with increased rabi frequencies. *Physical Review A*, **84**, 053416. 44, 54

BLAKE, T., KURCZ, A. & BEIGE, A. (2012). Rate-equation approach to cavity-mediated laser cooling. *Physical Review A*, **86**, 013419. 6, 54

BRENNER, M.P., HILGENFELDT, S. & LOHSE, D. (2002). Single-bubble sonoluminescence. *Rev. Mod. Phys.*, **74**, 425–484. 6, 7, 73

CAMARA, C., PUTTERMAN, S. & KIRILOV, E. (2004). Sonoluminescence from a single bubble driven at 1 megahertz. *Physical review letters*, **92**, 124301. 7

CHUAH, B.L., LEWTY, N.C., CAZAN, R. & BARRETT, M.D. (2013). Sub-doppler cavity cooling beyond the lamb-dicke regime. *Physical Review A*, **87**, 043420. 5, 29

CIRAC, J., PARKINS, A., BLATT, R. & ZOLLER, P. (1993). Cooling of a trapped ion coupled strongly to a quantized cavity mode. *Optics communications*, **97**, 353–359. 3, 5, 37

CIRAC, J., LEWENSTEIN, M. & ZOLLER, P. (1995). Laser cooling a trapped atom in a cavity: Bad-cavity limit. *Physical Review A*, **51**, 1650. 5

DIDENKO, Y.T., MCNAMARA III, W.B. & SUSLICK, K.S. (2000). Effect of noble gases on sonoluminescence temperatures during multibubble cavitation. *Physical review letters*, **84**, 777. 7

DIEDRICH, F., BERGQUIST, J.C., ITANO, W.M. & WINELAND, D.J. (1989). Laser cooling to the zero-point energy of motion. *Physical review letters*, **62**, 403–406. 4

DOMOKOS, P. & RITSCH, H. (2002). Collective cooling and self-organization of atoms in a cavity. *Physical review letters*, **89**, 253003. 1, 55

DOMOKOS, P. & RITSCH, H. (2003). Mechanical effects of light in optical resonators. *JOSA B*, **20**, 1098–1130. 5

FLANNIGAN, D.J. & SUSLICK, K.S. (2007). Emission from electronically excited metal atoms during single-bubble sonoluminescence. *Physical review letters*, **99**, 134301. 7, 73

GAITAN, D.F. (1990). Observation of sonoluminescence from a single, stable cavitation bubble in a water glycerin mixture. *Frontiers of Nonlinear Acoustics*. 73

GAITAN, D.F. & CRUM, L.A. (1990). Sonoluminescence from single bubbles. *The Journal of the Acoustical Society of America*, **87**. 73

GERRY, C. & KNIGHT, P. (2004). *Introductory Quantum Optics*. Cambridge University Press. 26

Gibbons, M.J., Kim, S.Y., Fortier, K.M., Ahmadi, P. & Chapman, M.S. (2008). Achieving very long lifetimes in optical lattices with pulsed cooling. *Physical Review A*, **78**, 043418. 6, 29

Hemmerling, M. & Robb, G. (2011). Cavity cooling using intense blue-detuned light. *Journal of Modern Optics*, **58**, 1336–1341. 5

Hiller, R., Weninger, K., Putterman, S.J. & Barber, B.P. (1994). Effect of noble gas doping in single-bubble sonoluminescence. *Science*, **266**, 248–250. 73

Kampschulte, T., Alt, W., Brakhane, S., Eckstein, M., Reimann, R., Widera, A. & Meschede, D. (2010). Optical control of the refractive index of a single atom. *Physical review letters*, **105**, 153603. 5, 29

Kim, O. & Beige, A. (2013). Mollow triplet for cavity-mediated laser cooling. *Physical Review A*, **88**, 053417. 3, 31, 97

Leibfried, D., Blatt, R., Monroe, C. & Wineland, D. (2003). Quantum dynamics of single trapped ions. *Rev. Mod. Phys.*, **75**, 281–324. 44

Lev, B.L., Vukics, A., Hudson, E.R., Sawyer, B.C., Domokos, P., Ritsch, H. & Ye, J. (2008). Prospects for the cavity-assisted laser cooling of molecules. *Physical Review A*, **77**, 023402. 4

Lohse, D. (2002). Sonoluminescence: Inside a micro-reactor. *Nature*, **418**, 381–383. 7

Loudon, R. (1992). *The Quantum Theory of Light*. Oxford University Press. 9, 21, 23

Madison, K.W., Wang, Y., Rey, A.M. & Bongs, K. (2013). *Annual Review of Cold Atoms and Molecules: Volume 1*, vol. 1 of *Annual Review of Cold Atoms and Molecules*. World Scientific. 1

Maunz, P., Puppe, T., Schuster, I., Syassen, N., Pinkse, P. & Rempe, G. (2004). Cavity cooling of a single atom. *Nature*, **428**, 50–52. 1, 4, 29

McKeever, J., Buck, J., Boozer, A., Kuzmich, A., Nägerl, H.C., Stamper-Kurn, D. & Kimble, H. (2003). State-insensitive cooling and trapping of single atoms in an optical cavity. *Physical review letters*, **90**, 133602. 1, 4, 29

Mishina, O.S. (2014). Cavity cooling of an atomic array. *New Journal of Physics*, **16**, 033021. 6

MOLLOW, B. (1969). Power spectrum of light scattered by two-level systems. *Physical Review*, **188**. 3

MORIGI, G. & ESCHNER, J. (2001). Doppler cooling of a coulomb crystal. *Physical Review A*, **64**, 063407. 6, 55

MOSS, W.C. (1997). Understanding the periodic driving pressure in the rayleigh–plesset equation. *The Journal of the Acoustical Society of America*, **101**, 1187–1190. 7

MOSSBERG, T., LEWENSTEIN, M. & GAUTHIER, D.J. (1991). Trapping and cooling of atoms in a vacuum perturbed in a frequency-dependent manner. *Physical review letters*, **67**, 1723. 5

MURR, K. (2006). Large velocity capture range and low temperatures with cavities. *Physical review letters*, **96**, 253001. 5

NEUHAUSER, W., HOHENSTATT, M., TOSCHEK, P. & DEHMELT, H. (1978). Optical-sideband cooling of visible atom cloud confined in parabolic well. *Physical review letters*, **41**, 233–236. 1, 4

NUSSMANN, S., MURR, K., HIJLKEMA, M., WEBER, B., KUHN, A. & REMPE, G. (2005). Vacuum-stimulated cooling of single atoms in three dimensions. *Nature Physics*, **1**, 122–125. 1, 5, 29

PUTTERMAN, S., EVANS, P., VAZQUEZ, G. & WENINGER, K. (2001). Cavitation science: Is there a simple theory of sonoluminescence? *Nature*, **409**, 782–783. 7

RITSCH, H., DOMOKOS, P., BRENNECKE, F. & ESSLINGER, T. (2013). Cold atoms in cavity-generated dynamical optical potentials. *Rev. Mod. Phys.*, **85**, 553–601. 6

SCHLEIER-SMITH, M.H., LEROUX, I.D., ZHANG, H., VAN CAMP, M.A. & VULETIĆ, V. (2011). Optomechanical cavity cooling of an atomic ensemble. *Physical review letters*, **107**, 143005. 6

STENHOLM, S. (1986). The semiclassical theory of laser cooling. *Rev. Mod. Phys.*, **58**, 699–739. 4, 29

SUSLICK, K.S. & FLANNIGAN, D.J. (2008). Inside a collapsing bubble: Sonoluminescence and the conditions during cavitation. *Annual Review of Physical Chemistry*, **59**, 659–683, pMID: 18393682. 7, 73

VIGNERON, K. (1995). Etude d'effets de bistabilite optique induits par des atomes froids places dans une cavite optique. Masters thesis Ecole Superieure d' Optique. 1, 4, 29

VULETIĆ, V. & CHU, S. (2000). Laser cooling of atoms, ions, or molecules by coherent scattering. *Physical Review Letters*, **84**, 3787. 5

WINELAND, D. & DEHMELT, H. (1975). Winelanddehmelt. *Bull. Am. Phys. Soc.*. 4, 44

WOLKE, M., KLINNER, J., KESSLER, H. & HEMMERICH, A. (2012). Cavity cooling below the recoil limit. *Science*, **337**, 75–78. 5, 29

ZAUGG, T., WILKENS, M., MEYSTRE, P. & LENZ, G. (1993). Adiabatic atomic cooling in microwave cavities. *Optics communications*, **97**, 189–193. 5

ZIPPILLI, S. & MORIGI, G. (2005). Cooling trapped atoms in optical resonators. *Physical review letters*, **95**, 143001. 6